SEISMIC PERFORMANCE OF YIELDING COLUMNS SUPPORTED BY ROCKING FOUNDATIONS: A COMPUTATIONAL STUDY

A Thesis
Submitted to the Graduate Faculty
of the
North Dakota State University
of Agriculture and Applied Science

By

Buddika Saranath Godagama

In Partial Fulfillment of the Requirements
for the Degree of
MASTER OF SCIENCE

Major Department:
Civil Engineering

November 2016

Fargo, North Dakota

North Dakota State University
Graduate School

Title

SIESMIC PERFORMANCE OF YIELDING COLUMNS SUPPORTED BY ROCKING FOUNDATIONS: A COMPUTATIONAL STUDY

By

Buddika Saranath Godagama

The Supervisory Committee certifies that this ***disquisition*** complies with North Dakota State University's regulations and meets the accepted standards for the degree of

MASTER OF SCIENCE

SUPERVISORY COMMITTEE:

Dr.Sivapalan Gajan
Chair

Dr. Dinesh Katti

Dr. Mijia Yang

Dr. Zhili Gao

Approved:

11/28/2016 — Date

Dr. Dinesh Katti — Department Chair

ABSTRACT

The effectiveness of foundation rocking as a seismic energy dissipation mechanism to reduce shake demands is studied by the use of a finite element numerical model consisting of a realistic structure and a soil-foundation interaction model. While both fixed base and rocking foundation systems performed satisfactorily during relatively small shaking events, rocking foundation systems exhibited superior performance during strong shaking events. Furthermore, rocking foundation design reduced the peak deck drift due to flexure, peak acceleration on the deck, and the column base moment by more than 50% when compared to conventional design. By intentionally reducing the rocking coefficient smaller than base shear coefficient, the beneficial effects of rocking foundations were fully utilized. It was shown that a slight increase in footing embedment and/or initial shear modulus of soil has the potential to improve settlement-rotation behavior of the foundation significantly, while still mobilizing rocking behavior and dissipating seismic energy.

ACKNOWLEDGEMENTS

I would like to thank my advisor Dr. Sivapalan Gajan for his guidance and support, without whom this research would have been impossible.

I would also like to thank my respective graduate committee Dr. Dinesh Katti, Dr. Mijia Yang and Dr. Zhili Gao for their invaluable input and guidance to complete this project.

My sincere gratitude to Mr. Roch Player and Mr. Timothy Wiles at Braun Intertec Corporation for their influence and support towards my graduate studies.

And finally, to the Department of Civil and Environmental Engineering at North Dakota State University for giving me the opportunity to complete this master's degree.

DEDICATION

To my loving parents Mr. Ubeysekera Godagama and Mrs. Sumana Wijewardena who taught me to believe in hard work. I am who I am because of their immense love, guidance and support.

To my wonderful in-laws, Mr. Christopher Crusz and Mrs. Sherine Crusz for their unending support and prayers.

Finally, to my amazing wife Shevonne who has been my source of inspiration and encouragement, which made graduate school possible.

TABLE OF CONTENTS

LIST OF TABLES

LIST OF FIGURES

Figure Page

LIST OF APPENDIX TABLES

1. INTRODUCTION

1.1. Background to Research

Effective seismic energy dissipation under rocking foundations by means of soil yielding is an area that has been studied to some extent in the field of civil engineering (particularly related to earthquake engineering design). However, there still exist several unanswered questions regarding the effectiveness of rocking foundations as a seismic energy dissipation mechanism. According to current accepted design practice, California Department of Transportation (Caltrans) require bridge column structures to be designed with deep foundations (pile or shafts) in order to keep the foundation within elastic range while the column reaches its over-strength capacity (Caltrans, 2004). This would result in a plastic "hinging" effect at the base of the column, which would act as a "fuse" in the presence of a large seismic load (Priestley et al., 1994). While this would provide and alternative route for the seismic energy dissipation away from the superstructure, it has been shown that bridge column damage or failure would be inevitable (Lehman & Moehle, 2000; Anastasopoulos et al., 2010; Anastasopoulos, 2010; Schoettler et al., 2015). Passive control techniques such as energy dissipation devices, which absorbs large plastic deformations within the superstructure by reducing structural acceleration through controlling inter-story drifts and seismic-isolation devices, which creates a discontinuity along the height of the structure and by decoupling the superstructure from foundation structure with the use of isolators and auxiliary devices (Dolce et al., 2000) are also integrated in to modern structures. However, the effectiveness of such "fuse" mechanisms depend on their load/ moment carrying capacity, ductility, self-centering characteristics and amount of energy that could be dissipated by those particular elements (Gajan & Kutter, 2008). According to Gajan & Saravanathiiban (2011), these passive control devices are not commonly used due to installation

complexities, maintenance and durability, replacement and restoration difficulties after a strong earthquake and most importantly the complicated nature of the design and the predicted behavior.

Earthquake engineering design emphasis the importance of incorporating nonlinear behavior of both structural and geotechnical components and the interaction between them (FEMA 356, 2000). Yet, current civil engineering practice does not fully take advantage of this nonlinear soil-footing interaction because of the limited understanding of the combined nonlinear load-deformation behavior, which includes complex material (plasticity) and geometrical (gap opening) nonlinearities (Gajan & Kutter, 2009). Rocking foundations are a relatively new philosophy that has been introduced as a possible alternative to the currently accepted earthquake design. Still in its infant stage, rocking foundations are not fully integrated into design manuals yet. However, considerable research is being conducted to evaluate the effects of combined nonlinear (cyclic vertical, shear and moment) loading on a shallow foundation.

The complicated nature of the soil response underneath a footing, subjected to a combined nonlinear and dynamic cyclic loading has been the primary reason to discourage the civil engineering community from accepting this new philosophy. Known issues such as possibility of excessive settlement due to reduced factor of safety and large footing rotations (Gajan & Kutter, 2008; Ntritsos, 2015), the uncertainty in soil properties and the perceived uncertainties in consequent nonlinear behavior of soil-foundation system and the complications involved in integrating such foundations into a structure (Kokkali et al., 2014) are among primary concerns related to this philosophy.

Historically, seismic related research predominantly has been done in either from a structurally dominant (conventional column capacity design) or a foundation dominant

(nonlinear foundations with simplified elastic structure) perspective. Structure related research has traditionally been focused on limiting ductility demands of the superstructure (for e.g. Aiken et al., 1988; Braga et al., 2002; Dolce et al., 2003) while geotechnical related research has been focused mainly on nonlinear behavior of soil-footing system with an idealized elastic structure (for e.g. Gajan et al., 2005; Ugalde et al., 2007; Gajan & Kutter, 2008 & 2009; Drosos et al., 2012). In this study, the investigation is focused on the nonlinear characteristics of a soil-footing-structure system with the use of realistic computational simulations that are subjected to historic ground motions. Using the moment-rotation-settlement results from these simulations, effectiveness of rocking foundation design is evaluated. Different types of soil conditions, footing sizes, column aspect ratios (ratio between column height and width) and footing embedment is used to produce an array of results in order to substantially evaluate the effects of a full-scale reinforced concrete bridge-column with a shallow foundation, which is allowed to rock at the base.

1.2. Scope of the Research

1.2.1. Objective

Recent studies have begun to understand the importance of studying the combined nonlinear behavior of both structural elements and foundation elements as a system. Deng et al., (2010) performed centrifuge experimented on two scaled-down bridge systems; one consisting of conventional foundation with a yielding column and the other one consisting of yielding foundation (small rocking footing) with a non-yielding column. The experimental results indicated that while both columns showed nonlinear behavior, yielding column reached higher moment and rotation values compared to the non-yielding column with rocking foundations for same excitation as conventional foundation design relies on the column to dissipate energy

(Deng et al., 2010). Furthermore, the smaller footing (yielding/ rocking foundation) reached foundation moment capacity without the presence of any capacity deterioration while the larger footing (conventional) remained well within the elastic range with much higher initial stiffness (resistance) to moment-rotation behavior. The permanent lateral displacement of the rocking foundation bridge system found to be comparatively less compared to the conventional bridge system, partly due to the self-centering characteristic of the rocking foundations. Similarly, Loli et al., (2014) conducted a series of centrifuge tests to study the nonlinear and inelastic response of both soil-foundation interface and structure using a scaled-down reinforced concrete bridge pier, where performance between a conventional foundation design and rocking isolated design is compared. The study emphasis the importance of the use of a reinforced concrete column rather than a metal structure when investigating inelastic deformations and strengths, referring to the differences in load-moment capacity interaction behavior and fuse development leading to degradation behavior under cyclic loading (Loli et al., 2014). Upon analyzing the behavior of the two structures, the study concluded that rocking foundations are a superior design based on the reduced acceleration transmitted to the structure, limited deck drift compared to the conventional pier and its overall ability to resist strong motions with minimal damages to the structure. By contrast, the conventional pier indicated linear elastic foundation response with increased rotation stiffness, while the column showed increased damage accumulation and eventual collapse. Both Deng et al., (2010) and Loli et al., (2014) acknowledge the excess settlement observed during the experiments and the need for remediation. The intention of this research is to extend this study of complex and strong coupling between the nonlinear behavior of the structure and nonlinear behavior of the soil during seismic loading. In order to achieve this goal, a realistic bridge pier computational model was developed then calibrated and validated against

experimental data to confirm accuracy and finally, combined with a nonlinear dynamic soil-foundation interaction model to study the soil-footing-structure interaction.

The primary objectives of this study are;

- To compare the ductility, acceleration and moment demands on the structure using current seismic design criteria with those of using rocking foundation design.
- To investigate the effects of rocking coefficient (Cr) and base shear coefficient (Cy) on combined structure-foundation system behavior.
- To evaluate the effects of soil improvement and footing embedment on moment-rotation-settlement behavior of a rocking foundation.

1.2.2. Methodology

The main purpose of this study is to compare the beneficial and detrimental effects of structural yielding and soil yielding using a realistic yet idealized structure, which can accurately depict the nonlinear behavior in both soil and structure. Additionally, characteristics of combined moment-rotation-settlement behavior of the soil-structure system and the resulting energy dissipation are also studied. Therefore, the development of a realistic but idealized structure was a paramount task. In order to neglect the complexities of a system behavior such as multiple span interactions due to deck coupling (such as a bridge) and focus more on the research objectives, it was decided that the use of a simpler structure such as a bridge pier would be ideal. The model was developed using the finite element software OpenSees (Open System for Earthquake Engineering Simulations) with the bridge pier column consisting of reinforced concrete sections to analyze the nonlinear behavior of the column element.

The development of the computational model essentially underwent three phases. First, the constitutive reinforced concrete column was constructed and calibrated using the well-

confined concrete bridge column experiments conducted by Lehman & Moehle (2000). Then, using the calibrated constitutive model a full-scale bridge-column computational model (Bridge-pier model) was developed and validated against a full-scale single column bridge shake table experiments (Schoettler et al., 2015) for accuracy. Finally, a complete soil-footing-structure model was constructed by placing the Bridge-pier model on a nonlinear dynamic soil-foundation interaction model (Contact Interface Model) available in OpenSees finite element platform. The completed numerical model was subjected to a series of ground shaking events to achieve the above-mentioned objectives.

1.3. Organization of the Thesis

This report consists of nine chapters and the following summarizes the content of each chapter.

- Chapter 1: Introduction to the research, which includes research background, research objectives, methodology and thesis organization.
- Chapter 2: Discusses the literature review of the effectiveness of rocking foundations in terms of moment capacity, settlement, self-centering ability and energy dissipation. Additionally, the current capacity design approach is also discussed.
- Chapter 3: Presents construction of the constitutive model including an introduction to material model behavior and model calibration.
- Chapter 4: Presents validation of the constitutive model and the development of the Bridge-pier model.
- Chapter 5: Introduces the experimental methodology

- Chapter 6: Evaluates the performance of capacity design approach in terms of moment-rotation behavior, ductility demands and energy dissipation characteristics to excitations and structural characteristics.
- Chapter 7: Evaluates the performance of rocking foundation design in terms of moment-rotation-settlement behavior and energy dissipation characteristics to excitations, footing embedment and structural characteristics.
- Chapter 8: Presents conclusions and recommendations for future work.

2. LITERATURE REVIEW

2.1. Introduction

In this chapter, a review of the current conventional capacity design approach is presented along with a discussion about the current research into rocking foundation design philosophy.

2.2. Structural Yielding versus Soil Yielding during Seismic Loading

The prevailing capacity design concept for bridge pier type structures ensures ductile flexural failure of the column while all other bridge components remain elastic, which meant heavy confining reinforcements with improved shear capacity (California Department of Transportation, 2006). According to this design approach, failure of the bridge column would likely to occur due to yielding and subsequent fracturing of the confining reinforcements after significant deformation. The hysteretic behavior of modern bridge columns under seismic loads and lateral loads is an area that has been thoroughly examined by the researchers. It has been observed that both the quality of concrete and the type of reinforcement and confinement determines the allowable ductility demands on this type of structure (Lehman & Moehle, 2000; Kawashima & Unjoh, 2004; Wibowo et al., 2014; Popa et al., 2014). The development of the "hinge" section within the column section due to excess flexural deformations potentially leading to shear failure is a characteristic of the capacity design concept (Park and Paulay, 1975; Park & Ang, 1989; Priestley et al., 1994). Since the column is used as the prime source for energy dissipation, the foundation is retained within the elastic range.

The incorporation of capacity design concept that ensures ductile flexural failure of the column while all other bridge components remain elastic meant heavy confining reinforcements with improved shear capacity (California Department of Transportation, 2006). According to this

design approach, failure of the bridge column would likely to occur towards the base of the reinforced column after significant damage (plastic deformation) to confining reinforcements where shear demand is primarily transferred (Watson & Park, 1994; California Department of Transportation, 2006).

The possibility of reducing ductility demands on the structure by the use of rocking foundations has been a heavily discussed topic for decades (Housner, 1963; Chopra & Yim, 1985; Priestley et al., 1996). These studies have shown that shallow foundations, by intentionally "under-designing", could be loaded well into their nonlinear range during intense earthquake loading. The Rocking foundations theory states this nonlinearity of soil could be used as an energy dissipation mechanism, potentially reducing shaking demands exerted on the structure (Gajan et al., 2005). The prevailing seismic design approach requires selecting an energy dissipation system such as base isolation method, use of passive energy dissipation method or column yielding depending on required specific performance level of earthquake demand (FEMA 356, 2000). However, the unpredictable nature of earthquakes make these approaches while quite effective when not exceeding the design limits, quite destructive once they do. The effectiveness of these mechanisms highly depends on the material's capacity, ductility, energy dissipation, isolation and self-centering characteristic (Gajan & Kutter, 2008). The rocking foundations on the other hand appears not to share the same weakness as damage from stronger motions are mostly contained within foundation soils with minimal structural damage (Anastasopoulos et al., 2010; Loli et al., 2014).

2.3. Characteristics of Rocking Foundations

This study primarily discusses the rocking behavior of an idealized single reinforced concrete bridge column type structures and the subsequent coupling of soil and structure nonlinear behavior. The discussion of this nonlinearity is considered using three specific characteristics;

- Moment-rotation response of the soil-footing-structure system
- Settlement-rotation characteristics in foundation soil
- Energy dissipation through moment-rotation response

2.3.1. Moment-Rotation Response

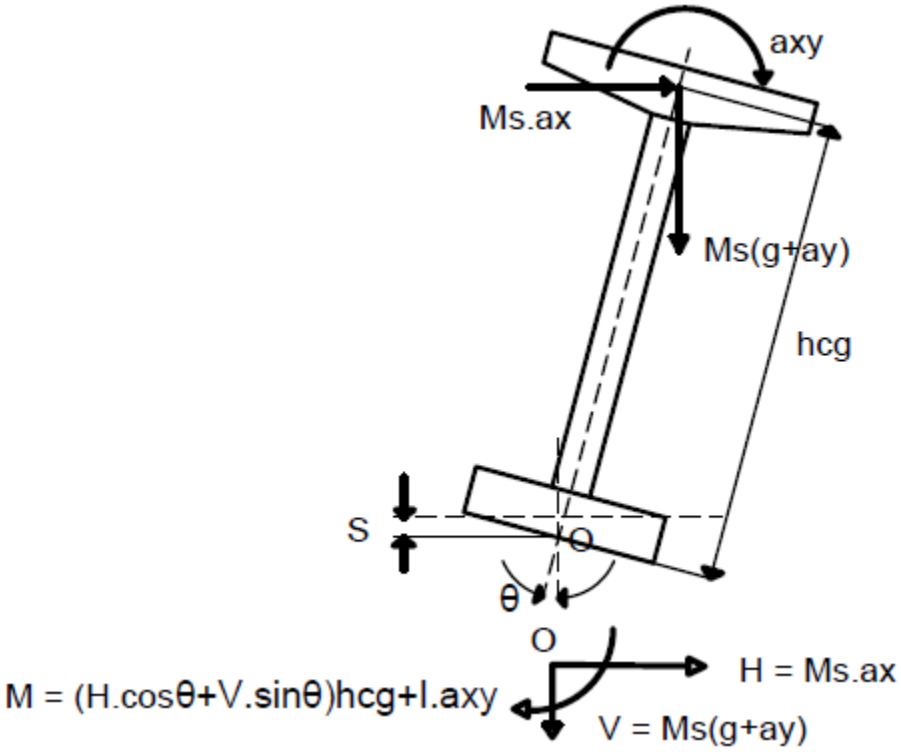

Figure 2.1. Vertical Load, Shear and Moment Acting on a Simplified Column-Footing Structure (after, Gajan & Kutter, 2008)

During seismic loading, inertial forces from the structure are transmitted to the foundation. Additionally the soil also directly transmits dynamic loads to the footing from the ground acceleration. The three external load components created due to dynamic loading as indicated in figure 2.1 are, vertical (V), lateral (H) and moment (M) as proposed by Gajan & Kutter (2008). The parameters of V, H and M loads are; structural mass (Ms), vertical and horizontal components of acceleration (ay & ax), angular acceleration (axy), gravitational acceleration (g), height of center of gravity for the structure (hcg), mass moment of inertia about the center of gravity (I) and rotation of the structure (θ). The combined cyclic vertical-shear-moment loading results in cyclic and permanent deformations in foundation soil in the form of settlement, sliding and rotation. The resulting hysteretic moment-rotation loop developed by the rocking behavior manifests the ability of a rocking foundation to dissipate energy at the soil-footing interface. Considerable amount of research has been done both computationally and experimentally to investigate various aspects of this moment-rotation behavior by means of soil type and condition, footing characteristics, structure type and excitation.

Anastasopoulos et al., (2010) evaluated the overall performance of 29 seismic excitations using a realistic bridge column simulation with a conventionally designed foundation and an under-designed foundation that utilizes soil yielding. Mobilization of moment both within the structure and in foundation soil was considered for both designs among other response. While the conventional design notably maintained the foundation soils within elastic range regardless of the excitation, the under-designed foundation responded with strong inelastic behavior for ground motions exceeding the design limits (Anastasopoulos et al., 2010). Despite the considerable soil deformations, the under-designed foundation exerted minimal ductility demands on the structure, while the conventionally designed foundation ultimately caused the

collapse of the structure once design limits were exceeded. Similarly, Loli et al., (2014) observed when compared to the conventional design, moment-rotation behavior of a rocking pier exerted much less structural deformations due to flexural movement and instead showing limited deck drifts mostly due to soil yielding. Furthermore, increasing nonlinear response in foundation soil for rocking foundations and increased flexural behavior within the structure for conventional foundations was observed with stronger ground motions indicating the ability of both designs to dissipate energy with increased demand.

For studying the nonlinear behavior of a system of rocking foundations, Deng et al., (2012) conducted a series of centrifuge experiments using bridge systems resting on dry sand. In the experiment, two identical two-span bridge decks were considered with two-pier support in the middle. One designed for soil yielding (smaller footing) and the other to resist plastic hinging moment in the column with a larger shallow foundation. The moment-rotation results indicated that while the small footing approached the moment capacity with relatively less initial stiffness, the larger conventional footing peaked well below moment capacity with much greater initial stiffness. It was noted that once soil has yielded, moment-rotation plots do not indicate any reduction in moment capacity with the number of cycles or with the amplitude of rotation. Similar behavior was observed by Gajan et al., (2005) and Gajan & Kutter, (2008 & 2009) when using idealized shear wall type structure experiments with centrifuge dynamic loading and cyclic push loading using Nevada sand and San Francisco Bay mud. The static factor of safety with respect to concentric vertical load (FS) values for these shear walls were varied between 2 to 10 by changing the axial loads, footing sizes and embedment. It was observed that for both dynamic loading and cyclic push loading, moment-rotation response was initially stiffer indicating low levels of rotation. However, as the rotation amplitude increases rotation stiffness

degrades as a result of soil yielding and mobilizing ultimate bearing capacity (Gajan & Kutter, 2008). Furthermore, it was observed that although embedment slightly increased the moment capacity of a footing (due to increased FS) it would also make the rocking behavior more stable by increasing its self-centering capability. Additionally, Gajan et al., (2005) also indicated that a clear correlation couldn't be determined between FS and rotational stiffness reduction.

The theoretical ultimate moment of a rocking foundation is defined as the maximum moment experienced by a footing at particular amplitude of rotation. As the amplitude of rotation increases, the mobilized moment increases as well (Gajan & Kutter, 2008).

$$M_{ult} = \frac{VB}{2}\left(1 - \frac{A_c}{A}\right) \quad (1)$$

The ultimate moment (Mult) can be indicated as a function vertical load (V), footing length in rocking direction (B) and critical contact area ratio (A/Ac), which is the ratio between footing area and minimum contact area required to support the vertical and shear loads. Deng et al., (2012) discussed that plastic hinging can be forced to occur at foundation soils by maintaining the foundation moment capacity smaller than the column moment capacity through the use of rocking coefficient (Cr) of the foundation and base shear coefficient (Cy) of the structure, which are non-dimensional moment capacities of soil-foundation system and column respectively. These two coefficients can be presented as follows;

$$C_r = \frac{B}{2H_g}\left(1 - \frac{A_c}{A}\right) \quad (2)$$

$$C_y = \frac{M_{column}}{VH} \quad (3)$$

H_g is the effective height of the structure and M_{column} is the moment capacity of the column. Assuming external shear forces are negligible, the following relationship between critical contact

ratio and FS_v can be developed provided the ultimate bearing pressure is independent of the shape and size of the loading area (Gajan & Kutter, 2008).

$$\frac{A}{A_c} \approx FS_v \tag{4}$$

Using this development, it can be shown that in order to create favorable conditions for rocking behavior, M_{ult} has to be minimized by reducing FS_v of the system and thereby reducing Cr.

2.3.2. Settlement-Rotation Characteristics

It has been understood that in order for rocking foundations to be a successfully integrated in to design, the amount of settlement has to be estimated with acceptable confidence and mitigated. Gajan & Kutter (2008) concluded that the main causes for the increased settlement are related to amplitude of rotation (footing), number of loading cycles and critical contact area ratio. Research related to rocking foundation has observed and tried to quantify this settlement issue by developing correlations.

The following correlation was developed by Deng et al. (2012) and provides a linear relationship between normalized settlement (S/B) and accumulative footing rotation (θcum). B is defined in equation 1, while accumulative rotation was defined essentially as the sum of all rotations that exceeds an arbitrary threshold (rotations below that value is not expected to cause any residual settlement) and C was indicated as a coefficient correlated to critical contact area ratio.

$$S = CB\theta_{cum} \tag{5}$$

Gajan & Kutter (2008) observed a similar linear trend during each cycle of loading as individual normalized settlement increase with amplitude of individual footing rotation. Furthermore, normalized settlement versus rotational amplitude plots indicated that smaller A/Ac

footings experience more permanent settlement and for a given A/Ac range, permanent settlement occurred during dynamic loading is larger compared to those that occurred during slow lateral cyclic loading for sand. Conversely, permanent settlements occurred in saturated clay during dynamic loading was observed to be smaller than those occurred during slow lateral cyclic loading. Gajan & Kutter (2008) concluded that the additional settlement in sand experiments could be contributed to the densification and the subsequent reduction in bearing capacity of soil material during dynamic shake as well as dynamic loading from footing. The reduced settlement observed in clay was contributed to the undrained behavior of saturated clay. Soil densification also accounts for the amount of permanent settlement as indicated by Kokkali et al., (2014). In a series of centrifuge and 1g tests performed on an idealized bridge pier, it was shown that for similar FS, the difference in permanent settlement between the two loading is more pronounced for loose sand (Dr=45%) compared to dense sand (Dr=90%). Additionally, less footing uplift accompanied by "sinking motion" was observed for the loose sand with lower FS whereas considerable footing uplift was noted for denser sand with higher FS.

The critical role of A/Ac (FS) on rocking foundation settlement is well documented by researchers such as Ntritsos et al., (2015); Gajan & Kutter, (2009 & 2008) and Ugalde et al., (2007). Ntritsos in particular investigated the undrained response of a square embedded and shallow footings using a lightly loaded (FS=5) and a heavily loaded (FS=2) footing placed in a homogenous clay stratum modelled as an elastoplastic material. In general an uplifting-dominant behavior was observed from the lightly loaded footing with strong self-centering capability while, a more sinking-dominant response was noted from the heavily loaded footing, which confirms to an observation later noted by (Kokkali et al., 2014). Notable effects of embedment were, considerable increase in plastic deformation of soil during rocking behavior leading to

abrupt moment decrease during unloading phase due to gapping effect and an abrupt moment increase when complete passive earth pressure is mobilized by the footing, reduction in P-Δ induced moment capacity degradation and considerable reduction in accumulated settlement as a results of reduced stress distribution onto the base soil (Ntritsos et al., 2015). Furthermore, it was conclude that based on the experimental results, the effect of embedment on increasing bearing capacity is much more than the effect of increasing soil stiffness (Ntritsos et al., 2015).

However, reducing foundation soil deformation by increased embedment or soil modification could hinder rocking behavior and subsequently limit the potential to dissipate energy. Since the rocking foundation theory relies on the plastic deformation of foundation-soil to dissipate seismic energy, hindering the potential of that soil deformation could results in limited energy dissipation. Deng et al., (2012), observed this in experiments using concrete pads to support rocking foundations. It was concluded that although the ground improvements successfully reduced the rocking-induced settlement, it was limited in its capacity to absorb energy compared to a non-supported rocking foundation (Deng et al., 2012). Therefore, an optimal design is necessary that has the capacity to dissipate seismic energy with minimal amount of settlement.

2.3.3. Self-Centering Behavior

Self-centering ability is an important aspect of a rocking foundation design. For a rocking foundation to effectively dissipate energy the rocking behavior needs to be well-mobilized, which relates back to the Cr value of the foundation. However, with better energy dissipation, soil deformation has to increase as well, which leads to higher structural rotation (Selvarajah & Gajan, 2015). Numerical simulations conducted by Anastasopoulos et al., (2010) on a full-scale bridge column indicated that even during strong motions such as Takatori, rocking foundations

has the capability to self-center while conventional columns could undergo considerable deformations leading to eventual collapse. Furthermore, according to Selvarajah & Gajan (2015) based on a series of centrifuge and shake table test data using a variety of structure, the experimental results indicate significant self-centering capacity in rocking foundations.

2.3.4. Energy Dissipation Ability

It has been identified that by allowing predominantly nonlinear behavior at soil-footing interface through rocking motion, considerable amounts of energy could be dissipated. This in turn would impose reduced acceleration and ductile demands on the structure. Gajan & Kutter (2008) stated that moment capacity, energy dissipation and settlement behavior could be closely related through the critical contact area ratio. This can be verified by formulas (4) and (5) as A/Ac (or FS) is closely related to the rocking potential of a structure and its ability to mobilize moment at foundation level. Kramer (1996) suggested the following relationship between damping ratio, moment and rotation as means of quantifying energy dissipation. Where the damping ratio is denoted by ξ , moment capacity by M_{max} and maximum rotation by θ_{max}. As evident from this relationship, with highly nonlinear behavior in foundation soil, the larger hysteretic moment-rotation loops indicate the potential to dissipate more energy at soil-footing interface.

$$\xi = \frac{1}{4\pi}\left(\frac{area\ of\ M-\theta\ hyteresis\ loop}{\frac{1}{2}xM_{max}x\theta_{max}}\right) \quad (6)$$

Selvarajah & Gajan (2015) observed correlations between normalized energy dissipation and normalized settlement (accumulative settlement per footing width) using Cr. The study concluded that systems with smaller Cr values (relatively) favor rocking behavior and the higher amplitude rotation and accumulative settlement would result in higher energy dissipation.

3. CONSTRUCTION OF THE CONSTITUTIVE MODEL: REINFORCED CONCRETE COLUMN

3.1. Introduction

In this chapter, a detailed discussion about the development of the constitutive reinforced concrete column is presented along with details of the structural material models used. As part of this development, the constitutive column model was calibrated for accuracy against a series of well-confined concrete columns subjected to a purely flexural behavior under cyclic loading.

3.2. Cyclic Loading Experiments

In 2000, Lehman & Moehle published the experimental results on seismic performance of a well-confined concrete bridge column, which investigates the response of a modern fixed-base bridge column to lateral loading (Lehman & Moehle, 2000). In this experiment, scaled down versions (1/3 of the original scale) of a modern bridge column with varying longitudinal reinforcement ratios (cross sectional area of concrete to cross sectional area of reinforcements) and column aspect ratios were subjected to controlled lateral displacements to assess strength, stiffness, force displacement response and element damage . Figure 3.1 indicates a schematic of these experimental setups used.

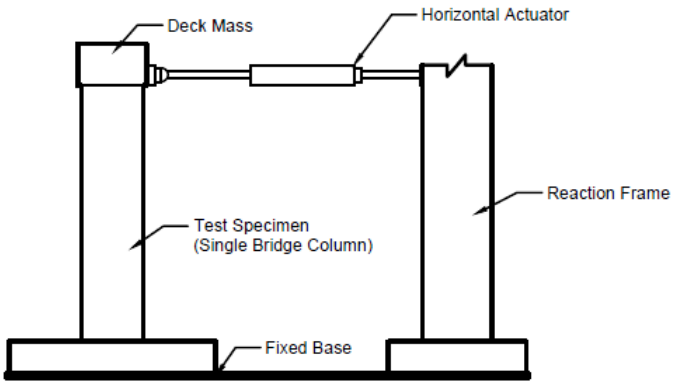

Figure 3.1. Cyclic Loading Experimental Configuration (after, Lehman & Moehle, 2000)

Lateral cyclic loading for the experiments was provided by a hydraulic actuator that was attached to the top of the column. All columns were firmly anchored to the ground so that the intended displacements would be purely flexural. The imposed displacement time-history consisted of five to six levels of monotonically increasing displacements with three cycles at each level as indicted in Figure 3.2. The loading was designed to produce degradation characteristics in the test specimens due to cyclic behavior while the monotonically increasing displacement was intended to create damage accumulation (Lehman & Moehle, 2000).

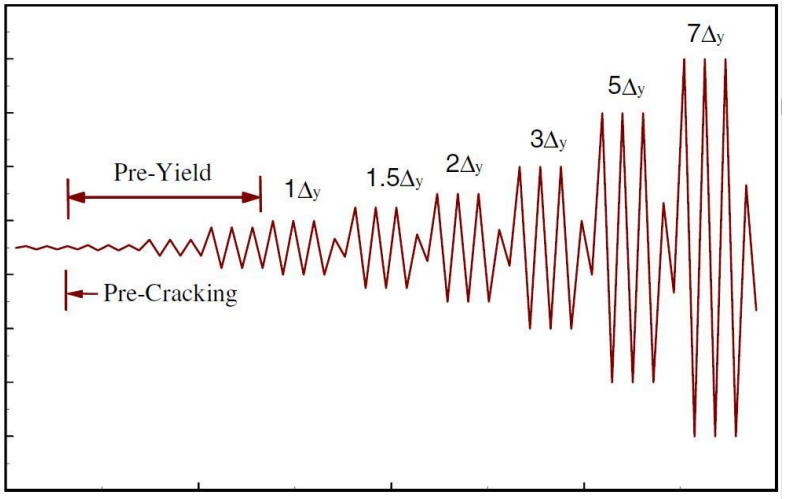

Figure 3.2. Input Loading History (Lehman & Moehle, 2000)
Note: Δy is the yield displacement of the column

3.3. Construction of the Reinforced Concrete Column

In order to capture the realistic cyclic stress-strain behavior of a modern bridge column/ pier, the numerical model must be accurately developed and calibrated using a realistic structure. An idealized yet simplified modern bridge column/ pier should consist of a circular column section typically consisting of reinforced concrete with an axial load applied at the top of column to simulate deck mass and inertial forces. The base of the column/ pier should be attached to a

footing firmly anchored to the ground to simulate elastic foundation-soil behavior. Therefore the fixed based well-confined concrete bridge column concept used by Lehman and Moehle (2000) was considered ideal to be used for the computational model development and calibration of the structural material since the experiments combine simplicity with realistic structural behavior.

3.3.1. Structural Material Model

In the proceeding sections, OpenSees material models used for the development of the reinforced concrete column are detailed. The calculations for the material model parameters are presented in the appendix section.

3.3.1.1. Concrete02 Material Model

Concrete02 material model available in OpenSees was chosen for developing confined and unconfined concrete for its accurate depiction of material behavior. This model, based on the theory developed by Yassin (1994), uses uniaxial Kent-Scott-Park concrete material (Concrete01) with degraded linear unloading /reloading stiffness according to the work of Karsan-Jirsa (1969) and linear tension softening. This model takes into account the damage of concrete and hysteresis, while retaining computational efficiency (Orakcal et al., 2006). Figure 3.3 presents concrete02 degradation behavior with linear tensions softening effect under cyclic loading as indicated by Opensees, while figure 3.4 indicates the stress-strain relationship.

The concrete02 material model employs seven user-defined input parameters consisting of unconfined compressive strength (fpc), strain at maximum strength (epsc0), concrete crushing strength (fpcu), strain at crushing strength (epscU), ratio between unloading slope at epscU and initial slope (lambda), tensile strength (ft) and tension softening stiffness (Ets) as can be seen from figure 3.4. All compressive strength and strain parameters are to be used with a negative (-) sign.

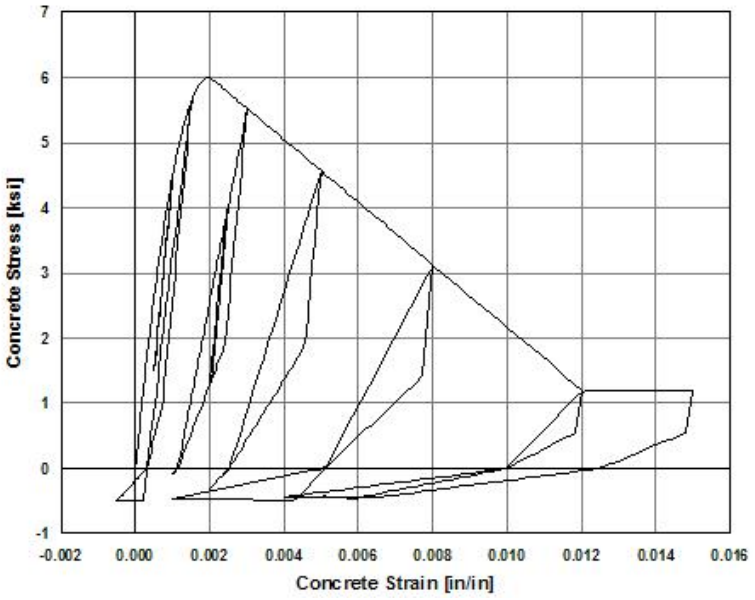

Figure 3.3. Concrete02 Material Behavior under Cyclic Loading (Mohd Hisham Mohd Yassin, 1994)

Confinement effects in concrete02 due to transverse reinforcements are an important aspect of the constitutive relationship. Proper inclusion of transverse reinforcement effects on confined concrete greatly influence material's strength and ductility behavior especially under severe cyclic loading conditions (Scott et al., 1982; Mander et al., 1988). For concret02 material model, these confinement effects are introduced through amplifying the strength and the corresponding strain based on the confined concrete model developed by Mander et al., (1988). Mander presents the stress-strain relationship of confined concrete as follows;

$$f'_{cc} = f'_{co}\left(-1.254 + 2.254\sqrt{1 + \frac{7.94f'_{l}}{f'_{co}} - 2\frac{f'_{l}}{f'_{co}}}\right) \tag{7}$$

$$\varepsilon_{cc} = \varepsilon_{co}\left[1 + 5\left(\frac{f'_{cc}}{f'_{co}} - 1\right)\right] \tag{8}$$

Where, f_{co} and ξ_{co} are unconfined compressive concrete strength and the corresponding strain, f_{cc} and ξ_{cc} are confined concrete compressive strength and its corresponding strain and f'_l is the lateral pressure applied by transverse reinforcements, which can be obtained by;

$$f'_l = \frac{1}{2} k_e \rho_s f_{yh} \tag{9}$$

$$k_e = \frac{1 - \frac{s}{2d_s}}{1 - \rho_{cc}} \tag{10}$$

$$\rho_s = \frac{A_{sp} \pi d_s}{\frac{\pi}{4} d_s^2 s} \tag{11}$$

Where, k_e is the effectiveness coefficient to consider ineffectively confined concrete at midway between two adjacent transverse reinforcements, s is the clear vertical spacing between transverse reinforcements, d_s is the diameter of spiral between bar centers, A_{sp} is the cross-sectional area of the transverse reinforcement bar, ρ_{cc} is the ratio between area of longitudinal reinforcements and are of core concrete section, ρ_s is the ratio of the volume of transverse confining steel to volume of confined concrete core and f_{yh} is the yield strength of transverse reinforcements (Mander et al., 1988). Based on this theory, OpenSees has suggested modifiers that can be used for calculating the confined concrete parameters and are presented in Appendix B.

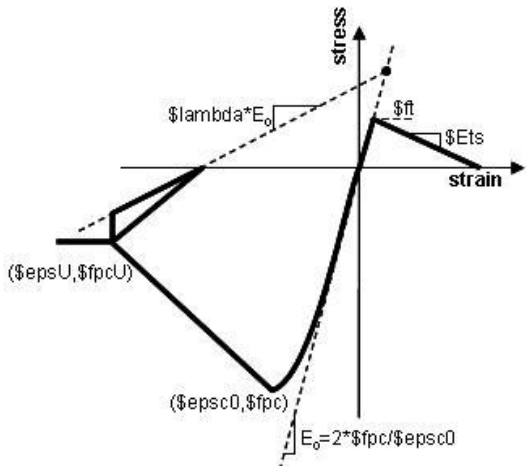

Figure 3.4. Input Parameters for Concrete02 Material Model (Mohd Hisham Mohd Yassin, 1994)
Note: Compressive forces in negative axes directions

3.3.1.2. Hysteretic Material Model (Steel)

The reinforcements for the numerical model were constructed using the hysteretic material model available in OpenSees. This uniaxial bilinear hysteretic material is capable of depicting pinching effect along with damage (deformation) and degradation of unloading stiffness, which can be modified based on maximum ductility demand of previous cycle or energy damage in the previous cycle as a function of the ratio of final to initial material stiffness of that cycle (OpenSees, 2007). The material behavior is primarily governed by points along the stress and strain failure envelope (figure 3.5), which makes the model behavior much more predictable compared to material such as steel02 or reinforcing steel. The material requires six user-defined stress strain input parameters; yield strength of steel (±Fy), yield strain (±epsY), post-yield maximum stress (±Fy1), post-yield maximum strain (±epsY1), ultimate stress (±Fu) and ultimate strain (±epsU) along with five material degradation related parameters, which require calibration; stress and strain points for pinch effect (pinch x & y), damage based on displacement/ cyclic loading (damage1), damage based on energy (damage2) and the degraded unloading stiffness for hysteretic material (betaMUsteel).

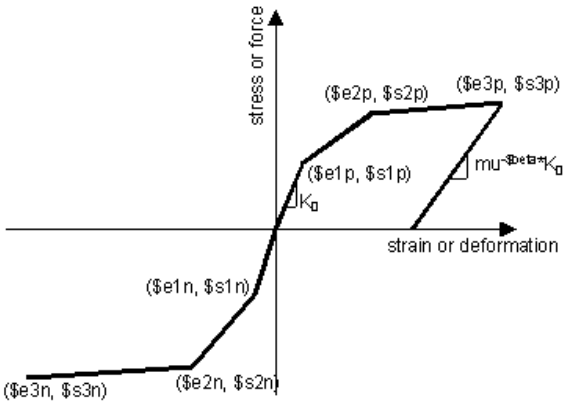

Figure 3.5. Backbone Curve for Hysteretic Material Model (OpenSees, 2007)
Note: All negative stress-strain values to be used with a (-) sign

3.3.2. The Constitutive Model

Model development is discussed in following subcategories; general layout of the constitutive reinforced concrete column, column section details, analysis step and loading and simulation recorders.

3.3.2.1. General Layout

Constitutive reinforced concrete column was modeled as a frame element connected by two nodes (two-dimensional), characterizing an idealized single bridge column structure. Frame element is essentially a straight line connecting two points (in this case two nodes) to which section properties such as confined concrete, cover concrete and reinforcements can be added (OpenSees, 2007). Element internal forces are produced at the element ends, where recorders are placed. Node 1 representing the column foundation is fixed in lateral, vertical and rotational directions for fixed-base analysis. Node 2 carrying the superstructure (characterized by an equivalent lumped mass in lateral, vertical and rotational directions), was connected to node 1 by a single force-based beam-column element characterizing a massless reinforced concrete column section (figure 3.6). This element type is based on force formulation and considers the spread of plasticity along the element (OpenSees, 2007) and is capable of tracing highly non-linear

behavior of reinforced concrete members under cyclic load combinations of bending moment and axial forces (Spacone et al., 1996).

3.3.2.2. Column Section Detail

The study of nonlinear behavior of the structure (column element) is an essential part of this research. Therefore, the development of a reinforced concrete column with the ability to accurately exhibit such behavior is pivotal. The column section properties were developed using "section" command available in OpenSees with the use of concrete02 and hysteretic material models. Fiber sections consisting of a core-concrete patch, a cover-concrete patch and reinforcement layer was integrated to the force-based beam-column element to determine the resultant force-deformation response. The core-concrete parameters, which are calculated based on the Mander's theory of confined-concrete model (Mander et al., 1988), offsets the need for providing confining reinforcements along the column (Opensees, 2007). Therefore, the only reinforcements provided in the column are the longitudinal reinforcements.

The confined-concrete, or rather core-concrete patch, expands from center to reinforcement layer and the unconfined-concrete, or rather cover-concrete patch expands from reinforcement layer to the outer edge. The section was discretized as the core-concrete patch in to 8 radial and tangential sections and the cover-concrete patch in to 4 radial and 8 tangential sections. This was because more numerical accuracy was demanded from the core-concrete patch rather than the cover-concrete patch. The reinforcements were evenly laid out in a concentric circle along the interface of core and cover concrete patches. A detailed cross-section of the column is indicated in Figure 3.6. Three integration points with section properties along the force-based beam-column element was created considering both the accuracy and calculation efficiency. Additionally, geometric linear transformation was assigned to include P-Δ effect in to

the column due to anticipated excessive displacement. This would enable the model to assume additional moments created during large displacements.

3.3.2.3. OpenSees Analysis Step for Static Lateral Pushover, Lateral Cyclic Loading and Dynamic Loading

For all simulations, gravity was as applied as a static constant vertical load prior to any other load inputs. Simulation load inputs for gravity, static pushover test and lateral cyclic loading test were applied at node 2 (superstructure) using Plain Pattern command while dynamic loading was applied at node 1 (footing) using Uniform Excitation Pattern command available in OpenSees. Simulation Analysis objects are the tools employed to analyze the system. In OpenSees analysis object is composed of several components which define the type of analysis and how it is executed. For static pushover test and lateral cyclic loading test, following analysis steps were constructed.

- *Plain constraints*; which is used for enforcing homogeneous single-point constraints such as fixed boundary conditions (OpenSees, 2007).
- *Plain numberer*; which provides mapping between degrees-of-freedom (DOF) to nodes based on how nodes are stored in the domain. A default method is employed by OpenSees to order equations when using this command and is recommended for small problems when Sparse solvers are used (OpenSees, 2007).
- *Sparse General* system; is used in order to construct a linear system of equations and linear solver objects to solve the system of equations using a sparse matrix system (Demmel et al., 1999).

- *Newton* algorithm; is used to construct a solution algorithm, which uses a Newton-Raphson method to solve non-linear equations. It is considered a rapidly converging method provided that the initial estimation is sufficiently close to the solution (OpenSess, 2007).
- *Norm Displacement Increment*; is the convergence test that is required to determine if the convergence has been achieved at the end of an iteration step. The convergence test is applied as follows where K is the stiffness matrix, ΔU is the displacement increment and R is the unbalanced force.

$$K\Delta U = R \tag{12}$$

  The positive force convergence is tested if the 2-norm of the ΔU vector in the linear system of equations is less than tolerance (OpenSees, 2007). In OpenSees, tolerance and the maximum number of iterations have to be specified by the user.
- *Static Analysis*; for static loads and time varying loads, which are less than one-third of the natural frequency of the structure (in the case of static lateral pushover and lateral cyclic loading), this method is used for solving the static response of the system without the effects of damping matrix(OpenSees, 2007).
- *Displacement Control* integrator; was used for the static analysis to construct a static integrator object. Displacement-controlled method was chosen due to its increased accuracy of the input method over the load-control method.

For dynamic loading, Newton algorithm and Plain constraints along with the following analysis steps were employed;

- *UmfPack General* system; which uses a UmfPack solver to construct a general sparse system of equations (OpenSees, 2007).

- *RCM numberer*; which uses a reverse Cuthill-McKee algorithm (Cuthill & McKee, 1969) to number the DOF. This algorithm has the capability to optimize node numbering to reduce bandwidth (OpensSees, 2007).
- *Energy Increment*; is the convergence test that constructs a test where positive force convergence is tested if one half of the product of ΔU and R vectors in the linear system of equations is less than specified tolerance (OpenSees, 2007).
- *Variable Transient* analysis; is used when the input loading function is an arbitrary time dependent function. In OpenSees, the transient response analysis is based on direct integration of the system equations and is proposed for systems with small time steps and potential convergence problems (OpenSees, 2007).
- *Newmark* integrator; this integrator is used with transient analysis object preferably for large scale linear analysis and assumes classical Newmark method (Newmark, 1959). Newmark integrator schemes employs the following equations;

$$D'_{t+\Delta t} = D'_t + [(1-\gamma)D''_t + \gamma_{t+\Delta t}D"]\Delta t \quad (13)$$

$$D_{t+\Delta t} = D_t + D'_t\Delta t + \left[\left(\frac{1}{2}-\beta\right)D"_t + \beta D"_{t+\Delta t}\right]\Delta t^2 \quad (14)$$

In which, D, D' and D'' are displacement, velocity and acceleration vectors of the finite element assembly, while β and γ are parameters for controlling the accuracy and stability of the results. Newmark proposed the values γ = 0.5 and β = 0.25 to provide unconditionally stable scheme (Newmark, 1959) and is suggested by OpenSees as a user-input parameters (OpenSees, 2007).

In dynamic analysis, the generalized form of solution can be indicated by equation 15. The time dependent response of all structural nodes is a relationship between inertial forces that

can be presented as a product of mass and acceleration and damping forces that can be presented as a product of damping coefficient and velocity.

$$[M]\{D''\} + [C]\{D'\} + [K]\{D\} = \{F\} \quad (15)$$

Where, [M] represents the structure mass matrix, {D''} is the nodal acceleration vector, [C] is the structural damping matrix, {D'} is the nodal velocity vector, [K] is the structural stiffness matrix, {D} is nodal displacement vector and [F] is the applied time dependent loading vector. In OpenSees, proportional damping [C] is considered in the following form (equation 16) and the 'Rayleigh' command is used for assigning damping to all elements and nodes, which is specified as a combination of stiffness and mass-proportional damping matrices.

$$[C] = \alpha[M] + \beta[K] \quad (16)$$

$$C = \alpha M.M + \beta K.K_{current} + \beta K_{initial}.K_{initial} + \beta K_{comm}.K_{lastcomm} \quad (17)$$

β and α are constants to be determined by damping ratios for two modes of vibrations, with αM as the mass proportional Rayleigh damping parameter, M as the mass matrix used for calculating Rayleigh damping, βK as the stiffness proportional damping parameter, $K_{current}$ as the stiffness matrix at current state determination used to calculate Rayleigh damping, $\beta K_{initial}$ as the initial stiffness proportional damping parameter, $K_{initial}$ as the stiffness matrix as initial state determination used for Rayleigh damping calculations, βK_{comm} as the committed stiffness proportional damping and $K_{lastcomm}$ as the stiffness matrix at last committed state determination used to calculate Rayleigh damping (OpenSees, 2007).

3.3.2.4. Recorders

Recorders were assigned to both nodes and column element of the model. While the nodes recorded displacement, rotation, and acceleration information the element recorded axial force, shear force and bending moment information.

3.4. Constitutive Model Calibration for Fixed-Base Analysis

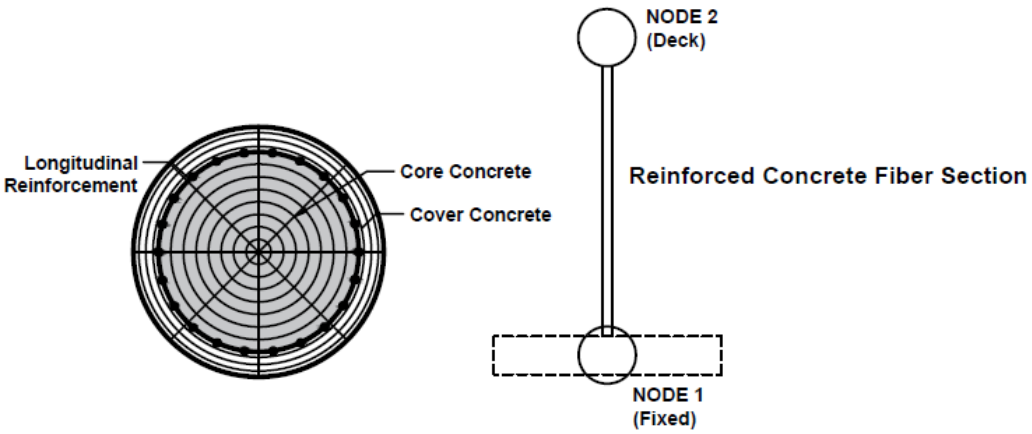

Figure 3.6. Reinforced Fiber Section and a Side Elevation of the Constitutive RC Column Model
Note: Node 1 is fixed in vertical, lateral and rotation directions only for fixed-base analysis

3.4.1. Test Specimens and Model Input Parameters

Input parameters of concrete02 and hysteretic material models are represented in table 3.1. Concrete02 input values were obtained from both physical properties of the specimens and as recommended by the OpenSees (OpenSees, 2007). Hysteretic material input values were obtained from a combination of physical properties of the material and by back-calculation of stress-strain results. The degradation parameters used in hysteretic material model were acquired through the comparison of the degradation behavior of well-confined concrete bridge columns. The constrained induced behavior (controlled lateral movement) of the well-confined concrete bridge column study made it ideal for calibrating material degradation parameters and to observe overall accuracy of the constitutive reinforced concrete column model without the effects of damping due to free vibration. For the purpose of this study, the degradation parameters were calibrated for a circular bridge column with a column aspect ratio between 4 to 10, reinforcement ratio of 1.5% and an axial load (structural weight) less than 0.2fc'Ag; where fc' is the compressive strength of concrete and Ag is the gross cross-sectional area of the column.

Three test specimens (specimen number 415, 815 and 1015) were chosen for the purpose of calibration (Lehman & Moehle, 2000). These specimens consisted of identical cross-sections in terms of column diameter, reinforcement ratio and reinforcement formation. Also, all specimens carried identical axial loads. However, specimen column heights varied from 2.44 m to 6.1 m giving a column aspect ratio range of 4 to 10. This range of different aspect ratios of the same structure was expected to provide a more comprehensive basis for calibrating material parameters with better accuracy. Physical characteristics of the test specimen are summarized in the table 3.2.

Table 3.1

Material Model Input

Concrete02 Parameters	Input Value	Hysteretic Material	Input Value
Confined		fy (Mpa)	±580
fpc (Mpa)	43	epsy	±0.003
epsc0	0.003	fy1 (Mpa)	±850
fpcu (Mpa)	34	epsy1	±0.1
epscu	0.015	fu (Mpa)	±700
ft (Mpa)	4.3	epsu	±0.2
Unconfined		pinchx	1
fpc (Mpa)	34	pinchy	1
epsc0	0.0026	damage1	0
fpcu (Mpa)	3.5	damage2	0.3
epscu	0.006	betaMUsteel	0
ft (Mpa)	3.5		
lambda	0.1		
Ets (Gpa)	2.7		

The three computational models 415N, 815N and 1015N (where, N stands for “numerical model”) were constructed for the purpose of calibration. These models consisted of the same constitutive reinforced concrete column section as described in “The Constitutive Model” and

were physically identical to their test specimen counterparts 415, 815 and 1015. Similar to the experiments, a lateral displacement was exerted at the top node to simulate the input loading.

Table 3.2

Test Specimen Characteristics

Column	Height (m)	Diameter (m)	Concrete/ Reinforcement	Deck Mass (Kg)	Aspect Ratio
415/ 415N	2.44	0.61	1.50%	$6.70x10^4$	4
815/ 815N	4.88	0.61	1.50%	$6.70x10^4$	8
1015/ 1015N	6.1	0.61	1.50%	$6.70x10^4$	10

The maximum displacements induced at top of each column (ductility values) were calculated using the effective yield displacement method presented in Priestley (1996). More details related to the calculation of ductility values are available at Lehman & Moehle (2000). Table 3.3 presents a summary of all maximum displacements experienced by the computational models.

Table 3.3

Expected Maximum Displacement at each Level

Displacement Level	Column 415 (mm)	Column 815 (mm)	Column 1015 (mm)
1Δy	25.4	88.9	127.0
1.5Δy	38.1	133.3	190.5
2Δy	50.8	177.8	254.0
3Δy	76.2	266.7	381.0
5Δy	127.0	444.5	635.0
7Δy	177.8		

3.4.2. Static Push Results

A displacement controlled static push was applied to 415N, 815N and 1015N for column moment capacity comparison purpose against the test specimens 415, 815 and 1015. All three models were subjected to a 10% lateral drift (compared to column height) at node 2. Then model push test results were plotted against experimental data for moment-curvature comparison. Based on figure 3.7, it can be seen that the effective column flexural rigidity (EI); where E is the combined elastic modulus of concrete and reinforcing steel and I is the moment of inertia (FEMA 356, 2000), of all three computational models compare quite well to the experimental results at first yield. Furthermore, all computational models appear to follow the same moment-curvature response regardless of the column height, which theoretically establishes the accuracy of the column behavior as the nominal moment capacity is a function of the cross sectional properties of the column. The anticipated nominal column capacity for test specimens 415, 815 and 1015 ranges between approximately 6300 to 6000 Kip-in (Lehman & Moehle, 2000), which is captured well by the computational models. However, the computational models indicate gradual capacity degradation upon reaching the moment capacity, which is not observed in the experimental specimens 415 and 815 and appears beyond 0.002/in. curvature in specimen 1015. It can be assumed this subtle difference could be due to the absence of confining reinforcements in the numerical models, which improves shear strength (even though confinement effects are assimilated in to confine concrete material) and the degradation behavior of the reinforced concrete column under flexural loading . Despite the subtle differences observed in the experimental results for 415 and 815, it can be concluded that 415N, 815N and 1015N is capable of accurately predicting flexural behavior of a reinforced concrete column under static lateral

load. The reduction in the moment capacity of test specimen 1015 is observed by Lehman & Moehle (2000), but does not provide an explanation.

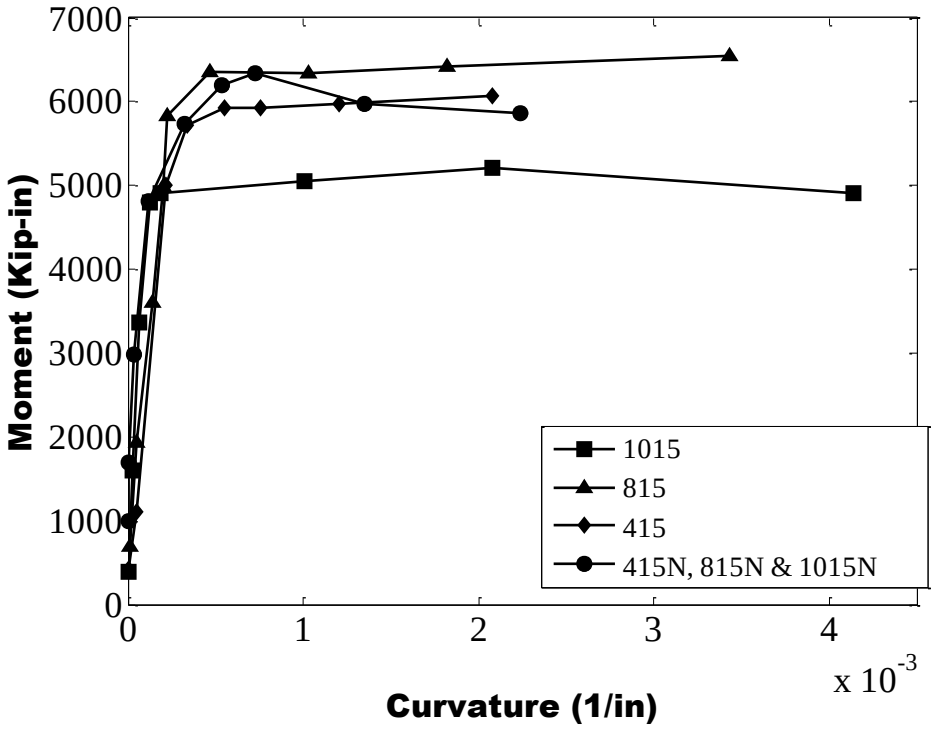

Figure 3.7. Monotonic Static Push Test Comparison for Fixed-Base Column

3.4.3. Cyclic Loading Results

One of most important aspects of this study is to investigate the nonlinear behavior of soil-footing-structure system incorporating a realistic idealized bridge column with an under-designed shallow foundation (compared to current design practice), which is allowed to rock. In order to exhibit realistic modern bridge column behavior under seismic loading, concrete02 and hysteric material models should be capable of capturing the accurate material nonlinear behavior as well as material degradation under cyclic loading. To reproduce the experimental behavior in numerical simulations, a range of numerical tests were conducted using different combinations of damage parameters for the hysteretic material model. Figure 3.8 presents comparison of force-

displacement results between test specimens and computational models in terms of maximum shear force, maximum lateral displacement, column stiffness and general ductile behavior.

The cyclic loading tests for the computational models were conducted in a same manner to the static push tests with lateral loading being applied at superstructure level (node 2). In general, it can be concluded that the computational models were able to capture the force-displacement behavior of 415, 815 and 1015 with considerable accuracy. The lateral displacements of the models in each cycle matched the experimental results along with peak shear force confirming the accuracy of the load input method and column construction. Capacity reduction was evident with increased amplitude for all simulations, indicating material degradation characteristics. However, the models appear to consistently underestimate the amount of degradation as seen from AR4, AR8 and AR10 towards the last two cycles. Subsequently the amount of energy dissipated due to inelastic behavior of the column can expected to be slightly reduced as well. The hysteretic material model damage parameter was calibrated to be only energy sensitive (damage2) as indicated in table 3.1. Although in actuality material degradation is a result of both ductility and energy, it was observed during calibration that it is difficult to manipulate both damage parameters simultaneously in order to obtain the desired results. Therefore, it was decided that the best approach would be to make the constitutive model sensitive to dissipated energy rather than ductility or a combination of both.

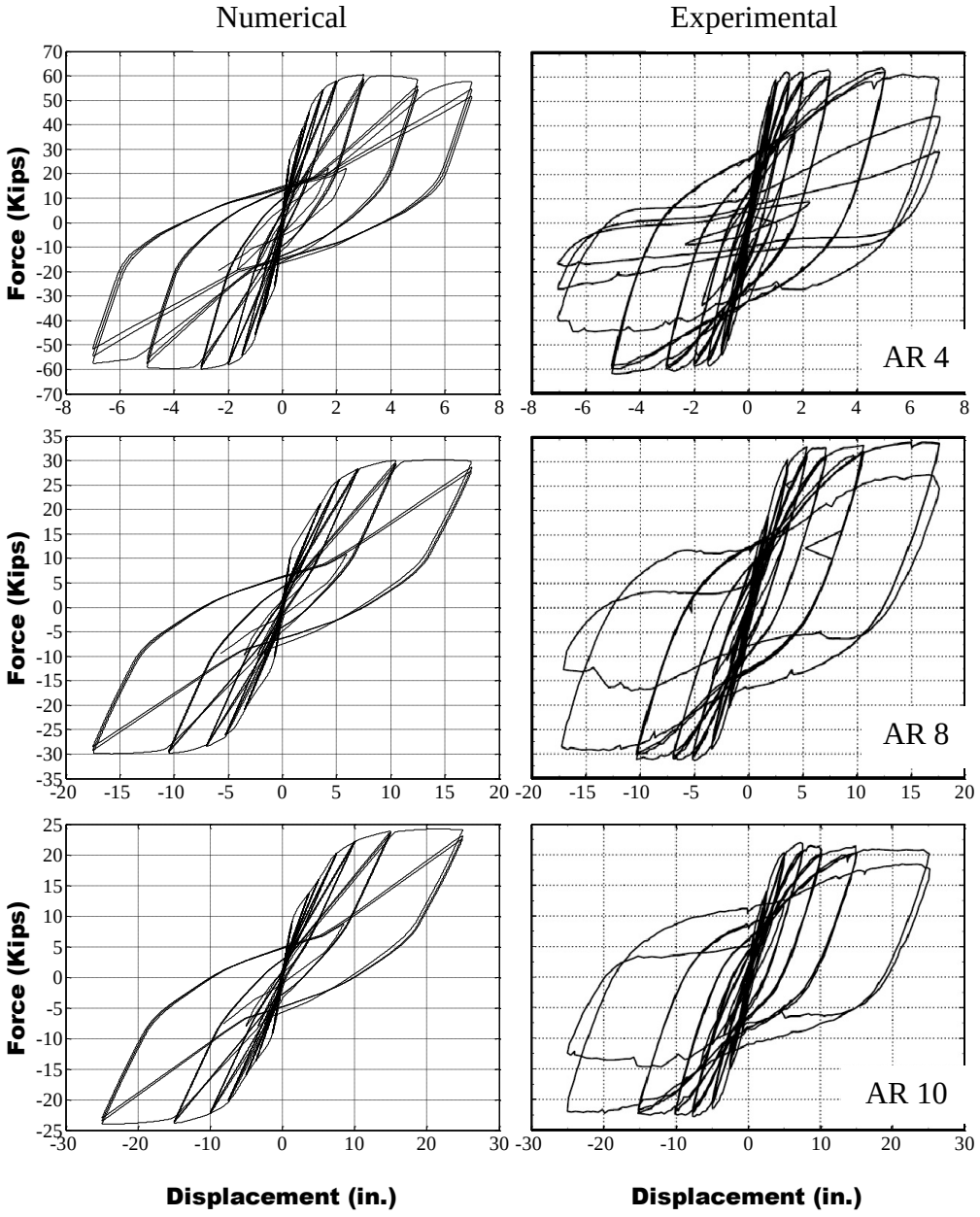

Figure 3.8. Comparison of Numerical Simulation Lateral Force-Displacement Results with Experimental Results (Experimental Results after, Lehman & Moehle, 2000)
Note: Column aspect ratio (AR) 4, 8 & 10 compared

4. THE BRIDGE-PIER MODEL

4.1. Introduction

This chapter details the development of the proposed Bridge-pier model that is to be used for the study of a typical conventional bridge column behavior during foundation rocking. The Bridge-pier model, which is design in accordance with Caltrans Seismic Design Criteria, uses the calibrated constitutive reinforced concrete column from the previous chapter as its platform. The completed model is then compared with the seismic performance of a full-scale single bridge-column for validation.

4.2. Full-Scale Bridge-Column Experiment

In order to investigate the dynamic response of a full-scale bridge-column for predetermined lateral displacement demands, Schoettler et al., (2015) conducted a series of shake table tests on a full-scale reinforced concrete bridge column that was designed according to Caltrans Seismic Design Criteria (Clatrans, 2004) and Bridge Design Specifications (California Department of Transportation, 2016). The reinforced concrete column characterizing a common single bridge pier consisted of a footing anchored to the shake table constraining movement in lateral, vertical and rotational directions. The reinforced concrete column consisted of 18, 35.8 mm diameter longitudinal reinforcements concentrically spaced around the column in a single layer. Column height from top of footing to the center of superstructure was 7.32 m and column diameter 1.22 m, creating a column aspect ratio of 6. The concrete to reinforcement ratio was 1.55% as specified by the design criteria with an axial load of 2.53 MN to produce axial load ratio (axial load/ Ag fc') of 5.3%, where Ag is the gross cross-sectional area of the column and fc' is the compressive strength of concrete. Schematic of the experimental structure is depicted in figure 4.1.

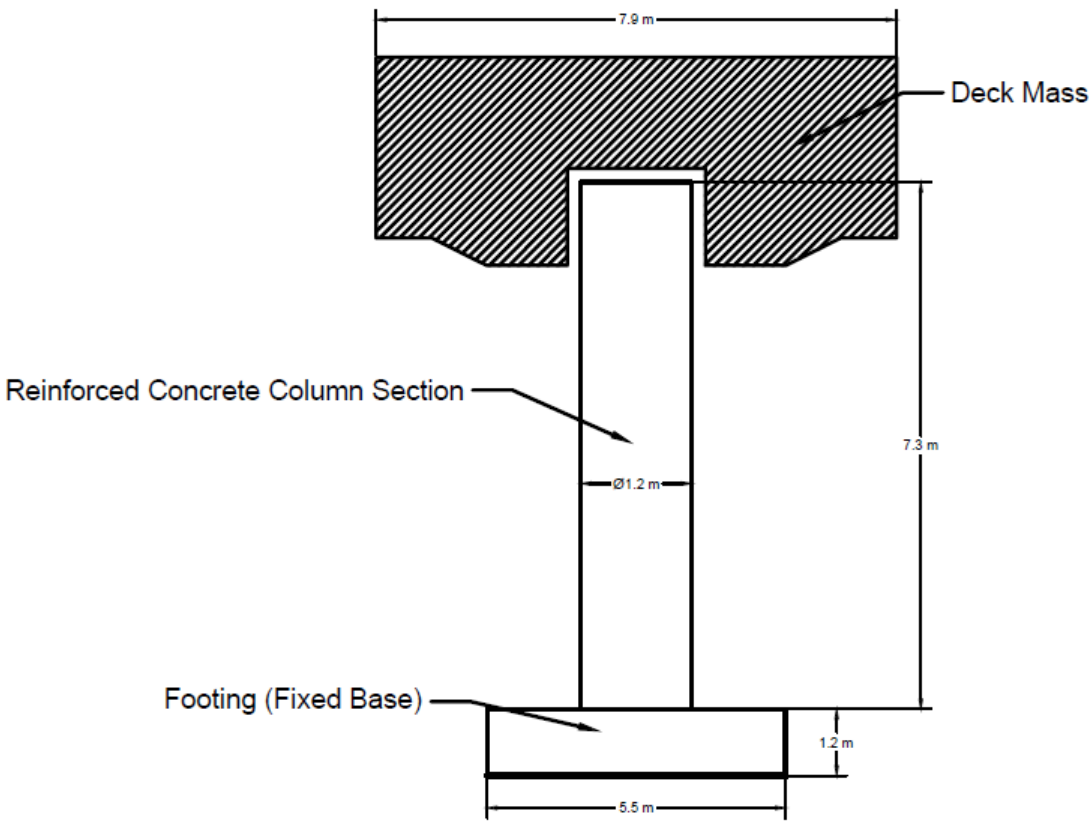

Figure 4.1. Full-Scale Bridge Column Test Setup (after, Schoettler et al., 2015)

The full-scale bridge-column experiment, which was the first to be design according to US seismic provisions, providing comprehensive performance evaluation of a modern single-column capacity-based design (Schoettler, et al., 2015). These evaluations included superstructure (bridge deck assembly) displacement response, column moment-rotation response and column shear force-displacement response under seismic inputs designed to gradually push the bridge column into nonlinear range.

4.3. Bridge-Pier Model Validation

Using the calibrated constitutive reinforced concrete column model as a platform, the Bridge-pier model was constructed based on the Schoettler's experimental work. This numerical model, which represents an idealized simplistic bridge pier, was constructed to maintain similar design properties to the full-scale bridge-column experiment.

4.3.1. Bridge-Pier Model Characteristics and Input Parameters

A cross-section detail and an elevation view of the Bridge-pier column model are indicated in figure 4.2. Input values of core concrete, cover concrete and longitudinal reinforcements are provided in table 4.1. Similar to the calibration phase, concrete02 input values were obtained from both physical properties of the specimens and as recommended by the OpenSees (OpenSees, 2007). For the hysteretic material, ASTM A706 grade 80 reinforcing steel was used to achieve the necessary yield and ultimate moment capacity as indicated in test protocol (Schoettler et al., 2015). The input values for the reinforcing material stress-strain behavior was selected as discussed in research report RD-15-15 (California Department of Transportation, 2015), while previously calibrated values were used for the degradation properties.

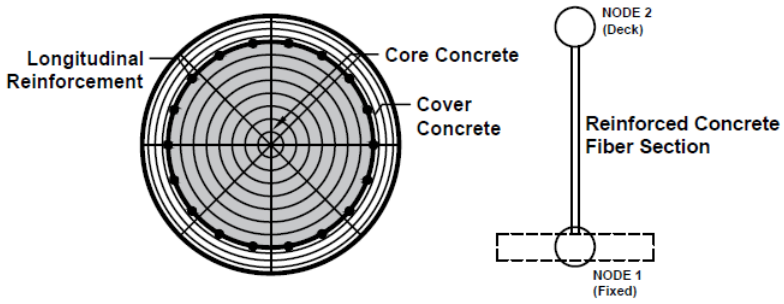

Figure 4.2. Reinforced Fiber Section and a Side Elevation of the Bridge-Pier Model for Fixed-Base Analysis

Table 4.1

Bridge Pier Model Input Parameters

Concrete02 Parameters	Input Value	Hysteretic Material	Input Value
Confined		fy (Mpa)	±710
fpc (Mpa)	53	epsy	±0.004
epsc0	0.003	fy1 (Mpa)	±800
fpcu (Mpa)	42	epsy1	±0.04
epscu	0.015	fu (Mpa)	±690
ft (Mpa)	5.3	epsu	±0.122
Unconfined		pinchx	1
fpc (Mpa)	42	pinchy	1
epsc0	0.0026	damage1	0
fpcu (Mpa)	4.2	damage2	0.3
epscu	0.006	betaMUsteel	0
ft (Mpa)	4.2		
lambda	0.1		
Ets (Gpa)	3		

As discussed before, the constitutive reinforced concrete column model served as the platform for the development of the Bridge-pier model. Details regarding the material models, general layout, column section details and analysis step for dynamic loading for the Bridge-pier model can be referenced in “Construction of the Reinforced Concrete Column”. Column height was modified to 7.9 m from top of footing to the assumed center of the deck mass, while column diameter was kept at1.22 m. only longitudinal reinforcements consisting of concentrically spaced18, 35.8 mm diameter rebar were considered. Node 1 was constrained in lateral, vertical and rotational directions for fixed-base analyses, while node 2 (deck node) was kept free from constrains. A structural mass of 260 Mg was applied in lateral, vertical and rotational directions to simulate structural loading, while the footing and column was considered massless in comparison. Prior to dynamic loading, the self-weight of the structure was applied at node 2 as

gravitational force. After gravity load, acceleration time histories were applied at node 1 to simulate the base shake shaking loading applied in the experiments. A uniform damping ratio of 5% for calculating Rayleigh damping coefficients was used. Based on the material properties provided in the experiment, an approximate elastic bending stiffness (K) for the reinforced concrete column was calculated using equation (18) for comparison purposes; Where, E denotes the equivalent elastic modulus for concrete and steel with I representing the moment of inertia for the column cross section and L representing the length of the column.

$$K = \frac{3EI}{L^3} \tag{18}$$

The full-scale bridge column bending stiffness was calculated to be approximately 28 MN/m using the idealized yield moment and curvature provided by Schoettler et al., (2015). The Bridge-pier model column bending stiffness of approximately 23 MN/m was calculated using the input parameters presented in table 4.1 and the Bridge-pier model physical characteristics discussed in "Development and Validation". OpenSees measured the elastic period for the Bridge-pier model as 0.78 s compared to the anticipated elastic period range of 0.7 – 1.2 s for the full-scale bridge column (Guerrini et al, 2011). The yield moment capacity of the Bridge-pier model was observed to be 5000 KNm, while the ultimate moment was observed to be 6330 KNm. Actual yield moment and ultimate moment values were not available from the full-scale bridge column experiment for comparison. However, according to the idealized monotonic response of the analytical model, a yield moment of 5790 KNm and an ultimate moment of 6280 KNm was anticipated (Schoettler et al., 2015). The details of the said analytical model were not provided in the study. For comparison purposes, a theoretical moment capacity based on the physical characteristics and the material properties of the full-scale bridge column was calculated

as well, the calculation results indicated a theoretical moment capacity of approximately 6300 KNm for the column.

4.3.2. Excitation Input

Among the four historical earthquake recordings (from four different stations) selected for bridge pier model validation, three motions were selected from the 1989 Loma Prieta earthquake. With peak ground acceleration (PGA) values ranging from 0.16g to 0.61g; these motions were expected to gradually push the model behavior from elastic to nonlinear plastic range. The 1995 Kobe earthquake was chosen as the fourth recording, which exceeds design limits of this structure (and model) and is expected to develop significant nonlinear plastic behavior. Table 4.2 presents the details of the selected ground motions, which were obtained from the Pacific Earthquake Research Engineering (PEER) Ground Motion database.

Table 4.2

Summary of Ground Motions

Test	Earthquake	Station	Component	Scale Factor	PGA* (g)	Duration (sec)
EQ1	Loma Prieta	Agnew	090	1.0	0.16	60
EQ2	Loma Prieta	Corralitos	090	1.0	0.48	40
EQ3	Loma Prieta	LGPC	000	1.0	0.57	25
EQ5	Kobe	Takatori	000	-0.8	0.49	41
EQ7	Kobe	Takatori	000	1.0	0.61	41

Note: *PGA - Peak Ground Acceleration

4.3.3. Bridge-Pier Model Performance

Figure 4.3 presents lateral force-displacement behavior of both numerical simulations and experiments while structure is initially within elastic range and then reaching the moment capacity. In figure 4.4, lateral force-displacement behavior for both numerical simulations and experiments are presented when pushed to nonlinear inelastic range.

The numerical simulation results for EQ1 and EQ2 show good comparison to experimental results in terms of peak base shear, maximum lateral displacement and column flexural rigidity (EI). Both Bridge-pier model and full-scale bridge column indicate slightly nonlinear behavior in EQ2 with increased ductility demand. With the results for elastic range behavior in good agreement, validation comparisons were extended to inelastic behavior to further evaluate the accuracy of the model.

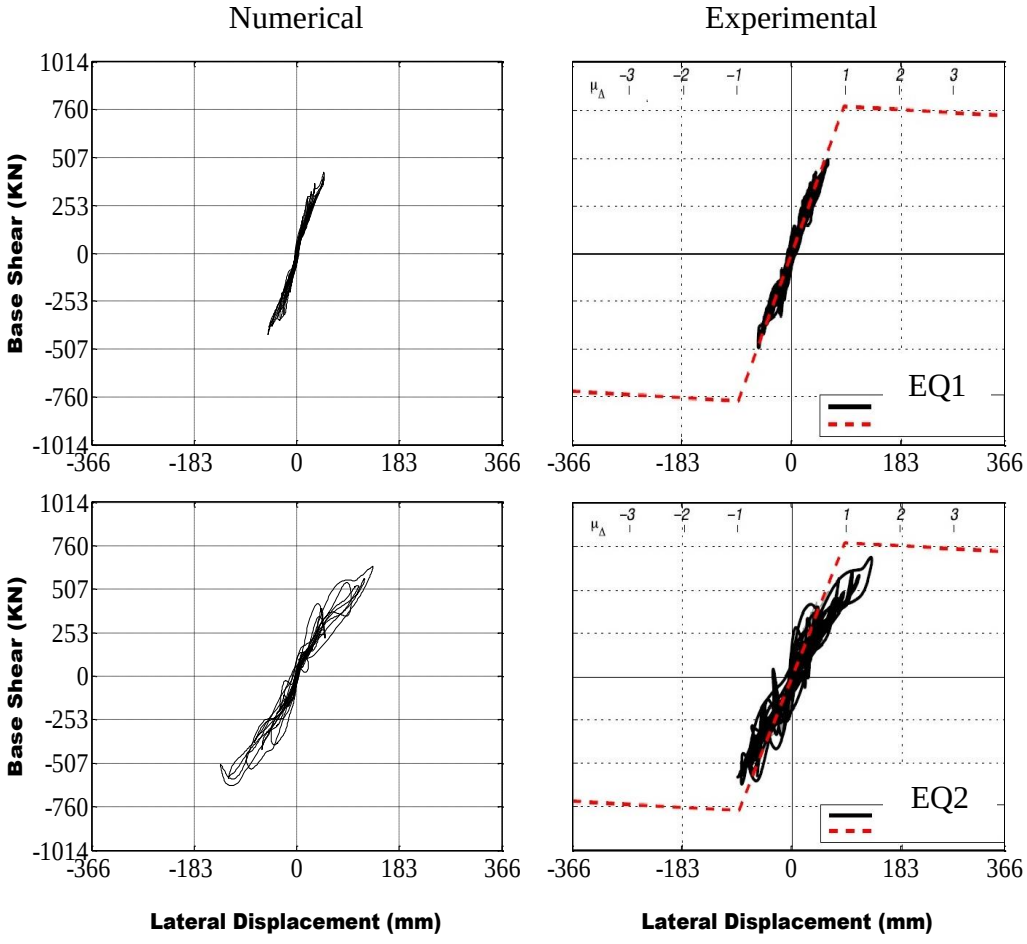

Figure 4.3. Experimental and Simulation Comparison for EQ1 & EQ2 (Experimental Results after, Schoettler et al., 2015)

For simulations EQ3, EQ5 and EQ7 the results generally indicate considerable similarities in terms of base shear, lateral displacement and overall degradation behavior. Base shear forces are in good comparison with the experimental results with slight over predictions in negative direction for EQ5 and in positive direction for EQ7. The Bridge-pier model's ability to capture the nonlinear behavior and the consequent material degradation of the structure is quite apparent from the results as well, which further establishes the model accuracy. The large hysteretic loops of both experimental results and numerical simulations are indicative of the capacity design's tendency towards dissipating energy through column yield. Apart from the minor deviations, it can be concluded that the simulation and experimental results are in good agreement.

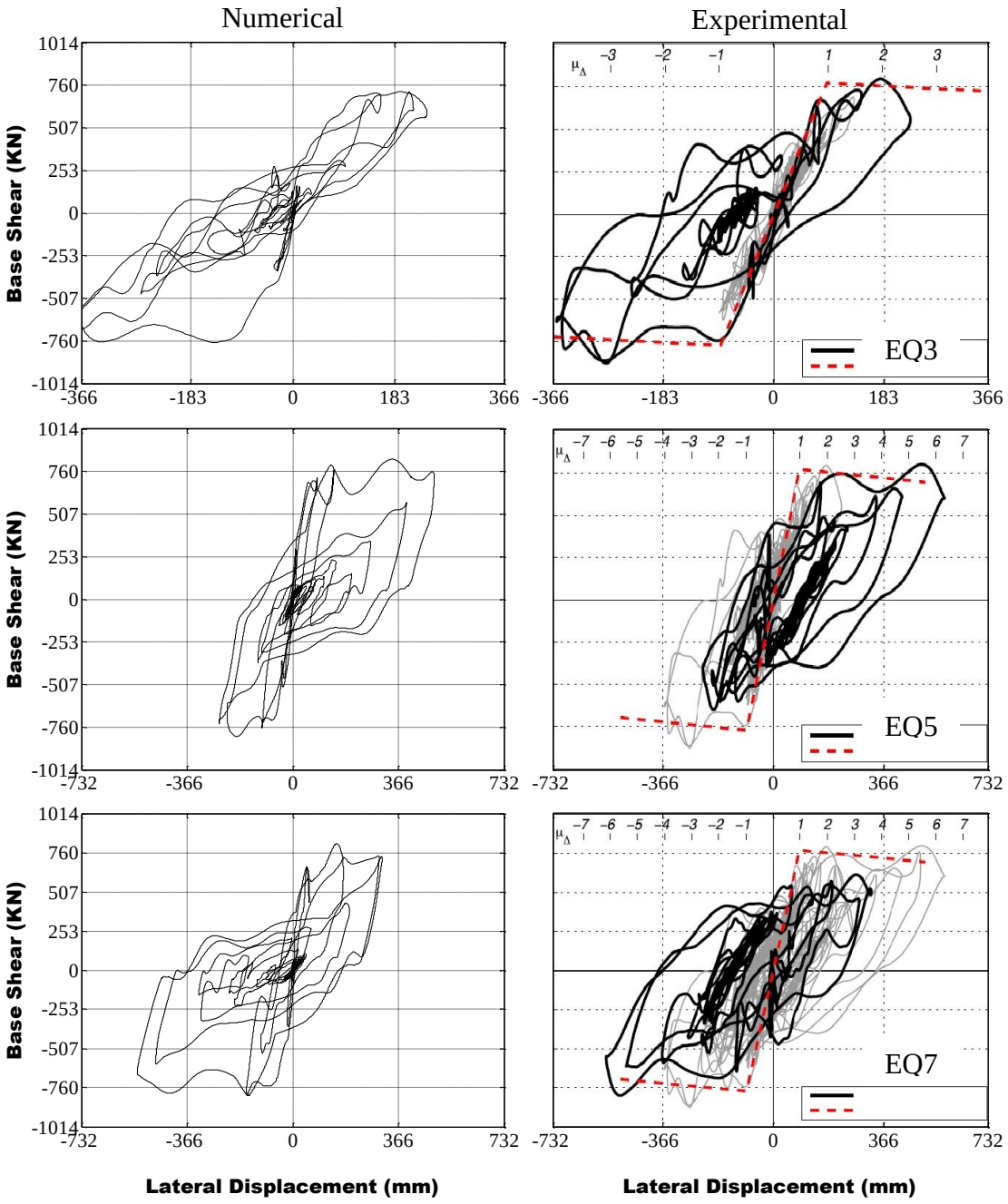

Figure 4.4. Experimental and Simulation Comparison for EQ3, EQ5 & EQ7 (Experimental Results after, Schoettler et al., 2015)

5. DYNAMIC ANALYSIS

5.1. Introduction

The essence of this study is to further the understanding of the complex nonlinear coupling behavior between soil and structure during the rocking motion of a shallow foundation.in this study, this is achieved through evaluation of soil-structure system moment-rotation behavior, foundation settlement-rotation response and system energy dissipation characteristics. In the previous chapters, the conception of an idealized yet realistic bridge column (Bridge-pier model) that agrees to the specified standards set forth by a regulatory agency (Caltrans) is discussed as part of this evaluation. In this chapter, the above-mentioned computational model is combined with a soil-foundation interaction model as presented in figure 5.1 to evaluate the nonlinear behavior of both soil and structure during seismic loading. A brief discussion about the soil-foundation interaction model and input parameters are also provided. Furthermore, the experimental method for this study is also introduced.

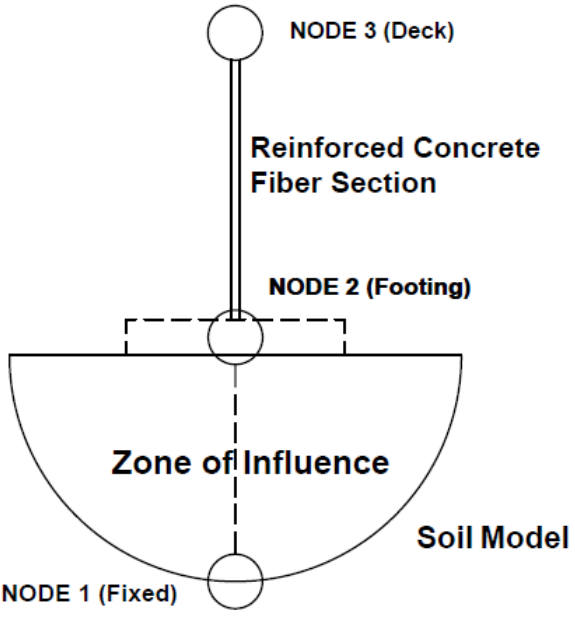

Figure 5.1. Rocking Foundation Assembly Combining the Bridge-Pier Model with the Nonlinear Soil Model (CIM)

5.2. Dynamic Excitations

Two historic ground motions were selected for this analysis; a medium intensity Kalamata motion (Greece 1986) and a relatively stronger intensity Takatori motion (Kobe 1995), characterized by a large number of significant cycles (Anastasopoulos et al., 2010). Using different scale factors for Kalamata (figure 5.1a) and Takatori (figure 5.1b) ground motions, six different input acceleration-time histories were created. The simulations and their assigned ground motion can be referenced from Appendix A. The input ground motions were obtained from the Pacific Earthquake Research Engineering (PEER) Ground Motion database. A summary of all input ground motions are presented in table 5.1.

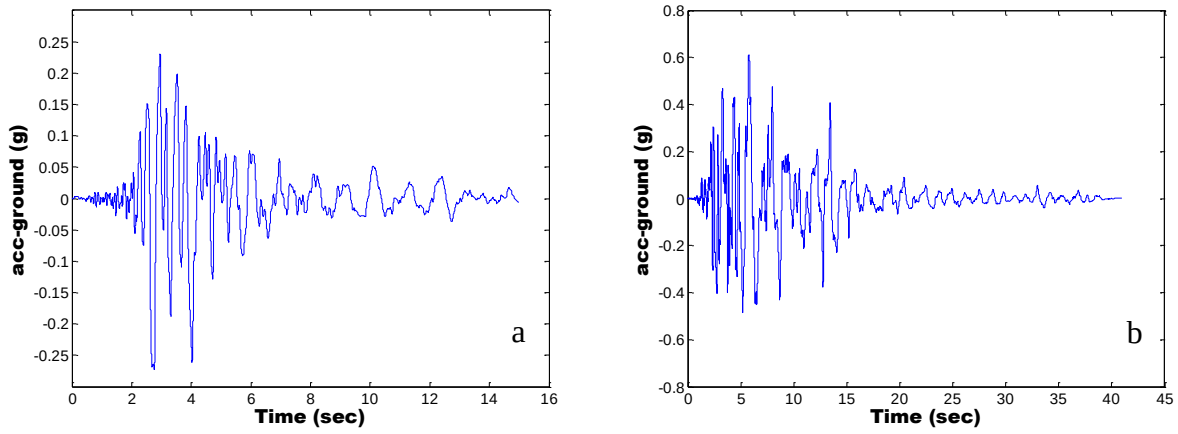

Figure 5.2. Input Excitations; Acceleration-Time Histories of (a) Takatori (b) Kalamata at Scale Factor 1.0

Table 5.1

Summary of Input Excitations

Earthquake	Component	Scale Factor	PGA (g)	PGD* (m)	Duration (sec)
Kalamata	N/A	1.0	0.271	0.054	15
Kalamata	N/A	1.5	0.406	0.081	15
Kalamata	N/A	2.0	0.542	0.107	15
Kalamata	N/A	3.0	0.813	0.161	15
Takatori	000	0.5	0.305	0.179	30
Takatori	000	0.8	0.489	0.286	30

Note: *PGD - Peak Ground Displacement

The acceleration response spectrum and the displacement response spectrum for original Kalamata and Takatori ground motions are presented in figure 5.3. According to the acceleration spectrum, structures within the natural period of 1 to 1.5 sec are expected to experience considerably high acceleration demands for Takatori motion. Whereas for Kalamata, increased accelerations are expected between natural periods of 0.1 and 0.9 sec. Based on the displacement response spectrum, the structure are anticipated to experience considerably increased displacements from 1.0 sec for Takatori motion, whereas for Kalamata the increased displacement is insignificant for the entire range. The spectrum was developed for an assumed damping ratio of 5%. Table 5.2 summarizes the ranges of natural periods (Tn) for all fixed-base and rocking foundation simulations as calculated by OpenSees.

Table 5.2

Natural Periods for Fixed-Base and Rocking Foundation Simulations

Structure Type	Tn (sec)
Fixed-Base	0.43 - 1.43*
Rocking Foundation	0.53 - 1.60

Note: *The analytical Tn for fixed-base AR 6.5 was calculated to be 0.67 sec

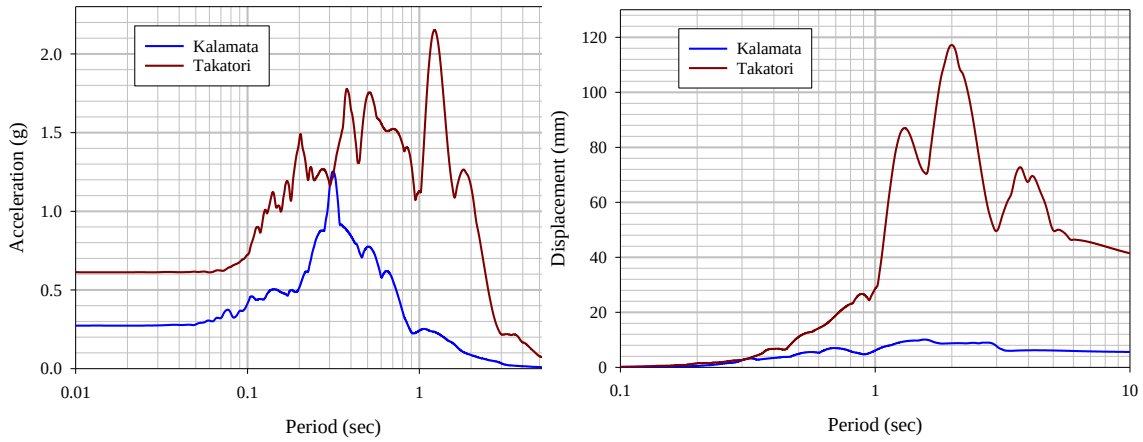

Figure 5.3. Acceleration and Displacement Reponses Spectra

5.3. Contact Interface Model

To study the rocking footing characteristics of a shallow foundation, the contact interface model (CIM) was chosen as the preferred soil model. Developed for OpenSees to provide nonlinear constitutive relations between cyclic loads and displacements of the footing-soil system during combined vertical, shear and moment loads, the model depicts rocking characteristics by tracking the geometry of the soil surface beneath the rigid footing and the kinematics of the footing-soil system (Gajan & Kutter, 2009).

In this research, the primary objective is the study of soil-structure interaction under dynamic loading. Therefore accurately capturing the permanent deformation, load capacities, stiffness degradation and energy dissipation of soil is quite important. Although the beam on nonlinear winkler foundation (BNWF) model has been used in previous experiments to model soil behavior (e.g. Allotey & Nagger, 2003; Harden & Hutchinson, 2005), the advantage of CIM over BNWF is its ability to couple moment, shear and vertical load capacities (Gajan et al., 2008). The coupling between the vertical and moment capacities results from the formation of the gap. The gap is formed between the footing and underlying soil while rocking is mobilized. Typically the moment capacity is reached upon the formation of the gap which causes the

vertical capacity to drop. The bounding surface proposed by Cremer et al. (2001) was adopted to include the coupling between moment, vertical and shear loads (M-V-H). This coupling is evaluated based on the diagram in figure 5.5. However, for our research purposes we would neglect the M-H coupling as the idealized bridge-column structure is purposefully designed for mobilizing rocking behavior over sliding.

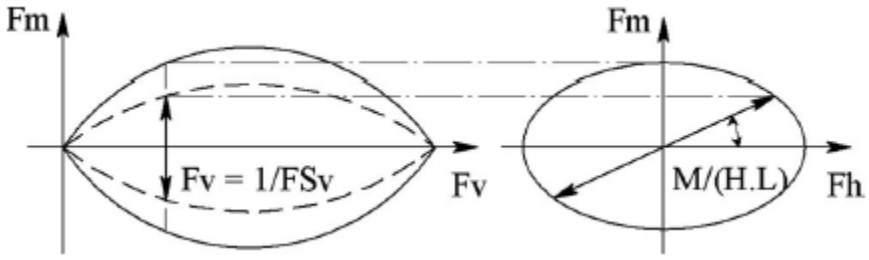

Figure 5.4. Constant Vertical and Moment to Shear Ratio Load Path and Bounding Surface in Normalized V-H-M Space (Gajan & Kutter, 2009)

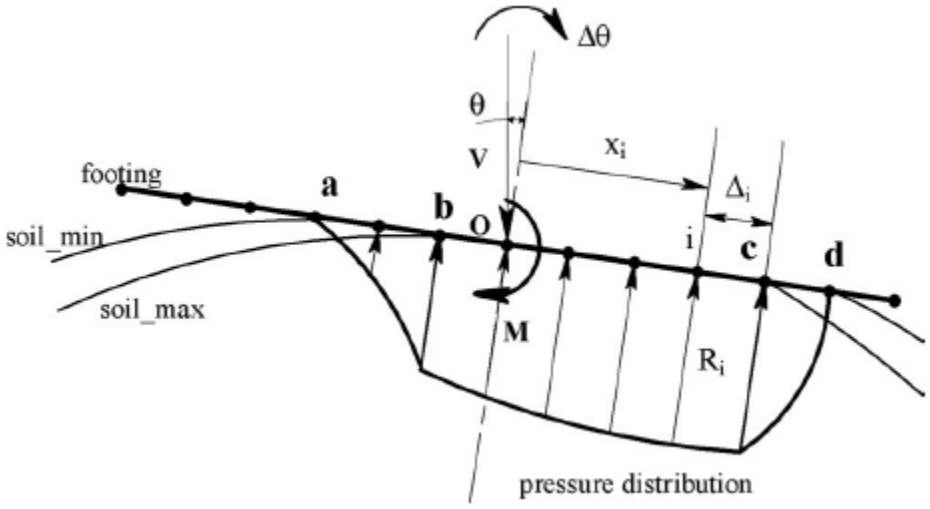

Figure 5.5. Pressure Distribution during the Rocking Behavior as Captured by CIM (Gajan & Kutter, 2009)

The rocking movement can be visualized as a moving contact problem, with the contact are moving from one side to the other with opening and closing gaps behind and in front of the

contact area (Gajan et al., 2009). The moment-rotation-settlement behavior of the soil-footing system is modelled by tracking the changing geometry and using reasonable assumptions about the bearing pressure distribution as indicated in figure 5.5 (Gajan et al., 2008). Identifying the ultimate moment of a given soil-footing system is an important factor for rocking foundations. The CIM model uses critical area concept to predict the ultimate moment. As the magnitude of rotation increases, the contact area would decrease while increasing the bearing pressure. However, once the bearing pressure becomes equal to the ultimate bearing resistance, no further reduction in contact area is possible (Gajan & Kutter, 2009). This minimal contact area is defined as the critical contact area Ac and moment obtain at that critical contact area is considered as the ultimate moment (M_{ult}) of the soil-footing system. This relationship between Ac, FS and M_{ult} is expressed in equations 4 and 1. However, this relationship ignores the passive resistance and side frictional resistance between footing sides and soil interface. Nevertheless, according to Gajan & Kutter (2008) for shallow embedment (embedment depth less than the height of footing) the relative error in predicted ultimate moment due to this negligence is up to about 5%.

The user defined input parameters used by CIM are indicated below. This section briefly describes how these values could be calculated using fundamental geotechnical engineering parameters and relationships.

- Ultimate vertical load (V_{ult}); corresponds to the ultimate bearing capacity of the soil. This value can be calculated using Meyerhof's bearing capacity formula (Das, 2011).
- Static vertical factor of safety (FS); is calculated using the ratio between V_{ult} and allowable bearing pressure. Together with V_{ult}, this allows the user to incorporate effects of footing embedment, footing shapes and soil surcharge.

- Footing width (L); denotes the linear dimension of the footing in the plane of rocking.
- Initial vertical and horizontal stiffness (K_v & K_h); are the elastic vertical stiffness and elastic horizontal stiffness of the foundation when footing is in full contact for pure vertical and shear loading (Gajan & Kutter, 2009). This value is determined by the procedure described in FEMA 356.

In this study, following equations were used for calculating V_{ult} and FS parameters. The shape factors and depth factors were calculated using relationships developed by DeBeer and Hansen (Das, 2011).

$$V_{ult} = \gamma D_f N_q F_{qd} F_{qs} + \frac{1}{2}\gamma B N_\gamma 0.6 \tag{19}$$

$$N_q = \left(\tan\left(45 + \frac{\phi'}{2}\right)\right)^2 e^{\pi \tan \phi'} \tag{20}$$

$$N_\gamma = 2\left(N_q + 1\right)\tan \phi' \tag{21}$$

$$F_{qd} = 1 + 2tan\phi'^{(1-sin\phi')^2}\left(\frac{D_f}{L}\right) \tag{22}$$

$$F_{qs} = 1 + tan\phi' \tag{23}$$

The depth of footing embedment is D_f, effective angle of friction in soil is ϕ' and unit weight of soil is γ. V_{total} is considered as the allowable bearing pressure applied by the structure.

$$FS = \frac{V_{ult}}{V_{total}} \tag{24}$$

The Initial soil modulus (G) is calculated using the following relationship as proposed by FEMA 356, where $(N_1)_{60}$ is normalized standard penetration test (SPT) blow counts and σ' is effective vertical stress (in psf) calculated at B/2 depth (B as defined in chapter 2);

$$G = 20{,}000\ (N_{1\,60})^{\frac{1}{3}}\sqrt{\sigma'} \tag{25}$$

Once *G* is calculated, K_h and K_v for foundations at surface was calculated by the equations below.

$$K_h = \left(\frac{GB}{2-\upsilon}\right)\left[3.4\left(\frac{L}{B}\right)^{0.65} + 1.2\right] \tag{26}$$

$$K_v = \left(\frac{GB}{1-\upsilon}\right)\left[1.55\left(\frac{L}{B}\right)^{0.75} + 0.8\right] \tag{27}$$

For embedded footings, the following modification factors were used;

$$\beta_h = \left(1 + 0.21\sqrt{\frac{D_f}{B}}\right)\left(1 + 1.6\left(\frac{hd(B+L)}{BL^2}\right)^{0.4}\right) \tag{28}$$

$$\beta_v = \left(1 + \frac{D}{21B}\left(2 + 2.6\frac{B}{L}\right)\right)\left(1 + 0.32\left(\frac{d(B+L)}{BL}\right)^{\frac{2}{3}}\right) \tag{29}$$

The K_h and K_v for embedded foundation could be calculated using the following relationship.

$$K_{h\ embed} = \beta_h K_h \tag{30}$$

$$K_{v\ embed} = \beta_v K_v \tag{31}$$

L is denoted as the footing length (for square footings, L equal to B) and h & d are taken as heights of sidewall contacts between footing and soil assumed to be $D_f/2$ for this application due to shallow embedment depths.

- Soil rebound ratio (Rv); is an empirical parameter to account for the elastic rebound and bulging of soil during rocking motion. Typical values of 0.1 – 0.12 (10% - 12%) was used for all simulations.
- Footing node spacing (deltaL); specifies the distance between the footing nodes internally created by the model. Typical range of 0.01 to 0.005 was used as suggested by the Gajan et al., (2008) and Gajan & Kutter (2009).

Gajan et al., (2008), validated results from CIM with previous shear wall experimental data presented in (Gajan 2005) and concluded that CIM has the ability to capture moment capacity and the degradation of rotational stiffness quite well. Additionally, the accuracy of permanent settlement per cycle between the experiential data and simulations along with the similar shape of settlement-rotation curves were also observed (Gajan et al., 2008). However, in its current implementation, radiation damping does not appear to be significant when rocking is fully mobilized due to the dominance of hysteretic damping (Gajan et al., 2008).

5.3.1. Soil Characteristics of CIM

The soil characteristics used for calculating the user-defined input parameters for CIM was assumed to be a dry clean sand consisting of a dry unit weight ranging from 16 to 19 KN/m^3 with a friction angle ranging from 32 to 38 degrees, that represented soil improvement effects in order to investigate the characteristics of rocking behavior. A Poisson ration of 0.3 was assumed for all calculations. An $(N_1)_{60}$ range of 15 to 50 SPT blow counts were assumed for G calculations. For G, a range of 56 – 115 MPa was calculated using equation 25 and soil characteristics mentioned above to be used for calculating K_v and K_h. The other user-defined CIM input parameters were calculated using the methods described in "contact interface model".

5.4. Fixed-Base and Rocking Foundation Setup

Two column heights were introduced in addition to 7.9 m, consisting of 5 m and 12 m (column aspect ratios of 4 and 10 respectively) to evaluate the effects of column aspect ratio (AR) on the Bridge-pier model nonlinear behavior . The column diameter remained at 1.22 m for all heights with column sections consisting of 18, 35.8 mm diameter longitudinal reinforcements concentrically spaced around the column in a single layer. The structural mass of 260 Mg remained applied in lateral, vertical and rotational directions to simulate structural loading (deck

assembly), while the column was considered massless in comparison. A uniform damping ratio of 5% for calculating Rayleigh damping coefficients was used. Prior to dynamic loading, the self-weight of the structure was applied at deck node as gravitational force.

Fixed-base approach was considered for the conventional capacity design simulations, which were to be compared with the performance of the rocking foundation design. This can be considered as a reasonable assumption as the foundation moment capacity for conventional capacity design bridge columns is much larger in comparison to the column moment capacity. For rocking foundation design simulations, a massless rigid square footing with footing width ranging from 3.5 to 6.5 m was considered. Furthermore, footing embedment of 0 (non-embedded), 1 and 1.5 m was used for evaluating the effects on rocking foundation behavior. The completed rocking foundation computational model consisting of the Bridge-pier model and CIM is presented in figure 5.1. The footing was connected to the nonlinear soil-foundation model using a ZeroLengthSection element to represent the soil-footing interface and the soil beneath the footing in the zone of influence to which CIM properties were added. Node 1, which was constrained in lateral, vertical and rotation movements represented the boundary condition at nonlinear soil-foundation model (CIM), while node 2 and node 3 represented the shallow Bridge-pier model footing and the deck assembly. In this study, in order to focus primarily on rocking behavior, the footing was constrained against lateral displacement allowing only vertical displacement and rotation. This is a reasonable assumption for higher aspect ratio structures-foundation systems (ratio between height to the center of gravity of the structure and length of the footing in the direction of rocking) where rocking behavior is dominant and sliding response is negligible when compared to rocking induced rotations (Gajan & Kutter, 2009). Acceleration-time histories of the excitations were applied at the fixed-base node (node 1) for fixed-base

simulations, while for rocking foundations, the acceleration-time histories were applied at the fixed node (node 1) within the nonlinear soil-foundation model.

5.5. Performance Parameters

In order to evaluate the seismic response of these structures properly, key performance parameters are introduced. These performance parameters are aimed at recognizing quantitatively, the beneficial and detrimental effects of column yielding versus soil yielding.

For fixed-base simulations (conventional capacity design), the primary performance parameters consisted of peak and permanent deck drift, peak structural acceleration, column base moment and shear force and structural rotation. The peak and permanent deck drift was defined as the maximum lateral displacement during the excitation and the residual displacement after the excitation experienced by the bridge deck respectively as measured by node 2 (figure 4.2). The maximum lateral acceleration recorded by node 2 was taken as the peak structural acceleration experienced by the bridge deck. Structural rotation for fixed-base simulations was considered as the flexural rotation experienced by the bridge column as recorded by deck node (node 2). The moment loads experienced by the bridge column during the excitation were plotted against structural rotation to evaluate the material degradation behavior and the resulting energy dissipation. The energy dissipation was calculated using the area enclosed by the moment–rotation plot. Foundation rotation was assumed negligible for fixed base simulations since in conventional capacity design typically deep foundations are provided for bridge pier design, which increases the foundation moment capacity significantly compared to the column moment capacity.

For rocking foundation simulations, the primary performance parameters consisted of peak and permanent deck drift, peak structural acceleration, column base moment and shear

forces, foundation moment, footing rotation θ_{found}, structural flexural rotation θ_{str} and foundation settlement. The peak structural acceleration was defined identically to the fixed-base simulation. Similar to fixed-base, the peak and permanent deck drift was considered as the maximum lateral displacement during the excitation and the residual displacement after the excitation experienced by the bridge deck respectively. All peak/ maximum and residual/permanent performance values rocking foundations were calculated based on equations 32 to 34, where θ_{total} is the total rotation of the soil-foundation system as measured by node 2 (figure 5.1), Δ_{str} is the lateral displacement of structure due to flexural rotation during rocking behavior, Δ_{total} and Δ_{rigid} are the lateral displacements of soil-structure system and due to rotation of the foundation respectively and H_g is the height of the bridge column.

$$\theta_{str} = \theta_{total} - \theta_{found} \tag{32}$$

$$\Delta_{rigid} = \theta_{found} . H_g \tag{33}$$

$$\Delta_{str} = \Delta_{total} - \Delta_{rigid} \tag{34}$$

$$\frac{\Delta_{str}}{H_g} = Drift\ ratio \tag{35}$$

The deck drift ratio for both fixed-base and rocking foundations is considered as the structural lateral displacement normalized by H_g (equation 35). For rocking foundation analysis, θ_{str} was measured as the difference between total rotation of the system measured at node 3 and the foundation rotation measured at node 2 (figure 5.1). Footing rotation was recorded at the rigid footing by node 2 during rocking behavior along with foundation settlement. The moment loads experienced by the bridge column and the foundation during the excitation were plotted against structural and footing rotation to evaluate the material degradation behavior and the resulting energy dissipation characteristics. Similar to fixed-base evaluation, the energy dissipation was calculated using the area enclosed by the moment–rotation plots.

6. FIXED-BASE PERFORMANCE OF THE BRIDGE-PIER MODEL

6.1. Introduction

The purpose of fixed-base performance analysis of the Bridge-pier model is to achieve a comprehensive knowledge about the modern reinforced bridge column behavior under seismic loads. The fixed-base behavior simulates the conventional deep foundation design, which is commonly adapted in modern bridge design. One of the main limitations of this design approach is the likelihood of failure of the bridge column due to yielding and subsequent fracturing of the confining reinforcements after significant deformation (California Department of Transportation, 2006). In this chapter, results from fixed-base Bridge-pier model simulations using different ground motions and three column aspect ratio (AR) are analyzed.

6.2. Excitation Sensitivity

Figure 6.1 and 6.2 presents the Bridge-pier model's column moment-rotation behavior and the column lateral displacement (deck drift) comparison for Kalamata and Takatori ground motions. The identical columns presented here consist of AR 6.5. In figure 6.1, the structural performance is indicated with increased scale factors of Kalamata (1.5, 2.0 and 3.0) ground motion to observe the nonlinear behavior with increased peak ground acceleration of 0.4g, 0.54g and 0.8g (respectively).

The increased moment-rotation behavior with increased ductility demands on the structure can be readily observed from the moment-rotation plot. For Kalamata1.5, the column behavior is within linear elastic range with maximum moment of 5300 KNm at 0.02 rad and a peak deck drift of 103 mm. Kalamata2.0 indicated slightly higher maximum moment of 6200 KNm at 0.03 rad with an increased peak deck drift of 177 mm. The tendency to dissipate energy through column yield is apparent at this stage with noticeable hysteretic loops in the moment-

rotation behavior. However, for Kalamata3.0 the column displayed obvious nonlinear plastic behavior with indications of column stiffness degradation. Maximum moment of 6700 KNm, which is higher than the theoretical moment capacity of the column with a maximum column rotation of 0.05 rad and a peak deck drift of 320 mm was observed.

In figure 6.2, the moment-rotation and lateral displacement behavior of the same structure is presented for Takatori0.8, where the peak ground acceleration experienced by the structure is about 0.49g. Considerable nonlinear plastic behavior of the structure coupled with serious material degradation is visible for this excitation, although the peak ground acceleration is less than Kalamata2.0 and Kalamata3.0. A maximum column moment of 6900 KNm is achieved at a structural rotation of 0.08 rad resulting in a substantial peak deck drift of 540 mm. Column stiffness degradation combined with considerable yield behavior is evident of the capacity design approach coupled with large amounts of energy dissipation.

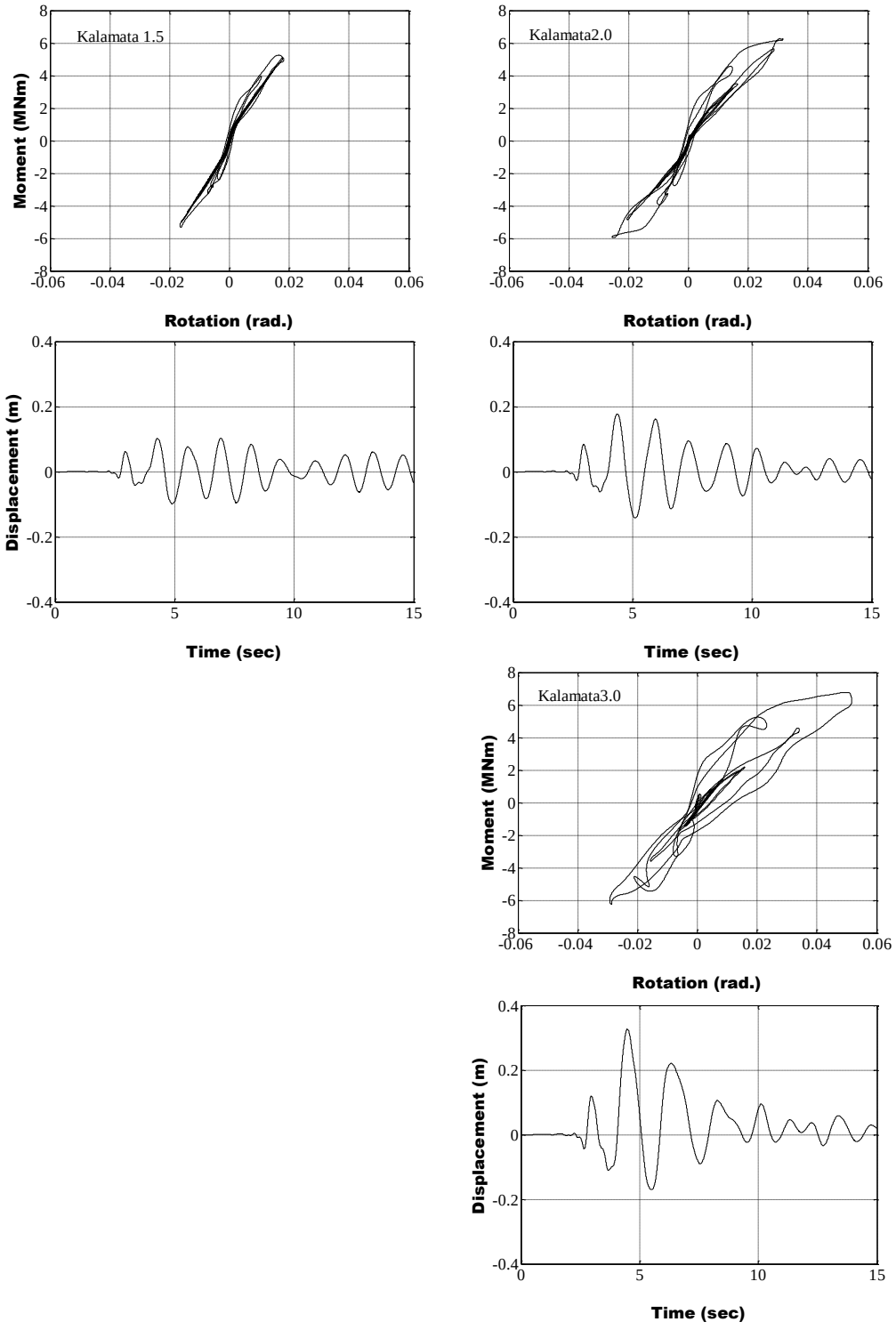

Figure 6.1. Fixed-Base Performance for Kalamata Ground Motion (Scale Factor 1.5, 2.0 & 3.0)

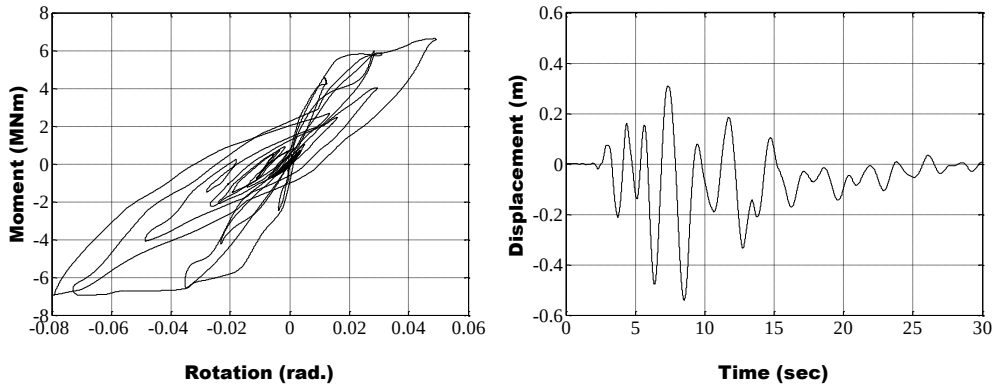

Figure 6.2. Fixed-Base Performance for Takatori Ground Motion (Scale Factor 0.8)

The peak structural acceleration experienced by the Bridge-pier model for the above simulations ranged from 0.25g for Kalamata1.5 to 0.3g for both Kalamata3.0 and Takatori0.8. However, despite difference of 0.05g in peak structural accelerations Takatori0.8 excitation induced approximately 220 mm additional lateral displacement demands at the peak on the bridge column compared to Kalamata3.0. This observation combined with large amounts of energy dissipation could be attributed to the nature of Takatori ground motion, where considerable amount of strong acceleration cycles are present relative to Kalamata and the natural period of the AR 6.5 structure. Although permanent deck drifts were not observed for the above simulations, peak deck drift ratios (peak deck drift compared to column height) ranging from 1% to 6.8% was observed during excitations.

Based on the observations of the full-scale bridge-column (that has similar characteristics to this column) experiments, permanent damages in form of spalling of concrete cover and significant development of cracking at the base of the column when reaching a peak drift ratio of 4.9% was observed by Schoettler et al., (2015). Therefore, it could be assumed that an actual bridge column designed according to current Caltrans seismic design criteria may experience detrimental damages for stronger excitations such as Takatori0.8.

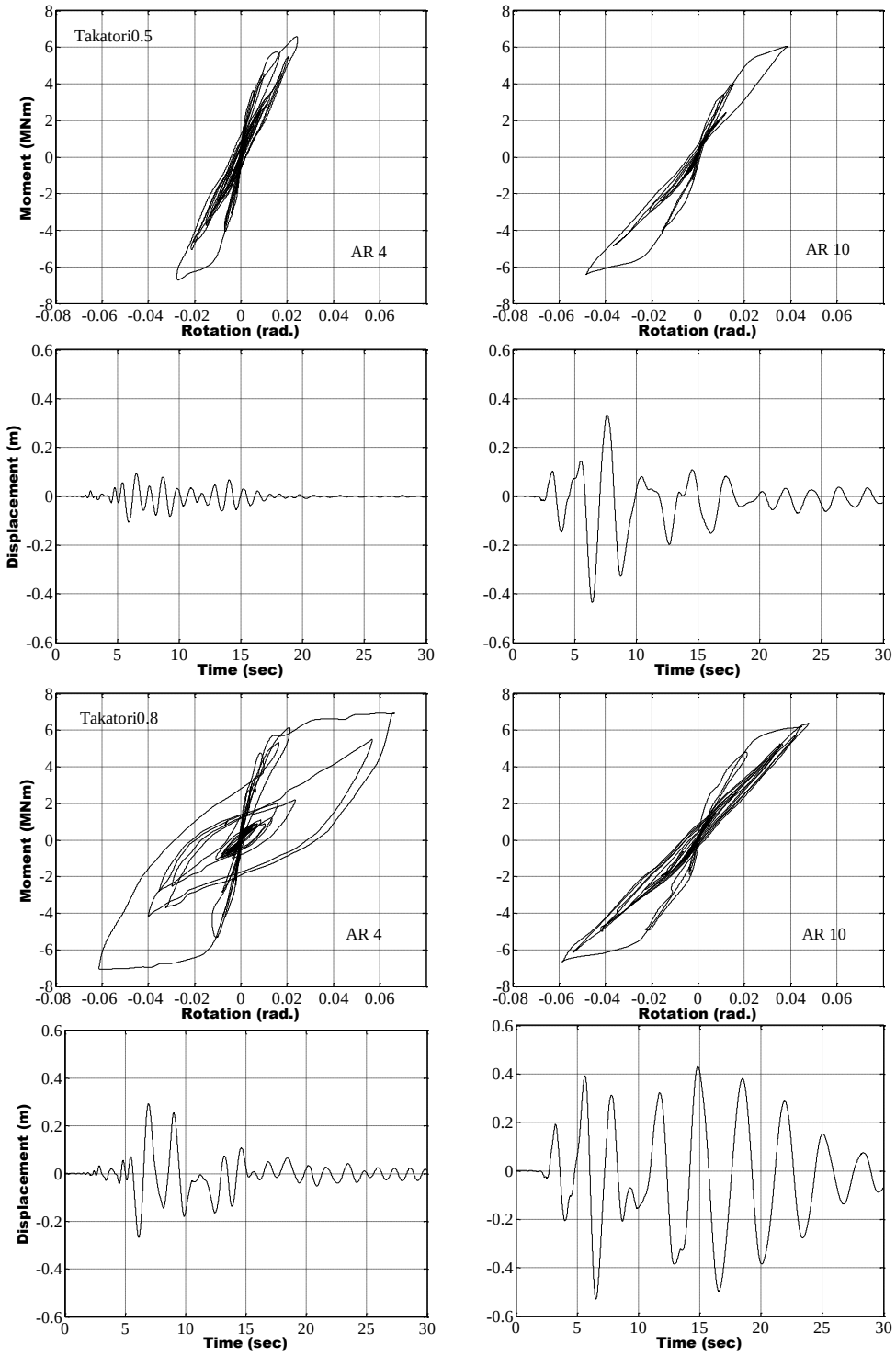

Figure 6.3. Effects of Column Aspect Ratio for Fixed-Base Simulations

6.3. Effects of Column Aspect Ratio

In figure 6.3, columns with AR 4 and AR 10 are compared with Takatori0.5 and Takatori0.8 excitations. With reduced column height for AR4 the natural elastic period of the structure was decreased to 0.43 s, while with increased column height for AR10 the natural elastic period was increased to 1.43 s. The moment-rotation and displacement-time plots are employed to evaluate the influence of natural period on the behavior of bridge-pier model.

For Takatori0.5, both structures reach the theoretical column moment capacity with peak deck drift ratios of 2% and 3.6% for AR4 and AR10 respectively. Some nonlinear behavior is indicated from both structures with minimal plastic deformation. Peak structural accelerations of 0.49g and 0.17g are experienced by the shorter and taller structure (respectively), indicating acceleration amplification by the shorter column. Furthermore, the shorter structure exhibit excessive plastic deformation while considerably exceeding the theoretical column moment capacity accompanied by a peak deck drift ratio of 5.8%. Acceleration amplification is also noted as the peak structural acceleration reached 0.53g, which was the highest of all simulations. In contrast, the taller structure achieved a peak deck drift ratio of 4.4%, with a slight increase in the column moment. Some plastic deformation was observed in the column behavior. interestingly, unlike other fixed-base simulations, the bridge column repeatedly reached higher deck drift as observed from the displacement-time plot. However, considerable material degradation due to this behavior is not observed.

6.4. Performance Summary

The fixed-base behavior of the Bridge-pier model confirms the conventional column capacity design philosophy, which is used in modern bridge column design. Based on the simulation performance, it can be concluded that the current Caltrans design seismic criteria is a

reasonable approach for intermediate ground motions recordings such as Kalamata (Greece 1986), Agnew (Loma Prieta 1989) and Corralitos (Loma Prieta 1989). However, for stronger ground motions recordings such as Takatori (Kobe 1995) and LGPC (Loma Prieta 1989) the structure is likely to undergo considerable deformations and as observed by Schoettler et al., (2015), column damage resulting in a permanent deck drift.

The use of column AR to evaluate the sensitivity of the natural elastic period in modern bridge column design to ground motions shed light on the importance of the incorporation of acceleration and displacement response spectra. From the simulations, it can be concluded that the structure was quite sensitive to Takatori excitation in general compared to Kalamata. Particularly, between AR 4 to 6.5, where the natural period was recorded as 0.43 s and 0.78 s, the structure generally indicated considerable nonlinear behavior accompanied by material degradation and considerable energy dissipation.

7. SHALLOW ROCKING FOUNDATION PERFORMANCE OF THE BRIDGE-PIER MODEL

7.1. Introduction

The rocking foundation philosophy intends to remove the plastic deformation from the reinforced concrete column to the foundation by intentionally under-designing the foundation and thereby subsequently leaving the superstructure undamaged. In this section, the performance of rocking foundation design is evaluated based on excitation intensity, soil characteristics, effects of footing embedment and energy dissipation characteristics.

7.2. Fixed-Base and Rocking Foundation Design Performance Comparison

Figure 7.1 compares the response for conventional and rocking foundation design between two identical full-scale bridge columns with a column height of 7.9 m and AR 6.5 subjected to Takatori0.5 ground motion. The moment-rotation plot for the fixed-base simulation tracks the column base moment against flexural rotation of the of the column, while the Moment-rotation plot for the rocking foundation tracks the column base moment against the flexural rotation of the column and the foundation moment against the footing rotation. Additionally, the settlement-rotation behavior of the foundation is also presented for rocking foundation, while base shear forces of the column is plotted against the lateral displacement (deck drift).

The conventional (fixed-base) design indicates highly nonlinear behavior and structural yielding as characterized by both large hysteretic loops exceeding the theoretical moment capacity and the sudden reduction in rotation stiffness. As shown by the base shear-lateral displacement plot, the structure reaches a maximum column base shear of 760 KN with a peak deck drift of 370 mm resulting a peak drift ratio of 4.6%. The peak acceleration experienced by

the structure is recorded as 0.3g indicating almost 99% acceleration transformations from ground to the structure.

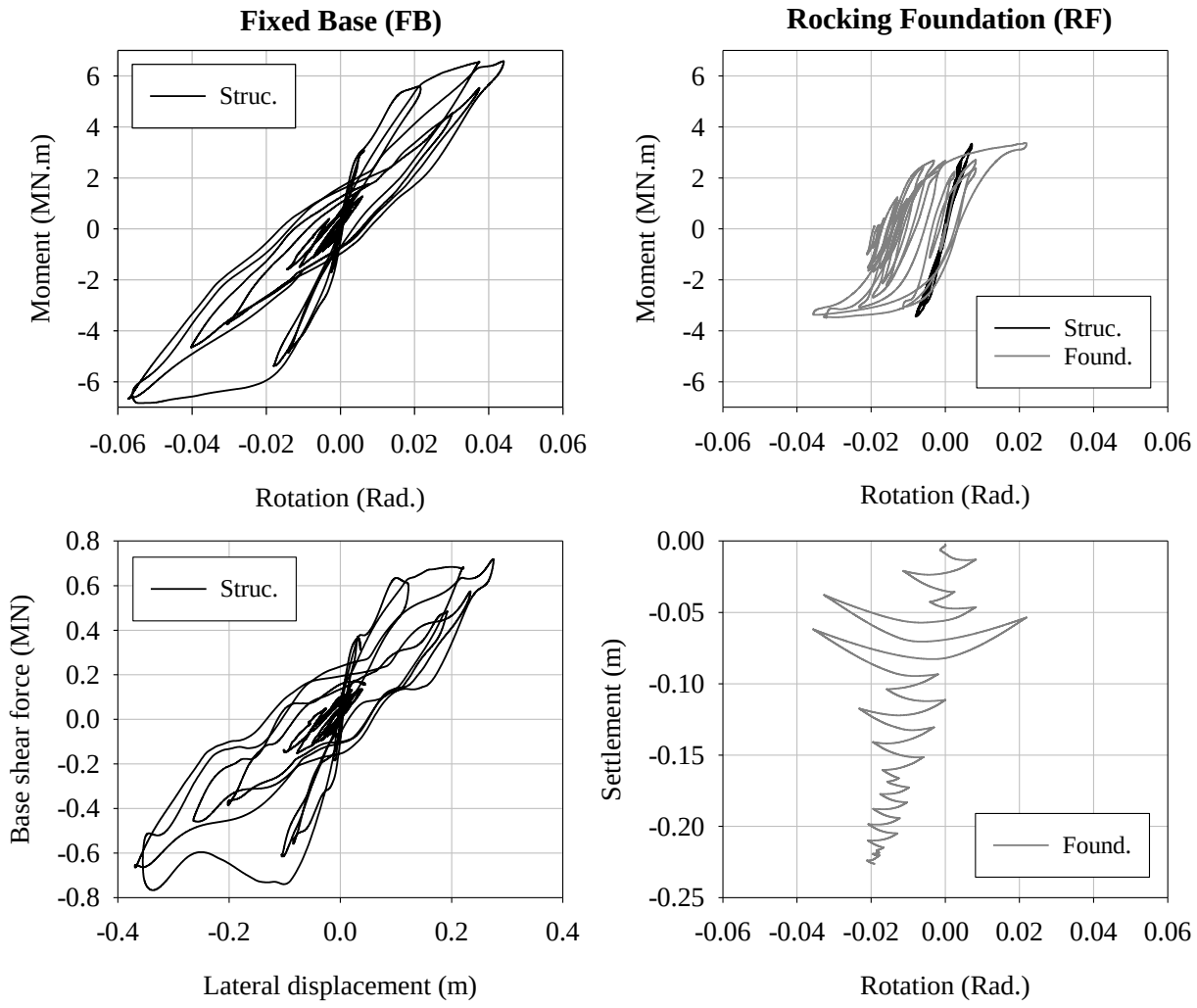

Figure 7.1. Comparison of Conventional Design to Rocking Foundation Design Behavior for Takatori0.5

In contrast, structural rotation (flexural) for the rocking foundation design appears very small all the while remaining well within linear elastic range. Although, the foundation exhibits considerable inelastic deformations foundation rotations are smaller than structural rotation from the conventional design. Soil reaches the moment capacity of 3200 KNm as observed from the plot and energy dissipation due to rocking behavior is evident by the large area enclosed by the moment-rotation hysteresis loop. Furthermore, similar to observations by Gajan & Kutter (2008)

moment-rotation behavior of the foundation indicate clear reduction in rotational stiffness without the degradation of moment capacity. Since sliding effects are constrained, the plastic deformation of soil is observed in form of footing settlement and rotation. The settlement-rotation plot indicates an accumulated settlement of 270 mm with a slight residual rotation of 0.02 rad after the shake. Footing uplift during the rocking motion is evident by the rebound in settlement-rotation curve. The structural acceleration was recoded as 0.13g indicating less than 45% acceleration transformation from the ground with a peak flexural deck drift of 41 mm (drift ratio of 1%).

7.3. Excitation Sensitivity of Rocking Foundations

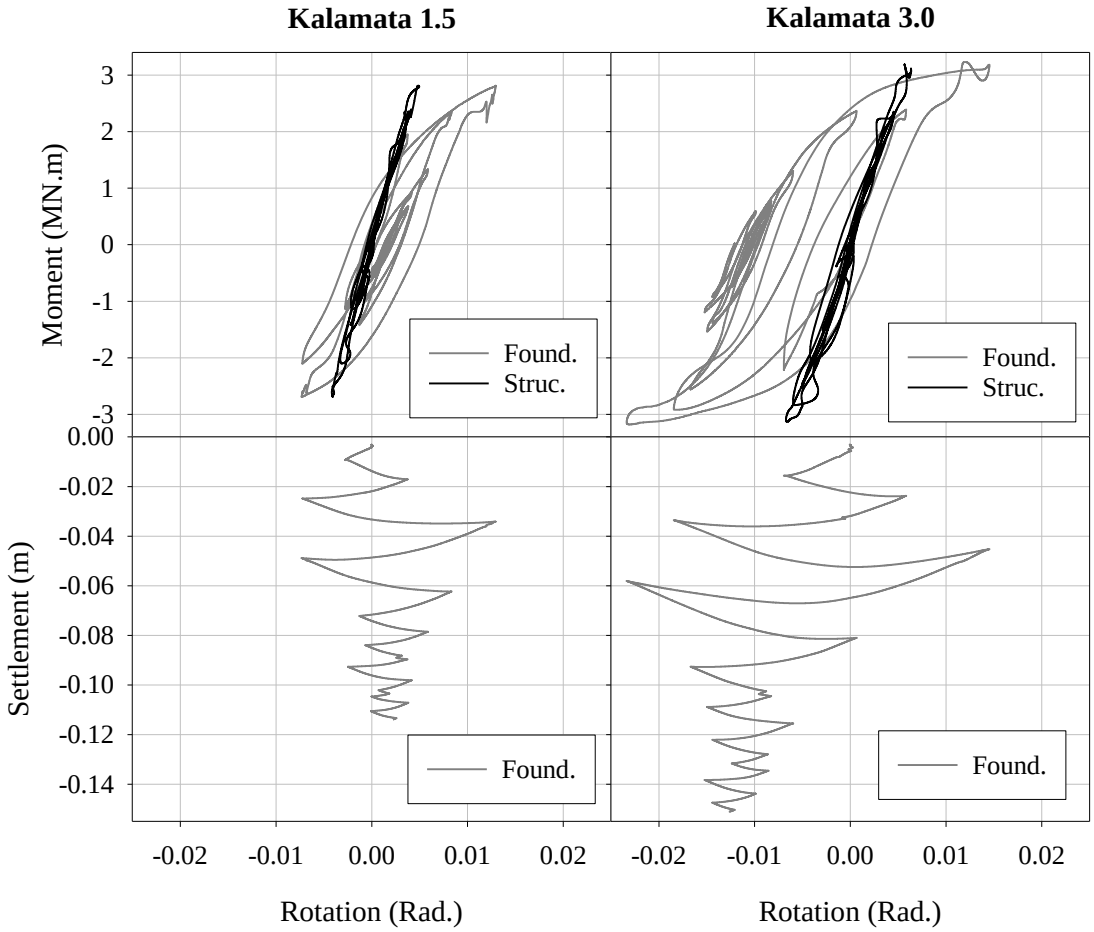

Figure 7.2. Moment-Rotation-Settlement Relationship for Kalamata1.5 and Kalamata3.0

Figure 7.2 presents moment-rotation-settlement relationship comparison for intensity of shaking using Kalamata1.5 and Kalamata3.0. Both structures consist of 6.5 column aspect ratio with 3.5 m wide footings and FS of 3.7 (Cr value of 0.16) allowing fully mobilized rocking behavior. For both cases, the structural moment-rotation response is contained well within the elastic range (approximately reaching 3000 KNm) while the foundation exhibits inelastic nonlinear deformations. With higher intensity shake, larger footing rotations are observed as soil reaches the moment capacity (M_{ult}) of 3200 KNm and increased energy dissipation due to increased rocking behavior is evident by the larger area enclosed by the moment-rotation hysteresis loop. The structural moment load and flexural rotation also appears to increase slightly with increased ground acceleration demand. However, the structure is still able to maintain the elastic behavior confirming the effectiveness of rocking foundation design. Similar to moment-rotation behavior, the settlement-rotation plots indicate increased footing rotational amplitude along with increased accumulated footing settlement for the larger intensity motion. The footing rotation amplitude is increased by over a 0.01 rad on the negative side due to the increased acceleration. The rocking behavior also develops a skewness as observed in the rotation-settlement response, which could result in the unbalanced rotational amplitude in the negative side. Footing uplift during increased rotation is indicated by the rebound in settlement-rotation curve, whereas the lower intensity shake (Kalamata1.5) indicates more of a sinking response with little footing uplift.

In figure 7.3, the same structure is subjected to a much stronger excitation than Kalamata3.0 to further understand the rocking sensitivity of the design. However, is should be noted that Takatori0.8 has a peak ground acceleration less than Kalamata3.0 (0.49g). Compared to Kalamata3.0, considerable amount of energy is dissipated through foundation as indicated by

the large hysteretic loops. The foundation not only reaches M_{ult} but mobilizes is to continuously dissipate energy during large rotation. The development of permanent rotation is apparent here as indicated from both moment-rotation and settlement-rotation curves. Considerable accumulative settlement is observed as a result of rocking induced plastic soil deformation.

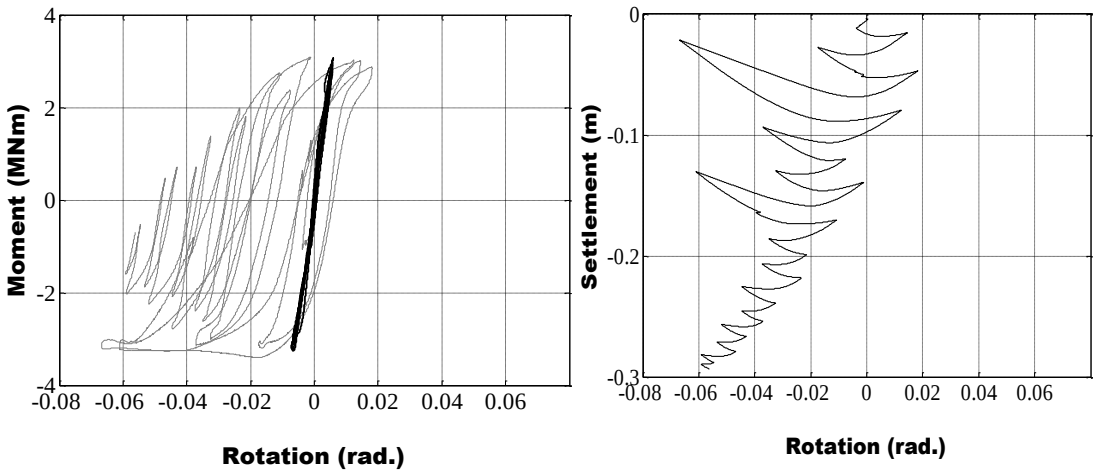

Figure 7.3. Moment-Rotation-Settlement Response for Takatori0.8

Between the rocking responses evaluated in figure 7.1, 7.2 and 7.3, Kalamata3.0 simulation was subjected to a higher peak ground acceleration (0.81g) than Takatori0.5 and Takatori0.8. However, the maximum footing rotation, accumulated footing settlement and the resulting residual rotation experienced by the Takatori simulations were larger in comparison despite the similarities in column AR, FS and footing size. This could be attributed to the characteristics of the Takatori excitation, which consists of stronger cycles and longer duration.

7.4. Effects of Shallow Footing Embedment and Soil Improvement

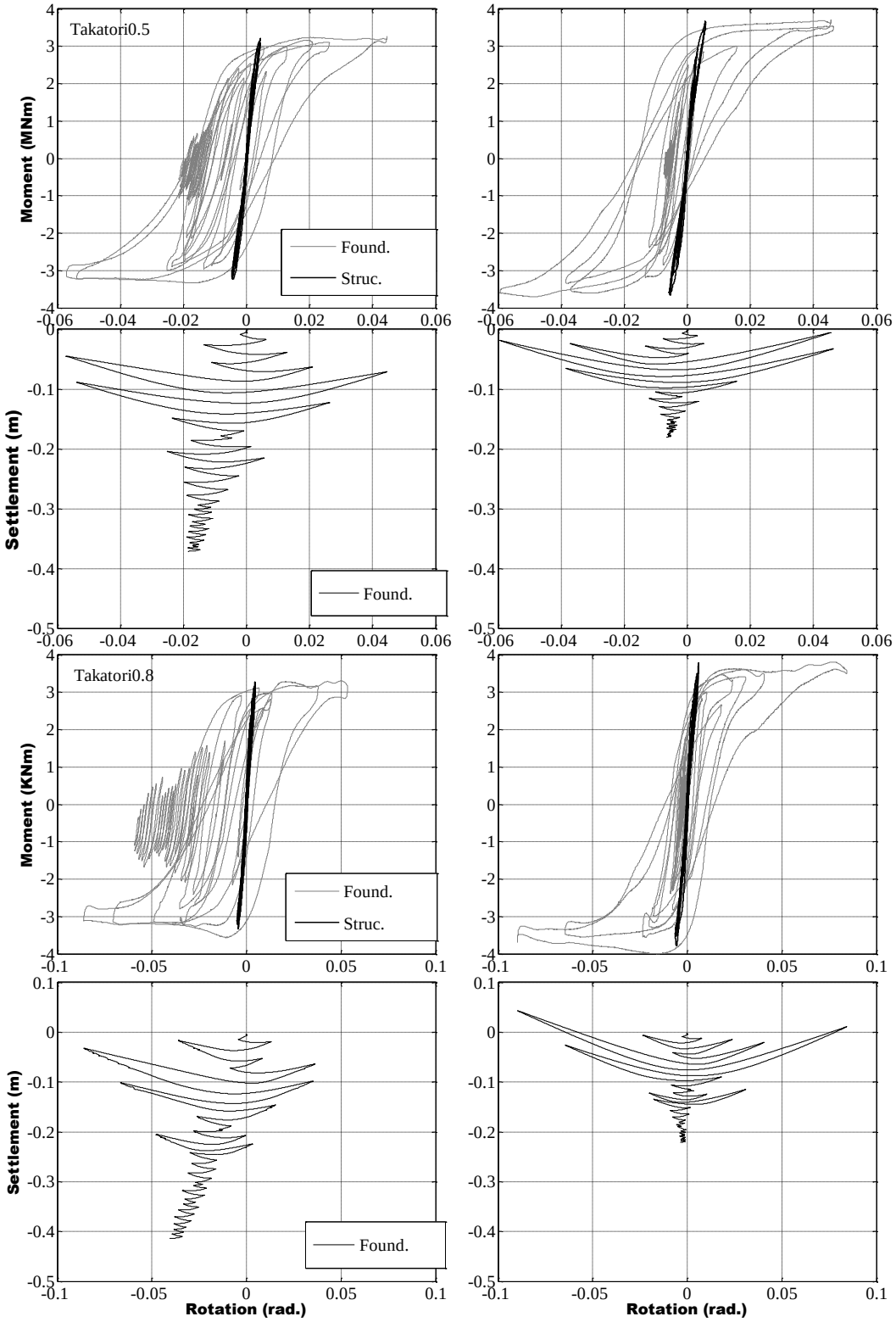

Figure 7.4. Effects of Embedment on Rocking Foundation Design for Takatori Excitations

The moment-rotation-settlement plots in figure 7.4 compare the effects of embedment on rocking foundations. The left side plots summarize the rocking behavior of zero embedment, while the right side plots summarize the rocking behavior of their embedded counterparts. The four plots on top show the moment-rotation and settlement-rotation response for Takatori0.5 and the bottom four plots show moment-rotation and settlement-rotation response for Takatori0.8. all simulations are expected to develop fully rocking behavior with FS = 8.3 for 1 m footing embedment (D_f =1) and FS = 3.7 for non-embedment (D_f = 0). Strong excitations were used for these simulations to evaluate the rocking induced moment-rotation-settlement behavior of a highly nonlinear soil-structure system with embedment.

In general, the non-embedded rocking behavior exhibit considerable accumulated settlement with large footing rotation as much as 0.09 rad for Takatori0.8, resulting substantial energy dissipation and large rotations as indicated by the moment-rotation plots. In contrast, the respective embedded structures exhibit considerably less accumulated settlement (reduction of approximately 50%) accompanied by little to non-existing residual total rotation. However, the large enclosing loops are indicative of its ability to dissipate energy at footing level similar to the zero embedment structure while maintaining the column rotation within elastic range. Also evident is the slight increase in M_{ult} due to increase FS as a result of embedment. From the plots, it appears that the shape of the moment-rotation hysteretic loops is slightly changed by the embedment. Specifically, because of the reduction in permanent rotation, most of the footing rotations are closer to 0.0 rad, even though they reach higher moment loads indicating increased foundation stiffness. However, few large rotations push the foundation to moment capacity, mobilizing the rocking behavior to dissipate energy. The foundation moment-rotation behavior shows what appears to be a slight reduction in moment capacity for Takatori0.8 once fully

mobilized. However, further investigations were not pursed to evaluate this phenomenon. Finally, Embedment also appears not to have affected the rocking motion from achieving moment capacity with rotational degradation, which further encourages the use of such method for limiting settlement and permanent structural rotation.

As discussed before, reduction in the residual rotation could be achieved through footing embedment, which also improves the stability of the overall rocking behavior. The embedded rocking behavior is further analyzed in figure 7.5 based on soil characteristics with initial soil shear modulus (G) ranging from 71 to 115 MPa. For the purpose of this discussion, soil consisting of G values 71, 89 and 115 MPa shall be identified as “loose sand”, “med. dense sand” and “dense sand” respectively. However, it should be noted that these terminologies do not constitute that soil characteristics used for these simulations consists of what may be considered typical characteristics of such soil type. All structures consist of D_f = 1 m and identical footing sizes aimed at mobilizing fully rocking behavior. The FS values of these structures are 5.5, 8.3 and 16.0 respectively and, subjected to Kalamata2.0 excitation. Based on the moment-rotation behavior, it appears that med. dense sand and dense sand simulations tend to rotate more towards positive direction (closer to 0.02 rad) as oppose to loose sand simulation where both negative and positive sides reach slightly higher than 0.01 rad, which depicts a more symmetrical movement. This is more apparent with the shift in the elastic range for foundation moment-rotation response. Due to the slight skewness, peak foundation rotation in the negative directions is slightly reduced for med. dense and dense sand as well. Nevertheless, the overall maximum foundation moment appears to remain relatively similar at approximately 3500 KNm for all three responses regardless of FS. Another observation is that med. dense and dense sand, potentially because of skewness, only able to fully mobilize moment capacity in the positive region. The absence of

moment capacity degradation regardless of soil characteristics reaffirms theoretical accuracy of the model. All three simulations exhibit capacity to dissipate energy at foundation level with med. dense sand and dense sand indicating relatively larger moment-rotation loops compared to loose sand meaning more dissipated energy.

The D_f = 0 m settlement-rotation behavior of the same simulation is plotted alongside embedded settlement-rotation behavior for comparison purposes. By observing the settlement-rotation plots, two main conclusions can be made. One is that with increasing FS (in this case due to soil conditions) the general trend is reduction in overall settlement along with gradually improving self-centering effect for D_f = 0 m simulations and second is that with D_f = 1 m, all three simulations have further improved the self-centering ability along with the improved accumulative settlement.

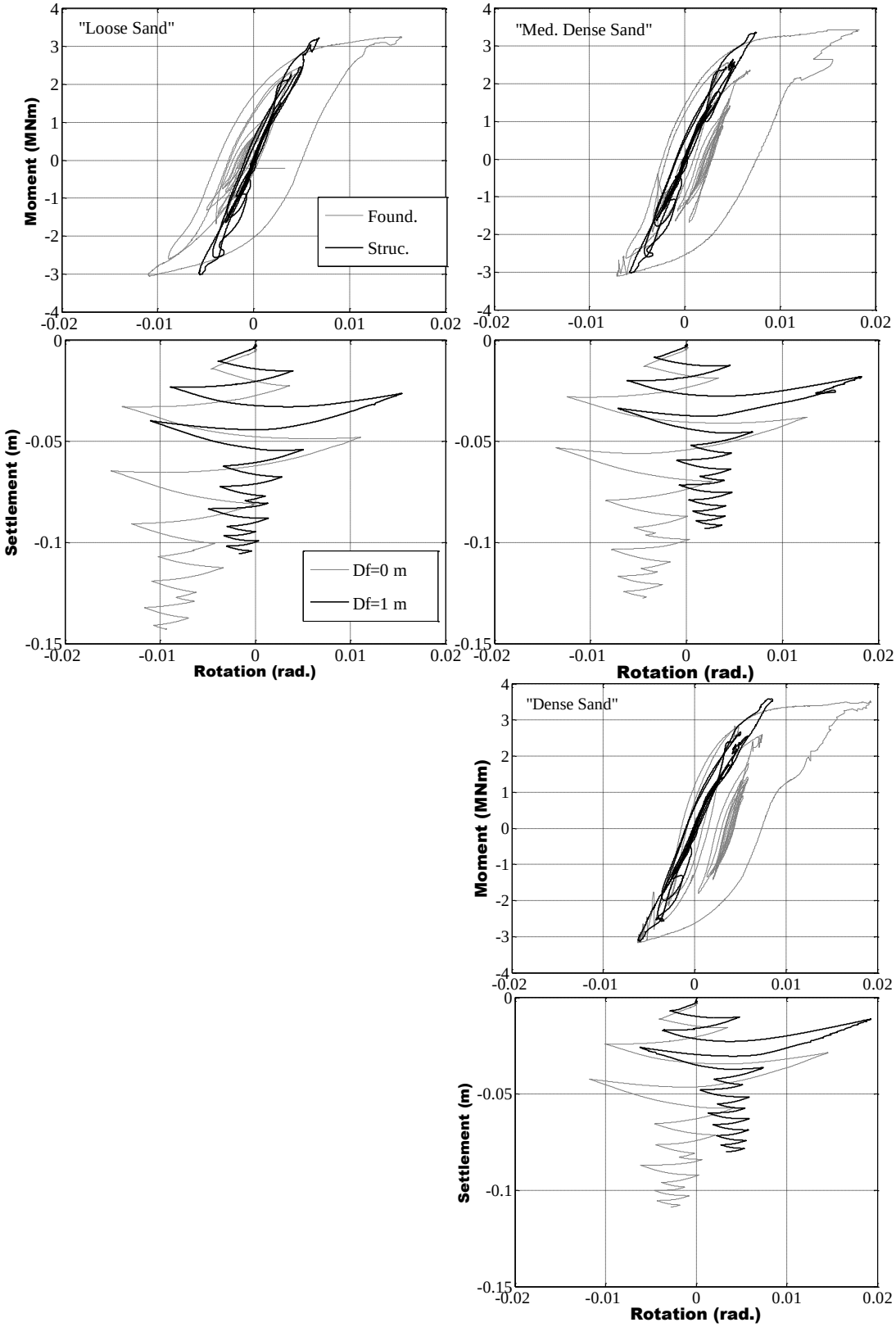

Figure 7.5. Response of Footing Embedment Combined with Increasing G

The study of the effects of column aspect ratio (AR) on moment-rotation-settlement relationship is another aspect of this research. A column aspect ratio range of 4 to 10 (column height ranging from 5 to 12 m) was introduced to the testing matrix in hopes of observing the changes in soil-structure nonlinear behavior. While figures 7.1 and 7.3 presents the moment-rotation-settlement behavior of a Bridge-pier model with AR 6.5, B3.5 and Takatori0.5 and Takatori0.8 excitations, the moment-rotation-settlement plot in figure 7.4 presents the same column with AR 4. Despite the similarities in FS and excitations, the shorter structures have a higher accumulative settlement for both excitations and more soil deformation judging by the peak rotations and the larger hysteretic loops, while achieving the same moment capacity (identical FS). Additionally, the shorter structures fully mobilize the moment capacity at foundation level on both sides (positive and negative) compared to $D_f = 0$ m counterpart. Therefore, it can be concluded that similar to fixed-base simulations, the shorter structure with reduced natural elastic period is more sensitive to the Takatori excitations resulting in large energy dissipations. However, unlike the fixed-base simulation, the energy is dissipated through foundation-soil for rocking foundations.

7.5. Self-Centering Ability of the Bridge-Pier Model

In the following summary plots, results of seventeen centrifuge experiments (Ugalde et al., 2007; Gajan & Kutter, 2008) and fifteen shake table experiments (Drosos et al., 2012; Anastasopoulos et al., 2013) are used along with simulation results of this study for comparison purposes.

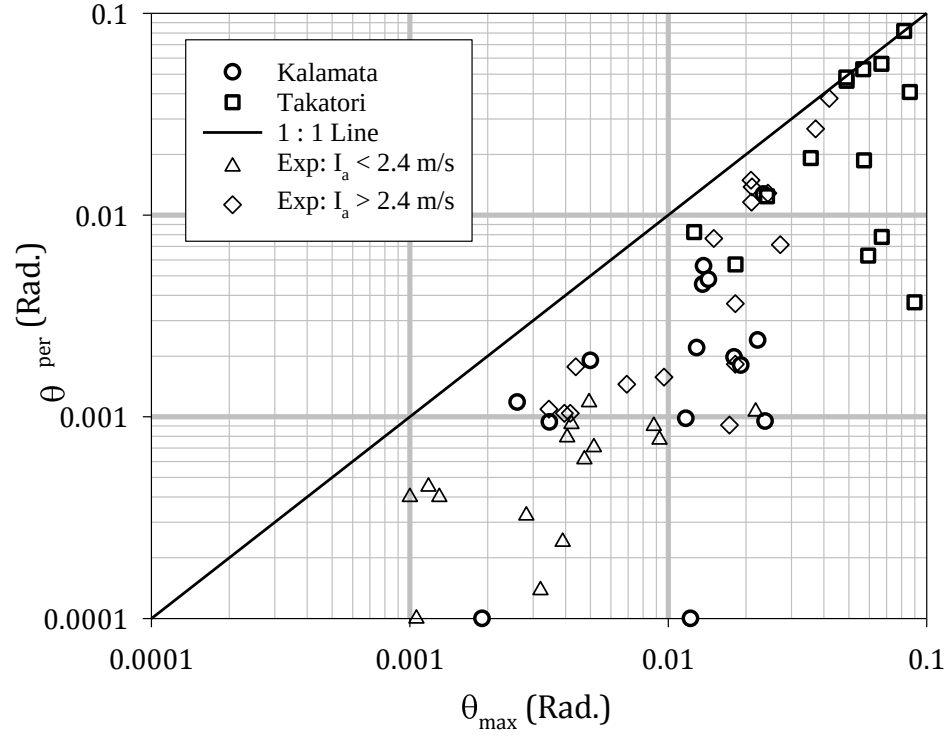

Figure 7.6. Simulation and Experimental Results of Maximum Foundation-Structure Rotation against Permanent Foundation-Structure Rotation

The results of maximum total rotation of the foundation-structure system during dynamic loading and the subsequent permanent total rotation at the end of the excitation are shown in figure 7.6. For comparison purposes, experimental results are classified by the Arias intensity (Ia), which is a measure of earthquake intensity. In general, the trend indicates increased maximum foundation rotation (θ_{max}) with higher intensity excitations for both experiments and simulations (Takatori is a strong ground motion compared to Kalamata). Another observation is,

apart from a few data points located on the 1:1 line closer to 0.1 rad, most data points fall below the 1:1 line. This indicate that despite the potential for higher maximum rotations during excitations, the permanent total rotation at the end still will be less in comparison thanks to the self-centering characteristic of the rocking foundation design.

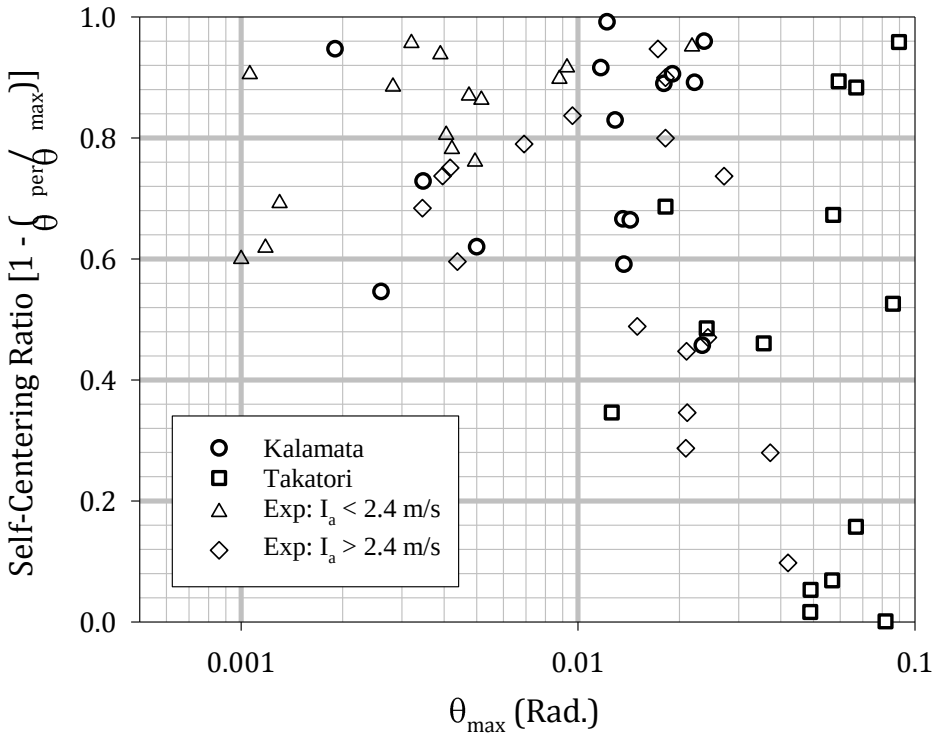

Figure 7.7. Self-Centering Ability of Rocking Foundations Compared with the Maximum Foundation-Structure Rotation

$$\eta = 1 - \frac{\theta_{perm}}{\theta_{max}} \tag{36}$$

The self-centering ability of a rocking foundation could be presented as a function of the ratio between residual foundation rotation at the end of the excitation (θ_{perm}) and θ_{max} (equation 36). Figure 7.7 further clarifies this observation (ability to self-center) with the use of self-centering ratio (η). As the permanent total rotation of the soil-structure system reaches maximum total rotation, the potential to self-center drastically reduces (self-centering ratio reaches 0.0) on

the other hand; if the permanent rotation is considerably small, the potential for self-centering ability increases (self-centering ratio reaches 1.0). As can be seen from figure 7.7, for θ_{mas} between 0.001 to 0.01 rad the self-centering ratio is relatively high for both experimental and simulation data indicating good potential for the structure returning back. However, between 0.01 to 0.1 rad the data points indicate a spread of data from both experimental and numerical simulations showing the potential to either self-center or maintain a permanent drift (due to permanent rotation at the footing). While Kalamata results mostly remain above $\eta = 0.5$, Takatori indicate results from nearly 0.0 to 1.0 range with a few extreme cases of permanent total rotation reaching the maximum total rotation. However, in general it can be said that based on the this study the potential to self-center is highly likely as long as θ_{max} is less than 0.04 rad.

7.6. Influence of Cr and Cy

Deng et al., (2012) proposed the use of Cr and Cy (rocking and base shear) coefficients to improve the rocking potential of structures and thereby increase the efficiency of energy dissipation through rocking. Figure 7.8 further enhances this theory through the relationship between normalized maximum structural acceleration and Cr value. Theoretically, Cr should be proportional to the maximum acceleration of the structure with results being on or below the theoretical limit line. In other words, smaller Cr values leading to higher rocking potential would result in reduced acceleration demands (due to reduced energy) to the superstructure. Apart from a few outliers, the general trend in figure 7.8 shows increased acceleration demands on the structure with increased Cr values, which confirms this theory. Also noticeable is the spread of numerical and experimental results beyond Cr value of 0.2 at which point numerical model results get closer to the Cy range of 0.2 to 0.5 resulting less optimized rocking behavior leading to more energy being transmitted to the structure.

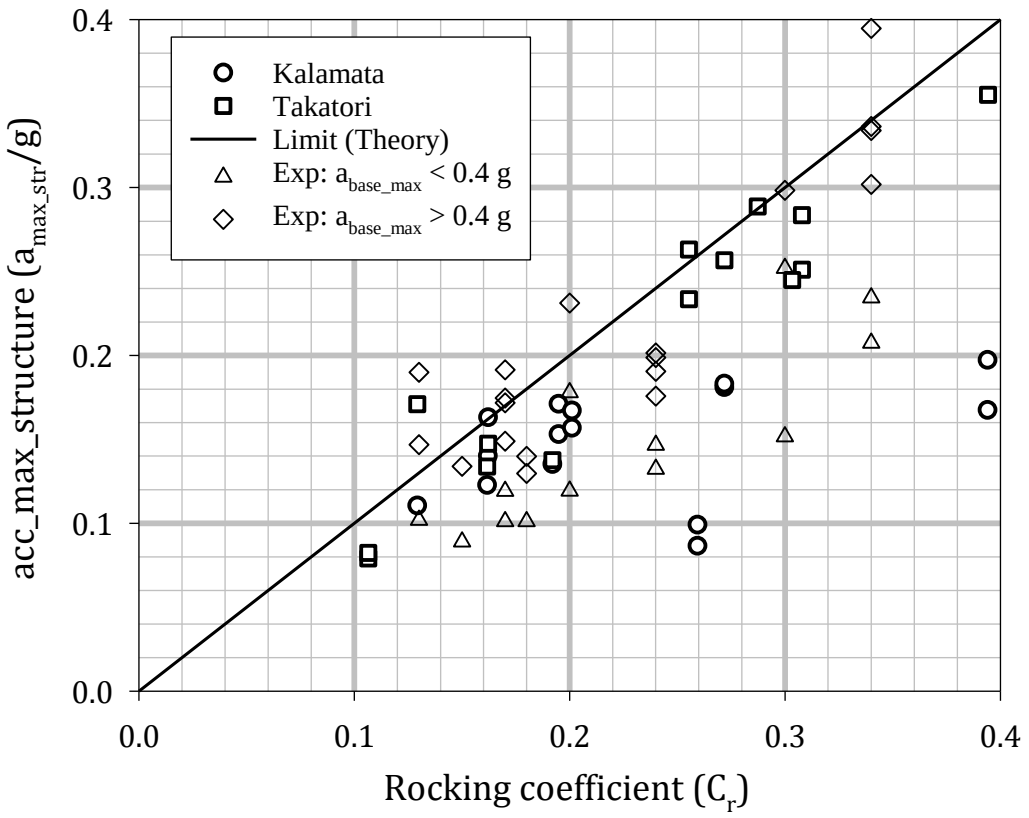

Figure7.8. Effects of Cr on Structural Acceleration of Rocking Foundations

The concept of Acceleration Amplification Ratio (AAR), which is a ratio of maximum acceleration experienced by the structure to the input maximum acceleration by the excitation, is introduced in figure 7.9 to further evaluate the effects of Cr on acceleration transmission to superstructure. Again, the general trend complements the previous observations of increased acceleration transmit to the structure with increasing Cr. The spread of numerical simulation results beyond Cr value 0f 0.2 could be contributed to the combined nonlinear behavior of both foundation and structure as the rocking behavior may no longer fully mobilized. If foundation moment capacity is not relatively smaller than the column moment capacity, the hinge location may not be completely moved to the foundation-soil causing a combined nonlinear behavior in

both column and foundation, and if Cr value is increasing beyond Cy, the structural behavior will revert to conventional design where most energy is dissipated through the column.

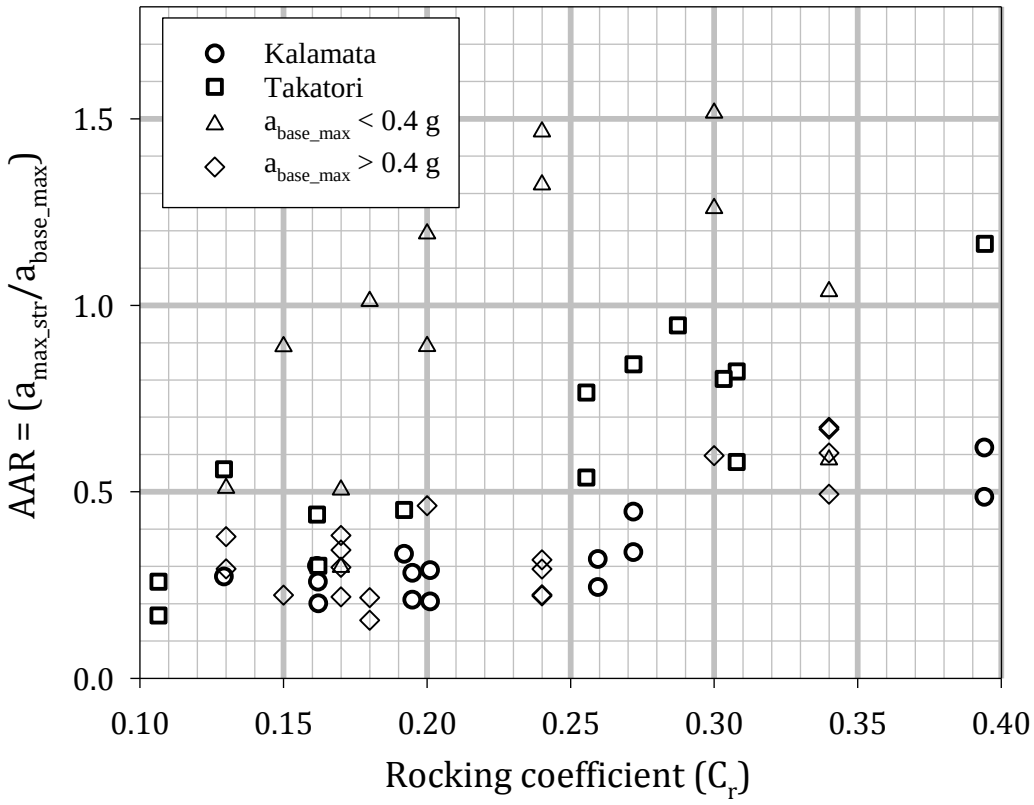

Figure7.9. Acceleration Amplification Effects of Cr

To study energy dissipation characteristics through the nonlinear behavior of the structure is one of the reasons for the use of a reinforced concrete structure for this numerical model. In figure 7.10, the ratio of energy dissipation of the foundation to the total energy dissipation of the foundation-structure system is plotted against the Cr/Cy ratio. The higher the energy dissipation ratio, the more effective the rocking foundation design would be. Likewise, when Cr/Cy ratio is smaller than 1 the system can be considered as rocking dominant whereas for values relatively closer to 1 and larger would result in the system being unable to completely mobilize the rocking behavior since foundation moment capacity has become closer-to or larger than the column

moment capacity. The results indicate a higher energy dissipation ratio of roughly 80% or higher for simulations with Cr/Cy values smaller than 1. in contrast, a considerable reduction in energy dissipation ratio is observed for Cr/Cy values larger than 1.0, indicating that noticeable amount of energy could be dissipating through the structural elements such as the column in addition to the inelastic nonlinear behavior of foundation-soil.

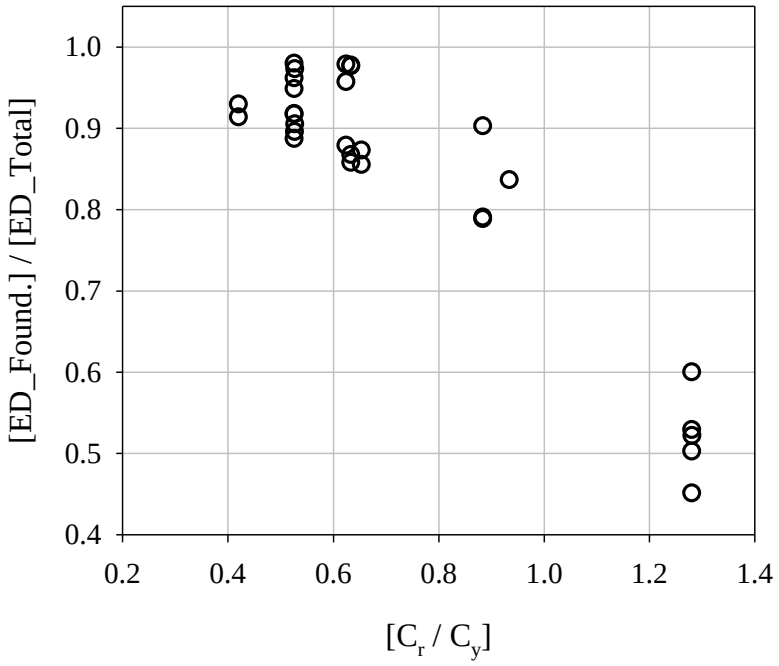

Figure 7.10. Energy Dissipation Ability of Rocking Foundations as a Function of Cr/Cy

7.7. Foundation Settlement Characteristics

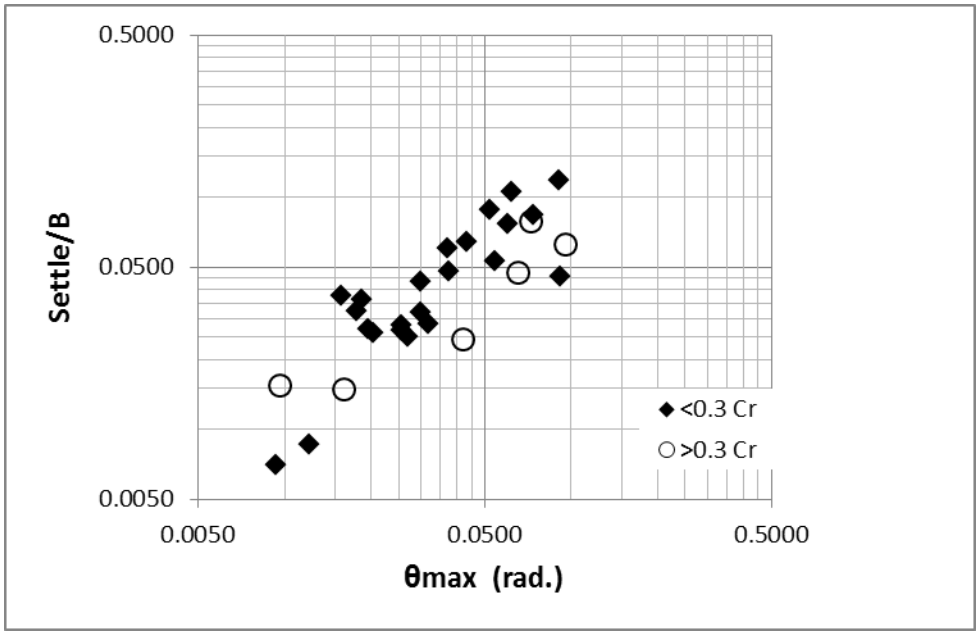

Figure 7.11. Normalized Settlement Based on Foundation-Structure Maximum Rotation

Understanding rocking induced settlement characteristics is crucial towards addressing foundation-soil settlement concerns of a rocking foundation design. Previous research had shown that FS, footing rotation amplitude, excitation characteristics such as intensity and base shake versus slow cyclic loading, and foundation-soil conditions could greatly influence the settlement behavior (e.g. Gajan& Kutter, 2008 & 2009; Ugalde et al., 2007; Drosos et al., 2012; Selvarajah & Gajan, 2015). In this study, the effects of footing embedment and G on settlement characteristics were discussed in previous sections, that discussion is extended in to the influence of total rotation of the soil-structure system and K_v using figure 7.11 and 7.12 in the following sections.

In figure 7.11, normalized settlement is compared with the peak total rotation of the system. The trend indicates normalized settlement being proportional to the maximum foundation rotation. The data are identified based on Cr values, however according to the data

spread the influence of Cr appears to be insignificant . This observation confirms the prior research observations by Gajan & Kutter (2008), whom concluded increased rotation and settlement with increased shake intensity and Selvarajah & Gajan (2015), whom noted the linear trend between rocking amplitude and footing settlement. Furthermore, Ugalde et al., (2007) also concluded that a strong correlation could be found between footing rotation and settlement that indicates most settlement is caused by moment and not by shear or vertical loading.

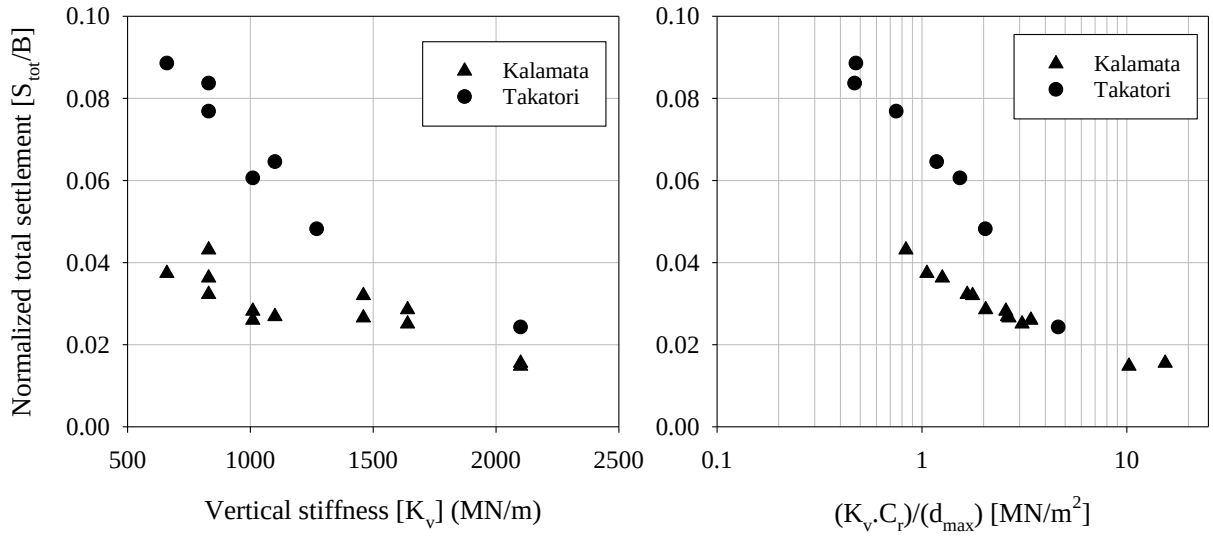

Figure 7.12. Normalized Settlement as a Function of Vertical Stiffness of Soil & Combined Effects of d_{max}, K_v and Cr on Normalized Settlement

Minimizing the settlement effects of rocking foundation design through soil improvement (e.g. Deng et al., 2012) or by footing embedment (e.g. Ntritsos et al., 2015) has been suggested by other researchers. A main objective of this study was to expand the investigation into potential use of footing embedment or soil improvement methods (through increase of G) for controlling rocking induced settlement. The left side plot in figure 7.12 analyze the relationship between normalized total settlements of all rocking foundation simulations with Kv, which is a function of G. The results are categorized based on the excitations and the trends indicate a

reduced settlement with increased K_v for both Kalamata and Takatori. Also noticeable is the large difference between the amounts of normalized settlement of Kalamata to Takatori when K_v is relatively less. However, as K_v increases this difference becomes insignificant.

Kokkali et al., (2014) investigated the rocking response of the single degree of freedom bridge pier supported on sand using centrifuge and 1g tests. During the investigation, the effects of FS on different systems were compared with normalized settlement (settlement/ footing width). The FS of the experimental systems consisted of 5, 11 and 14. In comparison, FS for this study ranged from 2.4 to 24. Based on the experimental results by Kokkali et al., (2014), the accumulated normalized settlement for "loose sand" with FS =5 using centrifuge test reached approximately 0.07, while using 1g test the accumulated normalized settlement reached approximately 0.15. Accumulated normalized settlement for "dense sand" using centrifuge test with FS = 11 reached approximately 0.025, while using 1g test with FS = 14 reached approximately 0.03. In this study based on figure 7.12, for FS = 2.4 (K_v = 660) the highest accumulated normalized settlement was 0.089 (Takatori) and 0.043 (Kalamata), while for FS = 24 (K_v = 2100) the lowest accumulated normalized settlements was 0.024 (Takatori) and 0.016 (Kalamata). For FS between 2.4 to 7.5, the simulations produced normalized accumulated settlements in the order of 0.07 to 0.09 (compared to 0.07 to 0.15 from experiments) while for FS between 8.3 to 10.8, the normalized settlement approached roughly 0.03 (compared to 0.025 to 0.03 from experiments). This comparison reinforces the results of these simulations by achieving strikingly close results in terms of settlement characteristics.

Based on the discussion so far regarding the characteristics of settlement due to rocking behavior, the following relationships could be summarized.

$$S \propto \frac{1}{K_v} \tag{37}$$

$$S \propto \frac{1}{C_r} \tag{38}$$

$$S \propto a_{max} \tag{39}$$

It can be proposed that rocking induced settlement is inversely proportional to K_v by observing trend of left side plot of figure 7.12. It can also be proposed that settlement is proportional to the peak ground acceleration (a_{max}) as shown in figure 7.2. Deng et al., (2012) proposed that by reducing Cr (compared to Cy) the rocking potential of the structure could be fully realized leading to increased θ_{max}. The increased θ_{max} of the structure results in increased permanent settlement is confirmed by figure 7.11 where the normalized settlement of all the numerical simulations show a proportional relationship to maximum foundation rotation regardless of Cr. An inversely proportional relationship of Cr to settlement can be concluded by considering the above discussion that concludes equation 38. Through integration of equation 39, the relationship between rocking induced settlement and maximum ground displacement could be realized (equation 40). Finally, by combining equations 37, 38 and 40, the relationship in equation 41 can be developed.

$$S \propto d_{max} \tag{40}$$

$$S \propto \frac{1}{\left(\frac{K_v . C_r}{d_{\max}}\right)} \tag{41}$$

This relationship is presented in the right side plot of figure7.12, where two trends can be developed for Takatori and Kalamata ground motions. Both curves show an inversely proportional relationship to normalized settlement. The units are in terms of $\frac{1}{MN/m^2}$ and combine the effects of soil, rocking and excitation characteristics to rocking induced settlement.

7.8. Rocking Foundation Performance Summary

The purpose of this chapter is to present a comprehensive evaluation of the rocking foundation design and discuss the beneficial effects of soil yielding design as oppose to conventional structural yielding design. An in-depth investigation in to the performance comparison of fixed-base versus rocking design, sensitivity of rocking design to excitation characteristics and rocking induced settlement response to footing embedment and initial shear soil modulus is performed to achieve substantial understanding of the rocking foundation design. Additionally, the self-centering characteristics of rocking design and the important role of rocking and base shear coefficients on rocking foundation design is also discussed. A summary of the findings from this chapter is presented below.

7.8.1. Conventional Design versus Rocking Foundation Design

Through comparison with chapter 6, the following about the two different design approaches could be concluded. (a). for intermediate excitations such as Kalamata1.5, the conventional design seemed quite resilient and performed quite well with a small peak deck drift (1%), while maintaining the moment loads well within linear elastic range. (b). once subjected to a stronger excitation such as Takatori0.8 excessive column deformations accompanied by material degradation and considerable energy dissipation was visible. (c). rocking foundations maintain the structure well within elastic range even at stronger excitations while indicating excessive plastic deformations in the foundation-soil.

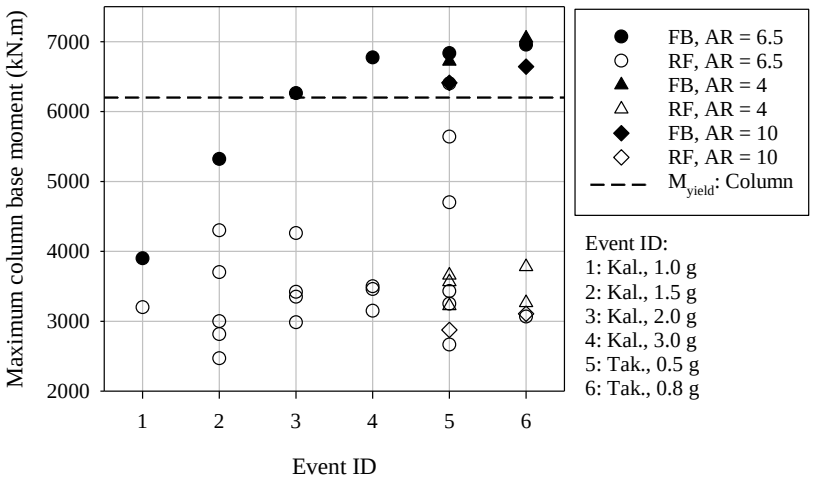

Figure 7.13. Bridge Column Moment Comparison between Fixed-Base and Rocking Foundations

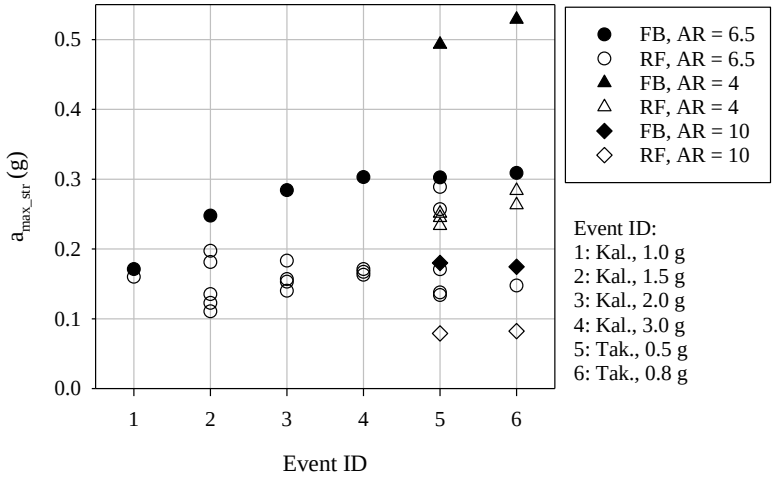

Figure 7.14. Bridge Column Acceleration Comparison between Fixed-Base and Rocking Foundations

Figure 7.13 and 7.14 summarizes the comparison between fixed-base and rocking foundation design in terms of acceleration and moment transmitted to the structure. The general observations indicate relatively higher moment and acceleration demands experienced by the fixed-base structure regardless of the shake event or AR compared to rocking foundations. From the column base moment plot, it appears that the structure is pushed beyond the theoretical

moment capacity during events 4, 5 and 6 that could be detrimental to the structural integrity. Furthermore, once rocking is fully mobilized, for excitation events 4, 5 and 6 the maximum column moment was reduced by approximately 50% (3200 KNm). The acceleration transformation from ground to the structure was effectively reduced by the rocking foundations, while subsequently reducing the peak deck drifts as discussed in the fixed-base- rocking foundation comparison. The taller structures in general regardless of fixed-base or rocking foundation design appear to experience comparatively lower accelerations, while shorter structures experience much higher accelerations.

7.8.2. Rocking Foundation Sensitivity to Excitations

From the results, it can be concluded that similar to conventional design, rocking behavior is also sensitive to the duration, peak acceleration and the intensity of the ground motion. By observing the rocking behavior between Kalamata1.5 to Kalamata3.0 and by comparing Kalamata3.0 with Takatori0.5 and Takatori0.8 a substantial understanding about the complex nature of the combined effects of duration and acceleration was achieved. While clearly increased acceleration would induce increased demands on the rocking behavior, motion duration and the number of strong acceleration cycles could further increased the demands on rocking behavior. However, as observed by Gajan & Kutter (2008, 2009), despite considerable foundation-soil deformations reduction in foundation moment capacity was not observed even after repeated mobilization. The only concerning observation from increased nonlinear plastic deformation of foundation-soil is the substantial accumulative settlement and the potential permanent footing rotations resulting from the increased rocking demand. Drosos et al., (2012) also acknowledged the sensitivity of rocking foundation design to excitation intensity by comparing structures with FS values 7.3, 3.5 and 2.3 to medium and high intensity base

accelerations. Noticeable increase in footing settlement and rotation was observed for all FS values for high intensity excitation with FS = 7.3 structure, which is identified as the conventional design even indicating slight acceleration amplification effects. The sensitivity of structural natural period to excitation is also evaluated through the comparison of AR within rocking foundation simulations, where AR 4 consistently indicated larger moment-settlement-rotation response for Takatori ground motion.

7.8.3. Settlement and Soil Improvement on Rocking Behavior

Shallow footing embedment and soil improvement can be considered as a means of controlling rocking induced settlement behavior. The relationship between vertical soil stiffness (K_v) and normalized settlement further reinforces this conclusion, as K_v includes combined effects of initial shear soil modulus and footing embedment. Additionally, another important aspect of embedment was the ability to provide a more stable rocking behavior by reducing not only settlement but also the permanent rotation of the rocking system as seen from figure 7.4. The amount of permanent rotation reduction due to embedment based on the settlement-rotation results from figure 7.4 calculated to be approximately between 70 to 90%. The effects of embedment can be further improved through soil improvement as seen from figure 7.5. Prior researchers have observed similar changes in rocking behavior as a result of embedment and soil improvement as discussed in literature review chapter. However, this study takes these two observations and combines them in hopes of achieving a substantial knowledge about the rocking induced settlement behavior. The said improvements in rocking induced settlement and foundation rotation was observed only for B = 3.5 m footing width with a maximum D_f of 1.5 m, which is less than half of the footing length. Also it was noted that despite the shallow embedment and increased initial shear soil modulus, the structural flexural rotation remained less

than 0.01 rad with deck drift ratios less than 0.5%, meaning that the structure was maintained well within linear elastic range.

Based on the relationships observed between normalized settlement and K_v, peak ground displacement (d_{max}) and rocking coefficient (Cr), a relationship is proposed as a means of quantifying potential rocking induced settlement. The ability to quantify and mitigate excess settlement would be quite beneficial towards wider recognition of rocking foundations as an alternative design approach. However, as discussed by Deng et al., (2012), the efficiency of energy dissipation in rocking foundations depends on its ability to induce plastic deformations on foundation-soils. Therefore, by considerably limiting the plastic deformations such as rocking induced settlement, the undissipated energy would potentially be transmitted on to the structure.

7.8.4. Self-Centering Behavior and Importance of Rocking and Base Shear Coefficients

This study further established that tip-over failure potential in rocking behavior is rare. From a series of 33 rocking simulations consisting of column heights 5, 7.9 and 12 m and AR 4, 6.5 and 10, none of the soil-structures systems indicated the potential for considerable system rotation that could have results in tip-over failure. Although, stronger motions tend to push the permanent rotation of few of the structures closer to the peak rotation, these models found to be of AR 10, which is not typical of a Caltrans bridge column design.

The importance of Cr and Cy coefficients on rocking behavior is also evaluated in this study. The potential use of this coefficient as a design parameter to maximize rocking potential and to control ductility demands through structural acceleration control is proposed along with use of Cr for quantifying settlement and the importance of establishing the Cr/Cy ratio for optimizing energy dissipation characteristics is discussed.

8. SUMMARY AND CONCLUSIONS

8.1. Introduction

This chapter briefly summarizes the research program and presents the conclusions derived from the study. Recommendations for future work are presented at the end of this chapter. The rocking foundation design seems to be proving its ability to dissipate seismic energy efficiently and safely without damaging the structural elements. The simulations results further substantiate this claim with high-energy dissipation ratios and effectively reducing ductility, acceleration and moment demands on the structure. With the use of "slight" embedment and soil improvement methods for containing accumulative settlement and permanent rotation problems, rocking foundations could be implemented as a successful alternate design strategy for earthquakes.

8.2. Summary of Research Program

In this study, the complicated nature of the foundation-soil behavior underneath a rocking foundation during seismic loading is evaluated with the use of an idealized yet realistic single column bridge pier and a realistic foundation-soil interaction model. Using the finite element platform OpenSees, a constitutive model for the reinforced concrete column was created. Then, the column material models were calibrated using well-confined concrete bridge column experiments by Lehman & Moehle (2000). The calibrated constitutive model was integrated in to a full-scale bridge-column computational model to develop the Bridge-pier model, which was validated against a full-scale single bridge column shake table experimental results (Schoettler et al., 2015). In order to compare the beneficial and detrimental effects of structural yielding and foundation yielding, a series of fixed-base simulations and rocking foundation simulations were conducted. For rocking foundation simulations, contact interface

model (CIM) available in OpenSees was used to develop the soil-structure combined nonlinear load-deformation behavior. Moment-rotation-settlement behavior of the foundation-soil system and structural ductility demands were considered for comparing the performance between conventional capacity design (fixed-base) and rocking foundation design. Upon establishing the superiority of the rocking foundation design, further investigations into the behavior of rocking foundations were conducted in terms of excitation sensitivity, effects of footing embedment and foundation-soil improvement on rocking response, influence of rocking coefficient and base shear coefficient on rocking performance and self-centering characteristics.

8.3. Conclusions

The conclusions derived from this research program are presented below, which are further discussed in the performance summary sections in chapter 6 and 7.

- The findings of this research clearly reveal that incorporating rocking shallow foundations into design reduces the ductility, acceleration, and moment demands transmitted to the structure during seismic loading when compared to conventional fixed base design. When the foundations are allowed to rock on soil, the reductions in peak flexural deck drift, peak deck acceleration, and the maximum moment at the base of the column are 50% or more when compared to their fixed base counterparts.
- For relatively small magnitude shakings, both fixed base and rocking foundation design show satisfactory performance. However, for relatively strong shaking events, rocking foundation systems exhibit superior performance. Fixed base columns experience moment demands that are beyond the yield moment of the column, which could be detrimental to the structural integrity, while columns supported by rocking foundations never reach their yield moment capacities.

- The results indicate that by intentionally making rocking coefficient (Cr) smaller than base shear coefficient (Cy), the rocking behavior can be fully mobilized and the beneficial effects of rocking can be fully utilized. As long as Cr is smaller than Cy, the foundation-soil dissipates about 80% of the total seismic energy while limiting the flexural deck drift to 0.5% or less. The maximum acceleration transmitted to the structure (and hence the maximum moment demand at column base) is limited by the value of Cr when Cr is smaller than Cy.
- Contrary to the popular perception, rocking foundations show well-defined stability against tipping-over failure by possessing excellent self-centering characteristics (thanks also to the reversing nature of the earthquake shaking). As long as the maximum rotation experienced by the foundation is smaller than 0.04 radians, the self-centering ratio of the rocking foundations are greater than 0.6 (a self-centering ratio of 1.0 corresponds to a perfectly self-centering system).
- Rocking foundation design keeps the structure well within the elastic range even for relatively stronger shaking events, while increased foundation rotation and permanent settlement being the detrimental effects. This study shows that a "slight" increase in footing embedment ($D < B/2$) and shear modulus have the potential to improve the settlement-rotation behavior of rocking foundation significantly (reduction in settlement up to 50% with reduced permanent rotation by approximately 30 to 90%), while still mobilizing rocking behavior and dissipating seismic energy.

8.4. Recommendations for Future Work

8.4.1. Limitations of the Bridge-Pier Model and CIM

The development of the Bridge-pier model was certainly one of the most important aspects of this study. Since the Bridge-pier model was developed based on a full-scale bridge column designed according to the current Caltrans seismic design criteria, the evaluations based on this model becomes much more substantial and could be readily applied to future studies where evaluation of current conventional design approach or rocking behavior of a full-scale reinforced bridge column is needed. Furthermore, this model can be considered superior in its performance authenticity compared to a computational model with an elastic-beam column section as it consists of realistic concrete and reinforcing material models with the capacity for nonlinear behavior. However, as with many numerical models, the Bridge-pier model does lack the ability to manifest microscopic effects of material damage such as spalling, crack development, and eventual loss of concrete to reinforcement bonding under heavy cyclic loading. Instead, the model manifests plastic deformation culminating from all the above-mentioned microscopic effects. The degradation parameters present in the hysteretic material require proper calibration with established results prior to any use. For this study, the material was calibrated for a circular bridge column with a column aspect ratio between 4 to 10, reinforcement ratio of 1.5% and an axial load (structural weight) less than 0.2fc'Ag. If this model is to be used for performance evaluation for a different study, performance validation prior to evaluation is highly recommended.

The rocking foundation simulations were performed using an assumed soil layer consisting of dry sand. The input parameters for the contact interface model (CIM) were calculated using the methods described in the dynamic analysis chapter for a dry sandy soil.

Therefore, the conclusions of this study may only be applicable for such soil types. Further analysis using clayey soils is suggested for evaluating influence of pore water pressure on the rocking response. Furthermore, generally seismic accelerations consist of vertical and horizontal components. However, in most rocking foundation related research, excitations are only subjected to the horizontal component. The combined effects of vertical and horizontal accelerations components could provide further insight in to the combined nonlinear behavior of the soil-structure system.

8.4.2. Improvements for the Future

Based on the conclusions of this research program, the following recommendations could be submitted as recommendations for future work related to rocking foundation assessments.

- Evaluating the rocking foundations response in a bridge system is the next evolutionary step of rocking foundation philosophy. Researchers such as Deng et al., (2010 & 2012) has experimented with small-scale systems using centrifuge-modeling methods. A computational model consisting of a full-scale bridge system could provide much valuable insight in to the complex nonlinear behavior of a rocking system.
- The inability to effectively mitigate the rocking induced settlement is an admitted concern of rocking foundation design. However, the factors that influence the settlement should be further evaluated. In this study, it was concluded that factors such as initial soil vertical stiffness (K_v), initial soil modulus (G), and embedment could influence the rocking characteristics considerably. In the future, the ability to incorporate these factors in to controlling rocking induced settlement could be further analyzed.

- The effects of pore-water pressure and the behavior of undrained soil conditions under rocking behavior is an area with limited study. For a more comprehensive understanding of the nonlinear behavior of foundation-soil, the importance of such conditions cannot be ignored.
- From the structural aspect, it is important to consider appropriate methods of incorporating rocking foundations in to the superstructure design. Due to the inherent nature of this design, the superstructure must be able to accommodate large movement in the foundation, which is in stark contrast to current design philosophy that permits only a limited range of movement at foundation level.

REFERENCES

Aiken, I. D., Kelly, J., and Pall, A. (1988). "Seismic response of a nine-story steel frame with friction damped cross-bracing." *Rep. No. UCB/EERC*, 88, 17.

Allotey, N. and Naggar, M. H. E. (2003), "Analytical moment–rotation curves for rigid foundations based on a Winkler model," *Soil Dynamics and Earthquake Engineering*, 23, 367–381

Anastasopoulos, I., Gazetas, G., Loli, M., Apostolou, M., and Gerolymos, N. (2010). "Soil failure can be used for seismic protection of structures." *Bulletin of Earthquake Engineering*, 8(2), 309-326.

Anastasopoulos, I. (2010). Beyond conventional capacity design: towards a new design philosophy. *Soil–Foundation–Structure Interaction*, 213-220.

Anastasopoulos, I., Loli, M., Georgarakos, T., and Drosos, V. (2013). "Shaking Table Testing of Rocking—Isolated Bridge Pier on Sand." *Journal of Earthquake Engineering*, 17(1), 1-32.

Antonellis, G., Gavras, A. G., Panagiotou, M., Kutter, B. L., Guerrini, G., Sander, A. C., and Fox, P. J. (2015). "Shake Table Test of Large-Scale Bridge Columns Supported on Rocking Shallow Foundations." *Journal of Geotechnical and Geoenvironmental Engineering*, 141(5).

Braga, F., Crew, A., D'Anzi, P., Dolce, M. and Ponzo, F. C. (2002), "Experimental and Numerical Behavior of R/C Building Frames Upgraded with Energy Dissipating Braces," *European Earthquake Engineering*, 16 (1), 27 - 39

Caltrans, S. (2004). "Caltrans Seismic Design Criteria." Version.

California Department of Transportation. (2006). “Visual Catalog of Reinforced Concrete Bridge Damage”. Version.

California Department of Transportation. (2016). “Bridge Design Specifications.” http://www.dot.ca.gov/hq/esc/techpubs/manual/bridgemanuals/bridge-design-specifications/bds.html (April,5 2016)

Chopra, A. K., and Yim, S. C.-S. (1985). "Simplified earthquake analysis of structures with foundation uplift." *Journal of Structural Engineering*, 111(4), 906-930.

Cremer, C., Pecker, A., and Davenne, L. (2001). "Cyclic macro-element for soil–structure interaction: material and geometrical non-linearities." *International Journal for Numerical and Analytical Methods in Geomechanics*, 25(13), 1257-1284.

Cuthill, E., and McKee, J. "Reducing the bandwidth of sparse symmetric matrices." *Proc., Proceedings of the 1969 24th national conference*, ACM, 157-172.

Demmel, J. W., Eisenstat, S. C., Gilbert, J. R., Li, X. S., and Liu, J. W. (1999). "A supernodal approach to sparse partial pivoting." *SIAM Journal on Matrix Analysis and Applications*, 20(3), 720-755.

Das, B. M. (2015). *Principles of foundation engineering*, Cengage learning.

Deng, L., Kutter, B. L., Kunnath, S., and Algie, T. B. (2010). "Centrifuge modelling of bridge system with rocking footings." *Physical Modelling in Geotechnics, Vols. 1 and 2*, 691-696.

Deng, L., & Kutter, B. L. (2012). Characterization of rocking shallow foundations using centrifuge model tests. *Earthquake Engineering & Structural Dynamics*, *41*(5), 1043-1060.

Dolce, M., and Cardone, D. (2003). "Seismic protection of light secondary systems through different base isolation systems." *Journal of Earthquake Engineering*, 7(2), 223-250.

Dolce, M., Cardone, D., and Marnetto, R. (2000). "Implementation and testing of passive control devices based on shape memory alloys." *Earthquake Engineering & Structural Dynamics*, 29(7), 945-968.

Drosos, V., Georgarakos, T., Loli, M., Anastasopoulos, I., Zarzouras, O., and Gazetas, G. (2012). "Soil-Foundation-Structure Interaction with Mobilization of Bearing Capacity: Experimental Study on Sand." *Journal of Geotechnical and Geoenvironmental Engineering*, 138(11), 1369-1386.

FEMA 356 (2000), "Prestandard and Commentary for the Seismic Rehabilitation of Buildings," Federal Emergency Management Agency, Washington, DC

Gajan, S., Hutchinson, T. C., Kutter, B. L., Raychowdhury, P., Ugalde, J. A., Stewart, J. P. (2008). *Numerical models for analysis and performance-based design of shallow foundations subjected to seismic loading*, Pacific Earthquake Engineering Research Center.

Gajan, S., and Kutter, B. L. (2008). "Capacity, settlement, and energy dissipation of shallow footings subjected to rocking." *Journal of Geotechnical and Geoenvironmental Engineering*, 134(8), 1129-1141.

Gajan, S., and Kutter, B. L. (2009). "Contact Interface Model for Shallow Foundations Subjected to Combined Cyclic Loading." *Journal of Geotechnical and Geoenvironmental Engineering*, 135(3), 407-419.

Gajan, S., and Kutter, B. L. (2009). "Effects of Moment-to-Shear Ratio on Combined Cyclic Load-Displacement Behavior of Shallow Foundations from Centrifuge Experiments." *Journal of Geotechnical and Geoenvironmental Engineering*, 135(8), 1044-1055.

Gajan, S., Kutter, B. L., Phalen, J. D., Hutchinson, T. C., and Martin, G. R. (2005). "Centrifuge modeling of load-deformation behavior of rocking shallow foundations." *Soil Dynamics and Earthquake Engineering*, 25(7-10), 773-783.

Gajan, S., and Saravanathiiban, D. S. (2011). "Modeling of energy dissipation in structural devices and foundation soil during seismic loading." *Soil Dynamics and Earthquake Engineering*, 31(8), 1106-1122.

Gajan, S., and Saravanathiiban, D. S. (2011). "Modeling of energy dissipation in structural devices and foundation soil during seismic loading." *Soil Dynamics and Earthquake Engineering*, 31(8), 1106-1122.

Harden, C. W, Hutchinson, T. C, Martin, G. R, and Kutter, B. L. (2005), “Numerical modeling of the nonlinear cyclic response of shallow foundations,” *Technical Report 2005/04*, Pacific Earthquake Engineering Research Center (PEER)

Housner, G. W. (1963). "The dynamic behavior of water tanks." *Bulletin of the seismological society of America*, 53(2), 381-387.

Kawashima, K., & Unjoh, S. (2004). Seismic design of highway bridges. *日本地震工学会論文集*, *4*(3), 174-183.

Karsan, I. D., & Jirsa, J. O. (1969). Behavior of concrete under compressive loadings. *Journal of the Structural Division*.

Kramer, S. L. (1996). *Geotechnical earthquake engineering*, Pearson Education India.

Kokkali, P., Abdoun, T., Anastasopoulos, I., Kourkoulis, R., Gelagoti, F., & Gazetas, G. (2014). Experimental investigation of the rocking response of SDOF systems on sand. In *ICPMG2014–Physical Modelling in Geotechnics: Proceedings of the 8th International Conference on Physical Modelling in Geotechnics* (Vol. 1, pp. 659-666). CRC Press, Boca Raton, FL, USA.

Lehman, D. E., & Moehle, J. P. (2000). *Seismic performance of well-confined concrete bridge columns*. Pacific Earthquake Engineering Research Center.

Loli, M., Knappett, J. A., Brown, M. J., Anastasopoulos, I., and Gazetas, G. (2014). "Centrifuge modeling of rocking-isolated inelastic RC bridge piers." *Earthquake Engineering & Structural Dynamics*, 43(15), 2341-2359.

McKenna, F. (2011). "OpenSees: Open System for Earthquake Engineering Simulation http://opensees.berkeley.edu.

Mander, J. B., Priestley, M. J. N., and Park, R. (1988). "THEORETICAL STRESS-STRAIN MODEL FOR CONFINED CONCRETE." *Journal of Structural Engineering-Asce*, 114(8), 1804-1826.

Mazzoni, S., McKenna, F., Scott, M. H., and Fenves, G. L. (2006). "OpenSees command language manual." *Pacific Earthquake Engineering Research (PEER) Center*.

Newmark, N. M. "A method of computation for structural dynamics." *Proc., Proc. ASCE*, 67-94.

Ntritsos, N., Anastasopoulos, I., and Gazetas, G. (2015). "Static and cyclic undrained response of square embedded foundations." *Geotechnique*, 65(10), 805-823.

Orakcal, K., Sanchez, L. M. M., & Wallace, J. W. (2006). *Analytical modeling of reinforced concrete walls for predicting flexural and coupled-shear-flexural responses*. Pacific

Earthquake Engineering Research Center, College of Engineering, University of California, Berkeley.

Overby, D., Kowalsky, M., and Seracino, R. (2015). "A706 Grade 80 Reinforcement for Seismic Applications."

Park, R., & Paulay, T. (1975). *Reinforced concrete structures*. John Wiley & Sons.

Park, Y.-J., and Ang, A. H.-S. (1985). "Mechanistic seismic damage model for reinforced concrete." *Journal of structural engineering*, 111(4), 722-739.

PEER Ground Motion Database (2013), Pacific Earthquake Engineering Research Center, http://ngawest2.berkeley.edu/.

Popa, V., Cotofana, D., and Vacareanu, R. (2014). "Effective stiffness and displacement capacity of short reinforced concrete columns with low concrete quality." *Bulletin of Earthquake Engineering*, 12(6), 2705-2721.

Priestley, M. N., Seible, F., and Calvi, G. M. (1996). *Seismic design and retrofit of bridges*, John Wiley & Sons.

Priestley, M. N., Verma, R., & Xiao, Y. (1994). Seismic shear strength of reinforced concrete columns. *Journal of structural engineering*, *120*(8), 2310-2329.

Schoettler, M. J., Restrepo, J. I., Guerrini, G., Duck, D. E., Carrea, F. (2015). *A full-scale, single-bridge bent tested by shake table excitation,* Pacific Earthquake Engineering Research Center.

Selvarajah, P. and Gajan, S. (2015), "The beneficial and detrimental effects of rocking shallow foundations on superstructure during seismic loading", Proc. Geo-Quebec 2015, Quebec City, Canada, September 20-23, 2015

Selvarajah, P. and Gajan, S. (2015), "Rocking shallow foundations as seismic energy dissipaters: Theoretical analyses of experimental findings", Proc. International Conference on Geotechnical Engineering, Colombo, Sri Lanka, August 10-11, 2015

Scott, B., Park, R., and Priestley, M. (1982). "Stress-strain behavior of concrete confined by overlapping hoops at low and high strain rates." *ACI journal*, 79(1), 13-27.

Spacone, E., Filippou, F., and Taucer, F. F. (1996). "Fibre beam-column model for non-linear analysis of R/C frames: Part II. Applications." *Earthquake Engineering and Structural Dynamics*, 25(7), 727-742.

Spacone, E., Filippou, F. C., and Taucer, F. F. (1996). "Fibre beam-column model for non-linear analysis of R/C frames: Part I. Formulation." *Earthquake engineering and structural dynamics*, 25(7), 711-726.

Ugalde, J. A., Kutter, B. L., Jeremic, B., and Gajan, S. (2007). "Centrifuge modeling of rocking behavior of bridges on shallow foundations." *Proc., Proceedings of the 4th international conference earthquake geotechnical engineering. Thessaloniki, Greece, Paper*, 25-28.

Watson, S., Zahn, F., and Park, R. (1994). "Confining reinforcement for concrete columns." *Journal of Structural Engineering*, 120(6), 1798-1824.

Wibowo, A., Wilson, J. L., Lam, N. T., & Gad, E. F. (2014). Drift capacity of lightly reinforced concrete columns. *Australian Journal of Structural Engineering*, *15*(2), 131-150.

Yassin, M. H. M. (1994). Nonlinear analysis of prestressed concrete structures under monotonic and cyclic loads. Dissertation. University of California. Berkeley, California.

APPENDIX A. TABLES

Table A1

Simulation Testing Matrix

#	Strucural Code	CIM Code	Excitation Code	H (m)	AR	Mass (Mg)	B (m)	Df (m)	Excitation	Scale Factor
1	BPM_6_0	N/A	K1.0	7.9	6.5	0.26	FIXED	N/A	KALAMATA	1.0
2	BPM_6_0	N/A	K1.5	7.9	6.5	0.26	FIXED	N/A	KALAMATA	1.5
3	BPM_6_0	N/A	K2.0	7.9	6.5	0.26	FIXED	N/A	KALAMATA	2.0
4	BPM_6_0	N/A	K3.0	7.9	6.5	0.26	FIXED	N/A	KALAMATA	3.0
5	BPM_6_0	N/A	T0.5	7.9	6.5	0.26	FIXED	N/A	TAKATORI	0.5
6	BPM_6_0	N/A	T0.8	7.9	6.5	0.26	FIXED	N/A	TAKATORI	0.8
7	BPM_4_0	N/A	T0.5	5	4	0.26	FIXED	N/A	TAKATORI	0.5
8	BPM_10_0	N/A	T0.5	12	10	0.26	FIXED	N/A	TAKATORI	0.5
9	BPM_4_0	N/A	T0.8	5	4	0.26	FIXED	N/A	TAKATORI	0.8
10	BPM_10_0	N/A	T0.8	12	10	0.26	FIXED	N/A	TAKATORI	0.8
11	BPM_6_6	0_M	K1.5	7.9	6.5	0.26	6.5	0	KALAMATA	1.5
12	BPM_6_6	0_M	T0.5	7.9	6.5	0.26	6.5	0	TAKATORI	0.5
13	BPM_6_3	0_M	K1.5	7.9	6.5	0.26	3.5	0	KALAMATA	1.5
14	BPM_6_3	0_L	K1.5	7.9	6.5	0.26	3.5	0	KALAMATA	1.5
15	BPM_6_3	0_D	K1.5	7.9	6.5	0.26	3.5	0	KALAMATA	1.5
16	BPM_6_3	0_M	K2.0	7.9	6.5	0.26	3.5	0	KALAMATA	2.0
17	BPM_6_3	0_M	K3.0	7.9	6.5	0.26	3.5	0	KALAMATA	3.0
18	BPM_6_3	0_M	T0.5	7.9	6.5	0.26	3.5	0	TAKATORI	0.5
19	BPM_6_3	0_L	T0.5	7.9	6.5	0.26	3.5	0	TAKATORI	0.5
20	BPM_6_3	0_D	T0.5	7.9	6.5	0.26	3.5	0	TAKATORI	0.5
21	BPM_4_3	0_M	T0.5	5	4	0.26	3.5	0	TAKATORI	0.5
22	BPM_4_3	0_M	T0.8	5	4	0.26	3.5	0	TAKATORI	0.8
23	BPM_10_3	0_M	T0.5	12	10	0.26	3.5	0	TAKATORI	0.5
24	BPM_10_3	0_M	T0.8	12	10	0.26	3.5	0	TAKATORI	0.8
25	BPM_6_5	0_L	K1.5	7.9	6.5	0.26	5	0	KALAMATA	1.5
26	BPM_10_6	0_M	K1.5	12	10	0.26	6.5	0	KALAMATA	1.5
27	BPM_6_6	0_M	K1.0	7.9	6.5	0.26	6.5	0	KALAMATA	1.0
28	BPM_10_6	0_M	T1.0	12	10	0.26	6.5	0	TAKATORI	1.0
29	BPM_6_5	0_L	K2.0	7.9	6.5	0.26	5	0	KALAMATA	2.0
30	BPM_6_5	0_L	T0.5	7.9	6.5	0.26	5	0	TAKATORI	0.5
31	BPM_6_3	0_M	T0.8	7.9	6.5	0.26	3.5	0	TAKATORI	0.8
32	BPM_4_3	0_D	T0.5	5	4	0.26	3.5	0	TAKATORI	0.5
33	BPM_6_5	0_M	T0.5	7.9	6.5	0.26	5	0	TAKATORI	0.5
34	BPM_6_3	1_M	K2.0	7.9	6.5	0.26	3.5	1	KALAMATA	2.0
35	BPM_6_3	1_M	K3.0	7.9	6.5	0.26	3.5	1	KALAMATA	3.0
36	BPM_6_3	1.5_M	K2.0	7.9	6.5	0.26	3.5	1.5	KALAMATA	2.0
37	BPM_6_3	1.5_M	K3.0	7.9	6.5	0.26	3.5	1.5	KALAMATA	3.0
38	BPM_4_3	1_M	T0.5	5	4	0.26	3.5	1	TAKATORI	0.5
39	BPM_6_3	1_M	T0.8	7.9	6.5	0.26	3.5	1	TAKATORI	0.8
40	BPM_6_3	1_L	K2.0	7.9	6.5	0.26	3.5	1	KALAMATA	2.0
41	BPM_6_3	1_D	K2.0	7.9	6.5	0.26	3.5	1	KALAMATA	2.0
42	BPM_6_3	0_L	K2.0	7.9	6.5	0.26	3.5	0	KALAMATA	2.0
43	BPM_6_3	0_D	K2.0	7.9	6.5	0.26	3.5	0	KALAMATA	2.0

Table A2

Foundation-Soil Parameters for CIM

#	Strucural Code	CIM Code	G (Mpa)	Kv (MN/m)	Kh (MN/m)	FS
11	BPM_6_6	0_M	97	2100	1700	23.8
12	BPM_6_6	0_M	97	2100	1700	24.0
13	BPM_6_3	0_M	71	830	670	3.7
14	BPM_6_3	0_L	56	660	530	2.4
15	BPM_6_3	0_D	92	1100	870	7.5
16	BPM_6_3	0_M	71	830	670	3.7
17	BPM_6_3	0_M	71	830	670	3.7
18	BPM_6_3	0_M	71	830	670	3.7
19	BPM_6_3	0_L	56	660	530	2.4
20	BPM_6_3	0_D	92	1100	870	7.5
21	BPM_4_3	0_M	71	830	670	3.7
22	BPM_4_3	0_M	71	830	670	3.7
23	BPM_10_3	0_M	71	830	670	3.7
24	BPM_10_3	0_M	71	830	670	3.7
25	BPM_6_5	0_L	61	1010	820	7.1
26	BPM_10_6	0_M	97	2100	1700	23.8
27	BPM_6_6	0_M	97	2100	1700	23.8
28	BPM_10_6	0_M	97	2100	1700	23.8
29	BPM_6_5	0_L	61	1010	820	7.1
30	BPM_6_5	0_L	61	1010	820	7.1
31	BPM_6_3	0_M	89	830	670	3.7
32	BPM_4_3	0_D	92	1100	870	7.5
33	BPM_6_5	0_M	76	1270	1020	10.9
34	BPM_6_3	1_M	89	1460	940	8.3
35	BPM_6_3	1_M	89	1460	940	8.3
36	BPM_6_3	1.5_M	96	1640	2190	10.8
37	BPM_6_3	1.5_M	96	1640	2190	10.8
38	BPM_4_3	1_M	89	1460	940	8.3
39	BPM_6_3	1_M	89	1460	940	8.3
40	BPM_6_3	1_L	71	1170	747	5.5
41	BPM_6_3	1_D	115	1900	1200	16
42	BPM_6_3	0_L	56	660	530	2.4
43	BPM_6_3	0_D	92	1100	870	7.5

APPENDIX B. OPENSEES EXAMPLE CODES

TCL Code for OpenSees Simulation of Rocking Foundation Using CIM (BPM63-0M-K1.5)

```
############ FULL-SCALE BRIDGE COLUMN CIM #################
######## UNITS USED: KG, NEWTON, SEC & METERS ########

# wipe out all previous input
wipe

#--------build a 2D model with 3 DOF----------#

model BasicBuilder -ndm 2 -ndf 3

#------structure properties-------#

set Hcol 7.9 #column height
set Mdeck 2.6e5 #structural deck mass
set Ideck 2.6e5 #structural deck rotational mass

#----define parameters for macro element use----#

set Rv 0.12
set deltaL 0.01
set L 3.5
set B $L
set Vtot [expr $Mdeck*9.81]
set Df 0 #footing embedment

#----soil parameters unit_weight angle_of_friction & cohesion----#

set gamma 18000 #soil unit weight
set phi 34 #friction angle
set c 0 #cohesion
set pi [expr acos(-1)]

source FScalc.tcl # recall factor of safety calculations

set Vult [expr $Vtot*$FS]

#--------CIM parameter calculation---------#

set nu 0.3 #Poisson ration
set N160 25 #SPT blow counts
#soil stiffness calculation
source surfacestiffness.tcl #recall soil stiffness calcuations
```

```
#-----------define nodes--------#

node 1 0 0
node 2 0 0
node 3 0 $Hcol

#---geometry of column elements----#

geomTransf PDelta 1

#------foundation/soil element-------#

#section SFS2d matID FS Vult L Kv Kh Rv deltaL
section soilFootingSection2d 1 $FS $Vult $L $Kv $Kh $Rv $deltaL
#element ZLS eleID ndi ndj matID
element zeroLengthSection 1 1 2 1 -orient 0 -1 0 1 0 0

#--------------define material for nonlinear column-----------------#

#confined concrete  mat.Tag fc1C eps1C fc2C eps2C lambda ftC Ets
uniaxialMaterial Concrete02 1 -53e6 -0.003 -42e6 -0.015 0.1 5.3e6 3e9

#unconfined concrete  mat.Tag fc1U eps1U fc2U eps2U lambda ftU Ets
uniaxialMaterial Concrete02 2 -42e6 -0.0026 -4.2e6 -0.006 0.1 4.2e6 3e9

#uniaxialMaterial Hysteretic $IDHysteretic $Fy $epsY $Fy1 $epsY1 $Fu $epsU -$Fy -$epsY -
$Fy1 -$epsY1 -$Fu -$epsU $pinchX $pinchY $damage1 $damage2 $betaMUsteel
uniaxialMaterial Hysteretic 3 710e6 0.005 800e6 0.04 690e6 0.122 -710e6 -0.005 -800e6 -0.04 -
690e6 -0.122 1 1 0.0 0.3 0

#--------------define column cross-section dimensions----------------#

#column diameter
set D 1.22
#number of reinforments
set numBar 18
#cover concrete
set Cover 0.051
#area of steel for each longitudinal
set  As 0.001006

#-------creating fiber sections for core/ cover concrete and reinforcements-------#

set ri 0
set r0 [expr $D/2]
set nfCoreR 8
```

```
set nfCoreT 8
set nfCoverR 4
set nfCoverT 8
set rc [expr $r0-$Cover]

section Fiber 2 {

#create core fiber mat.Tag numSubDivCirc numSubDivRad yCenter zCenter intRad extRad
startAng endAng
patch circ 1 $nfCoreT $nfCoreR 0 0 $ri $rc 0 360

#create cover fiber mat.Tag numSubDivCirc numSubDivRad yCenter zCenter intRad extRad
startAng endAng
patch circ 2 $nfCoverT $nfCoverR 0 0 $rc $r0 0 360

#create reinforcement fibers mat.Tag $numFiber $areaFiber $yCenter $zCenter $radius
<$startAng $endAng>
set theta [expr 360.0/$numBar]
layer circ 3 $numBar $As 0 0 $rc $theta 360
}

#-------------------define column elements----------------------#

#number of integration points along length of element
set npcolumn 3
set eleType forceBeamColumn

#create column using beam-column elements  tag ndI ndJ nsecs secID transferTag
element $eleType 2 2 3 $npcolumn 2 1

#-----------boundary condition-----------------------#

#fix base node in all directions nodetag x y rotation
fix 1 1 1 1
#fix node 2 in X-direction nodetag x y rotation
fix 2 1 0 0

#-------------gravity analysis-------------------------#

#define gravity loads - in 10 increments - deck mass
pattern Plain 1 Linear {
load 3 0 -2.55e5 0
}

#define analysis - gravity load
test NormDispIncr 1e-8 10 1
```

```
algorithm Newton
system UmfPack
constraints Plain
numberer Plain

analysis Static
analyze 10

#setting time back to 0 before dynamic analysis
loadConst -time 0.0

#-------define recorders--------#

set name "node"
for {set n 1} {$n <= 3} {incr n 1} {
set fileName [join [list $name $n] {} ]
recorder Node -file $fileName -node $n -dof 1 2 3 disp
}

set name "element"
for {set n 1} {$n <= 2} {incr n 1} {
set fileName [join [list $name $n] {} ]
recorder Element -file $fileName -time -ele $n force
}

recorder Node -file Accx -node 3 -dof 1 accel

recorder Node -file Accr -node 3 -dof 3 accel

puts "-----Gravity Analysis Done-----"

#indicate factor of safety
puts "----- Factor of Safety $FS -----"
puts "---Vult $Vult---"

#indicate CIM parameters
puts "---Kv $Kv---"
puts "---Kh $Kh---"

wipeAnalysis #wipe gravity analysis step

#----------stuperstructure node----------#

#define mass at node 3 in direction x y rotation
mass 3 $Mdeck $Mdeck $Ideck
```

```
#-----------dynamic analysis------------#

test EnergyIncr 1e-5 1000 1
algorithm Newton
system UmfPack
constraints Plain
numberer RCM
integrator Newmark 0.5 0.25
analysis VariableTransient

#-----------apply damping---------#

set xDamp 0.05
set lambda [eigen 1]
set omega {}
set f {}
set T {}
set pi [expr acos(-1)]

foreach lam $lambda {
lappend omega [expr sqrt($lam)]
lappend f [expr sqrt($lam)/(2*$pi)]
lappend T [expr (2*$pi)/sqrt($lam)]
}

puts "---Tn $T---"

set alphaM 0.0
set betaK 0
set betaKcomm [expr 2*$xDamp/$omega]
set betaKinit 0

rayleigh $alphaM $betaK $betaKinit $betaKcomm

#-----------define ground motion----------#

set dT 0.0001
set dTmin [expr $dT/100]
set dTmax $dT

# acceleration time history is read from an external file
set Series "Path -filePath Kalamatanew_input.txt -dt $dT -factor 14.7"
# acceleration is applied at the fixed node in horizontal direction (1)
pattern UniformExcitation 2 1 -accel $Series

#apply shake
```

```
set steps 150000
set itr 1000

for {set i 1} {$i < $steps} {incr i 1} {
test EnergyIncr 1e-5 $itr 0
set ok [analyze 1 $dT $dTmin $dTmax $itr]

        if {$ok != 0} {
        test EnergyIncr 1e-3 $itr 0
        set ok [analyze 1 $dT $dTmin $dTmax $itr]
        }
        if {$ok != 0} {
        test EnergyIncr 1e-2 $itr 0
        set ok [analyze 1 $dT $dTmin $dTmax $itr]
        }
}

# print out final node and element outputs on screen

for {set n 1} {$n <= 3} {incr n 1} {
    print node $n
}
print ele


puts "----TEST COMPLETE----"


#end
wipe
```

Concrete MATERIAL Properties Calculation Method for Bridge-pier Model (OpenSees, 2007)

```
# nominal concrete compressive strength
set fc [expr 6.1*$ksi]; # CONCRETE Compressive Strength, ksi (+Tension, -Compression)

# confined concrete
set Ec [expr 57*$ksi*sqrt(fc*1000)]; # Concrete Elastic Modulus
set fc1C [expr 1.26394*$fc];  # CONFINED concrete (mander model), maximum stress
set eps1C       [expr 2.*$fc1C/$Ec];  # strain at maximum stress
set fc2C $fc;   # ultimate stress
set eps2C [expr 5*$eps1C];    # strain at ultimate stress

# unconfined concrete
set fc1U $fc;   # UNCONFINED concrete (todeschini parabolic model), maximum stress
set eps1U       -0.003; # strain at maximum stress
set fc2U [expr 0.1*$fc];        # ultimate stress
set eps2U       -0.006; # strain at ultimate stress

# concrete02 material properties
set lambda 0.1 ;        # ratio between unloading slope at $epscu and initial slope
set ftC [expr -$fc1C/10.];      # tensile strength +tension
set ftU [expr -$fc1U/10.];      # tensile strength +tension
set Ets [expr $Ec/10.];# tension softening stiffness


########################################################################################
########################################################################################
#--------------------------CONCRETE02 PROPERTIES-------------------------------------#

#COMPRESSIVE STRENGTH (fc) = 6.1ksi
#ELASTIC MODULUS (Ec) 57*(sqrt(6100psi)) = 4450ksi
#lambda = 0.1
#Ets = Ec/10 = 445ksi (3Gpa)

#-----------------Confined Concrete-------------#

fc1C = 1.26*6.1ksi = 7.7ksi (53Mpa)
eps1C = 2*(fc1C/Ec) = 0.003
fc2C = fc = 6.1ksi (42Mpa)
eps2C = 5*eps1C = 0.015
ftc = fc1C/10 = 0.77ksi (5.3Mpa)

#-----------------Unconfined Concrete------------#
```

fc1U = fc = 6.1ksi (42Mpa)
eps1U = 0.0026
fc2U = 0.1*fc = 0.61ksi (4.2Mpa)
eps2U = 0.006
ftU = fc1U/10 = 0.61ksi (4.2Mpa)

##